C.1

RESTRICTED

NACA RM L52C11

UNCLASSIFIED

NACA

RESEARCH MEMORANDUM

LOW-SPEED LONGITUDINAL AERODYNAMIC CHARACTERISTICS OF A TWISTED AND CAMBERED WING OF 45° SWEEPBACK AND ASPECT RATIO 8 WITH AND WITHOUT HIGH-LIFT AND STALL-CONTROL DEVICES AND A FUSELAGE AT REYNOLDS NUMBERS FROM 1.5×10^6 TO 4.8×10^6

FOR REFERENCE

NOT TO BE TAKEN FROM THIS ROOM

By Reino J. Salmi

Langley Aeronautical Laboratory
Langley Field, Va.

CLASSIFICATION CANCELLED

Authority J. W. Crowley Date 12/7/53
CEO 1050K

By MHA 12/18/53 See NACA
RF 1660

CLASSIFIED DOCUMENT

This material contains information affecting the National Defense of the United States within the meaning of the espionage laws, Title 18, U.S.C., Secs. 793 and 794, the transmission or revelation of which in any manner to an unauthorized person is prohibited by law.

NATIONAL ADVISORY COMMITTEE FOR AERONAUTICS

WASHINGTON
June 11, 1952

UNCLASSIFIED

RESTRICTED

3 1176 01437 0770

NATIONAL ADVISORY COMMITTEE FOR AERONAUTICS

RESEARCH MEMORANDUM

LOW-SPEED LONGITUDINAL AERODYNAMIC CHARACTERISTICS OF A TWISTED AND CAMBERED WING OF 45° SWEEPBACK AND ASPECT RATIO 8 WITH AND WITHOUT HIGH-LIFT AND STALL-CONTROL DEVICES AND A FUSELAGE AT REYNOLDS NUMBERS FROM 1.5×10^6 TO 4.8×10^6

By Reino J. Salmi

SUMMARY

A low-speed investigation of the static longitudinal aerodynamic characteristics of a twisted and cambered wing having 45° of sweepback and an aspect ratio of 8.0 was conducted in the Langley 19-foot pressure tunnel. The tests included the effects of leading- and trailing-edge flaps, flow control fences, and a fuselage. The investigation was made through a Reynolds number range of 1.5×10^6 to 4.8×10^6.

A comparison of the results with those of a wing of similar plan form, but with no camber or twist, indicated that, for the flaps-neutral case, camber and twist improved the stability considerably in the lift-coefficient range below 0.7, increased the lift-drag ratios in the moderate and high lift-coefficient range, and increased the maximum lift coefficient from 1.01 to 1.30. With high-lift and stall-control devices on the wings, camber and twist increased the lift-drag ratios in the high-lift range and increased the maximum lift coefficient, although the forward shift of aerodynamic center near the maximum lift was somewhat greater for the twisted and cambered wing than for the untwisted wing. The fuselage had a destabilizing effect which increased greatly in the high angle-of-attack range. Reynolds number effects on the aerodynamic characteristics in the range investigated were, in general, small. Roughness on the leading edge of the plain wing caused an appreciable decrease in the lift coefficient at which the pitching moment became unstable and decreased the maximum lift coefficient about 0.2.

INTRODUCTION

As part of a broad program to investigate the low-speed aerodynamic characteristics of sweptback wings, the static longitudinal stability characteristics of a 45° sweptback wing of aspect ratio 8.0 were investigated in the Langley 19-foot pressure tunnel. The results are reported in references 1 to 3. Although a wing of such plan form is basically very unstable at moderate and high lift coefficients, it was pointed out in reference 1 that longitudinal stability could be obtained from the use of stall-control devices.

More recently, consideration has been given to the use of camber and twist variations along the span as a means of counteracting the undesirable induced effects of sweepback. Camber and twist also provide additional advantages, if properly applied, in that both the profile and induced drag would be reduced for high design lift coefficients.

With these considerations in mind, an experimental investigation was conducted to determine the low-speed longitudinal characteristics of a 45° sweptback wing of aspect ratio 8.0, which was cambered and twisted to provide an elliptical spanwise load distribution at a design lift coefficient of 0.7 and a Mach number of 0.9. The plan form of the present wing was similar to the plan form of the wing reported in references 1 to 3, which had no camber or twist.

The present paper contains the results of force tests to determine the effects of high-lift and stall-control devices on the cambered and twisted wing. The investigation was conducted at Reynolds numbers ranging from 1.5×10^6 to 4.8×10^6.

SYMBOLS

All forces and moments are referred to a point 9.34 percent of the mean aerodynamic chord above the quarter-chord point of the mean aerodynamic chord projected to the plane of symmetry.

A	aspect ratio
a	speed of sound
b	wing span
c	wing chord

$\bar{c}$	mean aerodynamic chord $\left(\frac{2}{S}\int_0^{b/2} c^2 dy\right)$
C_D	drag coefficient (Drag/qS)
C_L	lift coefficient (Lift/qS)
C_{l_i}	design section lift coefficient
ΔC_L	increment in lift coefficient
C_m	pitching-moment coefficient (Pitching moment/$qS\bar{c}$)
ΔC_{m_f}	C_m (fuselage on) - C_m (fuselage off)
dC_m/dC_L	rate of change of pitching-moment coefficient with lift coefficient
L/D	lift-drag ratio
M	Mach number (V/a)
q	dynamic pressure $\left(1/2\rho V^2\right)$
R	Reynolds number $(\rho V\bar{c}/\mu)$
S	wing area
t	wing thickness at any section
V	free-stream velocity
x	distance along chord line from leading edge
y	spanwise coordinate
z	distance normal to chord line
α	angle of attack of wing root chord line
δ_f	flap deflection angle measured in a plane parallel to plane of symmetry
ρ	mass density of air

μ coefficient of viscosity

Subscripts:

max maximum

MODEL

The wing (fig. 1) was similar in plan form to the untwisted wing reported in references 1 to 3, and had 45° of sweepback at the quarter-chord line, an aspect ratio of 8.0, and a taper ratio of 0.45. The wing was designed to provide an elliptical spanwise loading and a uniform chordwise loading at a lift coefficient of 0.7 and a Mach number of 0.9. The corresponding twist and camber were calculated by the method of reference 4. Figure 2 presents the spanwise variation of the geometric twist and the design section lift coefficient. The mean line used was a very close approximation of the mean line derived from reference 4 and was obtained by increasing slightly the curvature near the nose of a mean line of the type $a = 1$. The equations giving the shape of the mean line together with tabulated ordinates for a design section lift coefficient of 1.0 are given in table I. The mean-line ordinates at any spanwise station are obtained by multiplying the ordinates given in table I by the proper values of C_{l_i} given in figure 2. The thickness distribution of the NACA 63_1A012 section was used. The twisted wing represents a series of sections sheared parallel to the plane of symmetry and rotated about the 80-percent-chord point, so that true sections were maintained parallel to the plane of symmetry.

The wing construction consisted of a steel core with an outer layer of an alloy of bismuth and tin. The various flaps and fences used on the wing were made of sheet steel. The details of these devices and their locations on the wing are shown in figure 1.

The fuselage was circular in cross section and had a fineness ratio of 10.0. The fuselage had removable sections which permitted the wing to be set at incidence angles of 0° or 4°. For each incidence angle, the leading edge of the root chord remained fixed relative to the fuselage, that is, 3.182 inches above the fuselage center line. The following equations define the fuselage nose and afterbody shapes:

Nose shape

$$\left(\frac{r}{r_o}\right)_n = \left[1 - \left(1 - \frac{x_n}{l_n}\right)^2\right]^{1/2}$$

Afterbody shape

$$\left(\frac{r}{r_o}\right)_a = \left[1 - \left(1 - \frac{x_a}{l_a}\right)^2\right]^{3/4}$$

where the length of the constant-diameter section was equal to 41.680 inches and

r	radius
r_o	radius of constant-diameter section (6.36 in.)
x_n	distance measured toward center of fuselage from fuselage nose
l_n	length of curved portion of fuselage nose (33.344 in.)
x_a	distance measured toward center of fuselage from the stern
l_a	length of curved portion of fuselage afterbody (52.236 in.)

TESTS

The tests were conducted in the Langley 19-foot pressure tunnel at an air pressure of about 33 pounds per square inch absolute and at Reynolds numbers ranging from 1.5×10^6 to 4.8×10^6. Figure 3 shows the model mounted in the tunnel.

Measurements of the forces and moments on the model were made for an angle-of-attack range from -4° to 30°. Most of the data were obtained with the fuselage off. Various combinations of the leading-edge flaps, trailing-edge flaps, and fences were tested, and the results are summarized in table II. The fuselage-on data were obtained for wing incidence angles of 0° and 4°. An indication of the air-flow characteristics near the surface of wing was obtained from observations of wool tufts fastened to the wing surface with cellulose tape.

The test Reynolds numbers and corresponding Mach numbers were as follows:

R	M
1.5×10^6	0.07
2.2	.11
3.0	.14
4.0	.19
4.8	.25

The effects of roughness of the type described in reference 5 on the aerodynamic characteristics of the plain wing were determined at Reynolds numbers of 1.5×10^6 and 4.0×10^6.

RESULTS AND DISCUSSION

The data have been corrected for the support tare and interference effects, air-stream misalinement, model blockage, and jet-boundary interference. The jet-boundary corrections were determined by the method shown in reference 6. In the following discussion, reference is made to unpublished pressure-distribution data which were obtained on the present wing.

Longitudinal Stability Characteristics

Wing alone.- The lift and pitching-moment characteristics of the cambered and twisted wing and those of the uncambered and untwisted wing (reference 2), which will hereinafter be referred to as the flat wing, are presented in figure 4. It is readily apparent that the camber and twist increased the lift-coefficient range in which the wings did not experience any decrease in stability and that the twisted and cambered wing had an abrupt unstable break, whereas the flat wing had a more gradual unstable change. From reference 2 and from unpublished section-lift data for the twisted and cambered wing, it was noted that a loss in lift for the wing sections near the tips began at a wing lift coefficient of about 0.4 for the flat wing and 0.7 for the cambered and twisted wing. The pitching-moment data of figure 4, however, indicate a forward movement of the center of pressure for the flat wing which begins at a lift coefficient of about 0.2. Analysis of the pressure-distribution data of reference 2 indicates that the section centers of

pressure do not move enough to account for much of the wing center-of-pressure movement. The initial movement of the wing center of pressure is evidently due mainly to small reductions in the lift-curve slope of the tip sections, possibly even outboard of the $0.96\frac{b}{2}$ station (the farthest outboard row of orifices). Lift changes outboard of this station would not be large enough to affect the wing lift-curve slope but would have a noticeable effect on the wing pitching moment and center of pressure because of the distance of those sections behind the moment center. The lift curves were nearly linear for the tip sections of the twisted and cambered wing so that the pitching-moment-coefficient curve for that wing (fig. 4) was almost linear in the lift-coefficient range below 0.7.

Stall-control devices.- As in the case of the flat wing (reference 1), an appreciable improvement in the stability of the cambered and twisted wing resulted from the use of upper-surface fences (figs. 5 to 9). A comparison of the pitching-moment curves of the various fence configurations indicated that the most favorable stability characteristics were obtained for a combination of three complete fences located at 0.450b/2, 0.700b/2, and 0.890b/2 (fig. 7). When more than three fences were used, the stability characteristics in the lift-coefficient range below the maximum lift coefficient were further improved, but an unstable break resulted at the maximum lift coefficient. The results of the present investigation, however, indicate that, as in the case of the flat wing, the instability of the cambered and twisted wing could not be completely eliminated by the use of fences alone.

Some indication of the effects of the fences on the boundary-layer cross flow may be obtained from the tuft studies of figure 10. It can be seen that the cross flow was obtained between the fences even at the lowest lift coefficient for which the tuft-study data are presented. The cross flow between the fences is believed to be independent of the cross flow on the wing inboard of the fences, since the stalled areas on the wing in the high lift-coefficient range are prevented from spreading to the wing areas just outboard of each of the fences.

Figure 9 gives the results of a brief investigation of the effect of fence height. The effectiveness of the fences in promoting stability increased somewhat with size, but the fences having a height of $0.15t_{max}$ were almost as effective as those having a height of $0.60t_{max}$.

An appreciable improvement in the stability of the wing was also obtained with the leading-edge flaps (fig. 11). It can be seen that, as in the case of the flat wing, the leading-edge flaps of about half of the semispan provided the greatest reductions in the instability of the twisted and cambered wing. The tuft studies of figure 12 indicate

that the leading-edge flaps tended to reduce the cross flow at the forward part of the outboard sections and delay the separation to higher lift-coefficients.

When a combination of both leading-edge flaps and fences was used on the wing, the greatest stabilizing influence of the stall-control devices was obtained. From figures 13 and 14 it can be seen that the most favorable pitching-moment characteristics in the region of the maximum lift coefficient were obtained with a combination of 0.450b/2 leading-edge flaps and 0.575b/2 and 0.800b/2 chord fences on the wing. From figure 14 it can be seen that when the leading-edge flaps were on, the use of more than two fences on the wing reduced the instability in the lift-coefficient range below the maximum lift coefficient but caused larger unstable variations near the maximum lift coefficient.

Combinations of stall-control devices and trailing-edge flaps.- When the stall-control devices were off, the trailing-edge flaps increased the lift coefficient at which the large unstable pitching-moment change occurred (fig. 15). The greatest increase occurred with the longest-span trailing-edge flaps.

With the trailing-edge flaps on, the addition of fences to the wing reduced the instability to approximately the same degree as with the flaps off, as indicated by a comparison of figures 16 and 17 with figures 6 and 7. From a comparison of figures 16, 17, and 18, it can be seen that, with the trailing-edge flaps on, the unstable pitching-moment break occurred at a higher lift-coefficient with leading-edge flaps than with fences, but the instability prior to $C_{L_{max}}$ was greater with the leading-edge flaps.

As in the case with the trailing-edge flaps off, the greatest stabilizing influence of the stall-control devices when the trailing-edge flaps were on, was obtained with a combination of both the leading-edge flaps and fences. Figures 19 and 20 present the results obtained with various spans of both split and extended-split flaps at deflection angles of 23° and 52°, on the wing with 0.500b/2 leading-edge flaps and 0.575b/2 and 0.800b/2 chord fences. In general, the effects of trailing-edge split-flaps on the stability were similar to those noted for the flat wing (reference 1) and a lower-aspect-ratio wing (reference 7). It can be seen from figures 19 and 20 that the shortest-span trailing-edge flaps tested $\left(0.350\frac{b}{2}\right)$ improved the stability slightly, but with longer spans of trailing-edge flaps, the stability in the high-lift-coefficient range progressively decreased as the trailing-edge flap span was increased. With both types of trailing-edge flaps, smaller unstable variations in the pitching moment occurred at the lower flap deflection angle (23°). Except for the differences in the lift-coefficients at

which the unstable pitching-moment variations occurred, the differences in the stability characteristics for the two types of split flaps tested were, in general, small (fig. 21).

An indication of the effects on the stability of the number of fences used when both the leading- and trailing-edge flaps were on the wing can be seen from figure 22. The curves indicate that a single fence was less than half as effective as two fences in reducing the instability.

Both the split flaps and the extended-split flaps effected a positive trim change, as would be expected from the geometry of the wing. Through the range of span investigated, the trim change decreased as the trailing-edge-flap span was increased.

A direct comparison of the stability of the various combinations of devices tested can be seen from figure 23 in which the variation of dC_m/dC_L with lift coefficient is shown for the most favorable arrangement of the devices from the viewpoint of stability for each case.

Lift Characteristics

Wing alone.- A maximum lift coefficient of 1.30 was obtained for the plain cambered and twisted wing in the angle-of-attack range tested (fig. 4). The increase in the maximum lift coefficient over the value of 1.01 obtained for the flat wing was approximately equal to the amount that would be expected because of the addition of the camber (reference 5). A decrease in the lift-curve slope occurred at a wing lift coefficient of about 0.7 and corresponded with the unstable break in the pitching moment. In the region near the maximum lift coefficient the variation of the lift coefficient with angle of attack was small.

High-lift and stall-control devices.- A maximum lift coefficient of 1.47 was obtained with the combination of 0.450b/2 leading-edge flaps and 0.575b/2 and 0.800b/2 chord fences on the wing, which was the most favorable combination of stall-control devices from the viewpoint of stability with the trailing-edge flaps neutral (fig. 13).

As shown by figure 24, the split flaps were very poor high-lift devices regardless of their span or deflection angle. The extended-split flaps, however, increased the maximum lift coefficient appreciably. The maximum lift coefficient increased with an increase in the span of the extended split flaps for both deflection angles tested. The increments in the maximum lift coefficient obtained with the extended-split flaps were greater at the lower deflection angle. The optimum flap deflection angle for maximum lift is probably in the range between 23° and 52°. This conclusion is in agreement with the results obtained in reference 8,

where an optimum deflection angle of 40° was obtained for extended-split flaps.

The highest value of the maximum lift coefficient obtained in the tests was 1.78 with the combination of 0.600b/2 extended-split flaps deflected 23° and with leading-edge flaps and fences (fig. 20). A large unstable variation in the pitching moment occurred near the maximum lift coefficient for this combination, however. As previously noted, the most favorable pitching-moment characteristics were obtained with the shortest-span trailing-edge flaps in combination with the leading-edge flaps and fences. For this configuration (using extended-split flaps) a maximum lift coefficient of 1.61 was obtained with a forward movement of the aerodynamic center of about 17 percent of the mean aerodynamic chord in the high-lift range, as shown by figure 23. In the case of the flat wing, a maximum lift coefficient of 1.50 was obtained with an aerodynamic-center shift of about 6 percent mean aerodynamic chord for a combination of 0.500b/2 extended-split flaps and a similar arrangement of stall-control devices as that used on the cambered and twisted wing.

Drag Characteristics

The drag characteristics of the cambered and twisted wing are presented as variations of the lift-drag ratios with lift coefficient (figs. 25 and 26). The maximum value of the lift-drag ratio of the twisted and cambered wing was slightly less than that of the flat wing, but the L/D curve for the cambered and twisted wing had a much broader peak and considerably higher values of L/D in the lift-coefficient range above approximately 0.45.

From figure 26 it can be seen that, although fences reduced the maximum value of L/D of the cambered and twisted wing, they increased the lift-drag ratios in the high-lift range. With similar arrangements of trailing-edge flaps, leading-edge flaps and fences on the wings, the cambered and twisted wing exhibited greater values of L/D at lift coefficients above about 1.35 (fig. 26). The L/D values in the low lift-coefficient range may be smaller for the cambered and twisted wing because of the large negative angles of attack of the tip sections at low lift coefficients.

Fuselage Effects

The variations of the lift and pitching-moment characteristics of the cambered and twisted wing with and without a fuselage are presented in figure 27. From figure 28 which shows the variation with angle of attack of the increment in pitching moment between the wing alone and

wing-fuselage combination $\left(\Delta C_{m_f}\right)$, it can be seen that a sharp increase in ΔC_{m_f} occurred at approximately 26° angle of attack. It can also be seen from the curves of ΔC_{m_f} for the various flap configurations that the angle of attack at which the increase occurred was dependent to some degree on the wing flap configuration. Inasmuch as ΔC_{m_f} represents the summation of all the mutual interference effects between the wing and fuselage in addition to the basic fuselage pitching-moment characteristics, the causes of the sharp increase in ΔC_{m_f} cannot be isolated from the data available. Because the fuselage caused the pitching moment to break unstable at the maximum lift coefficient as shown in figure 27, it seems that a more detailed investigation of the fuselage effects in the high-angle-of-attack range would be desirable.

From a comparison of the curves of figure 27 the effects on the stability of a change in the wing incidence angle from 0° to 4° relative to the fuselage center line appeared mainly as a trim shift.

Both the maximum lift coefficient and the lift-curve slope were slightly higher with the fuselage on, for both values of the wing-fuselage incidence tested. At zero angle of attack, the fuselage caused a slight decrement in the lift coefficient (fig. 27). The decrement in lift was greater for a wing incidence angle of 4° than 0° because of the greater negative attitude of the fuselage.

Reynolds Number Effects

In the Reynolds number range investigated $\left(1.5 \times 10^6 \text{ to } 4.8 \times 10^6\right)$, the maximum lift coefficient obtained on the plain wing in the angle-of-attack range tested increased from 1.22 at a Reynolds number of 1.5×10^6 to 1.30 at a Reynolds number of 4.8×10^6. An examination of the lift curves of figure 29 indicated, however, that the maximum lift coefficient may not have been reached in the angle-of-attack range tested. The pitching-moment curves of figure 29 indicate that the stable moment break in the region of the maximum lift coefficient was more pronounced at the higher Reynolds numbers.

With a combination of four fences on the wing (fig. 30) the maximum lift coefficient increased from approximately 1.30 to about 1.39 as the Reynolds number was increased from 1.5×10^6 to 4.0×10^6. Figure 30 also indicates that the angle of attack and the lift coefficient at which the unstable pitching-moment break occurred increased as the Reynolds number was increased.

With a combination of split flaps, leading-edge flaps and fences (fig. 31) an increase in the maximum lift coefficient of about 0.12 resulted for an increase in the Reynolds number from 1.5×10^6 to 4.0×10^6. The point at which the maximum lift coefficient occurred also became more definite as the Reynolds number was increased. The pitching-moment curves of figure 31 indicate that the instability in the lift-coefficient range just below the maximum lift coefficient decreased as the Reynolds number was increased.

The Reynolds number effects on the lift-drag ratios were not distinct in the region of $(L/D)_{max}$ but in the higher lift-coefficient range, where increasing the Reynolds number would tend to delay separation, the lift-drag ratios increased slightly with increasing Reynolds numbers (fig. 32).

Effects of Wing Roughness

The effects of roughness (of the type described in reference 5) on the lift and pitching-moment characteristics of the cambered and twisted wing are presented in figure 33. At a Reynolds number of 4.0×10^6, the roughness decreased the maximum lift coefficient about 0.13. A decrease in the lift-curve slope in the low lift-coefficient range began at an angle of attack of about 3°. The pressure-distribution data indicated that, with roughness on, the lift-curve slopes of the outboard wing sections were lower and that the curves began rounding off at a lower angle of attack. The effects of the wing roughness on the lift characteristics of the outboard wing sections are also reflected in the pitching-moment curves of figure 33, which indicate that both the large unstable break and the initial decrease in stability began at much lower lift coefficients.

At a Reynolds number of 1.5×10^6, the decrease in maximum lift due to the roughness was not as great as at the higher Reynolds number, but the effects of roughness on the pitching-moment characteristcs in the low lift-coefficient range were almost as large as at the higher Reynolds number.

CONCLUSIONS

The following concluding remarks are based on the investigation in the Langley 19-foot pressure tunnel of a 45° sweptback wing of aspect ratio 8.0, which incorporated twist and camber:

1. The plain twisted and cambered wing exhibited almost linear stable pitching-moment characteristics up to a lift coefficient of about 0.7 at which point a severe unstable break occurred.

2. Both upper-surface wing fences and leading-edge flaps reduced the instability between lift coefficients of 0.7 and the maximum lift coefficient but in no case was the instability completely eliminated. The greatest stabilizing effect was obtained from the use of both leading-edge flaps and fences in combination.

3. In general, the stability decreased with increasing trailing-edge flap span, but with leading-edge flaps and fences on the wing, a slight improvement in the stability resulted from the use of 0.350-semispan extended-split flaps deflected 23°. The stability was generally more favorable with the flap deflected 23° than deflected 52°.

4. The cambered and twisted wing had a maximum lift coefficient of 1.30 as compared with 1.01 for a similar wing of no camber or twist. A maximum lift coefficient of 1.61 was obtained with 0.350-semispan extended-split flaps in combination with leading-edge flaps and fences, for which case the least forward shift in aerodynamic center (about 17 percent mean aerodynamic chord) was obtained. In the case of the untwisted and uncambered wing, a maximum lift coefficient of 1.50 was obtained with 0.500-semispan extended-split flaps and a similar arrangement of stall-control devices as used on the untwisted and cambered wing. The aerodynamic-center shift in the latter case was about 6 percent mean aerodynamic chord.

5. In general, camber and twist increased the lift-drag ratios at high lift coefficients.

6. A large increase in the destabilizing influence of the fuselage occurred at high angles of attack. The addition of the fuselage caused an unstable pitching-moment break at the maximum lift coefficient for fuselage-off configurations that originally exhibited stable pitching-moment breaks at the maximum lift.

7. Reynolds number effects on the aerodynamic characteristics in the range investigated were, in general, small.

8. Roughness on the leading edge of the plain wing caused a considerable decrease in the lift coefficient at which the pitching moment became unstable and decreased the maximum lift coefficient about 0.2.

Langley Aeronautical Laboratory
National Advisory Committee for Aeronautics
Langley Field, Va.

REFERENCES

1. Pratt, George L. and Shields, E. Rousseau: Low-Speed Longitudinal Characteristics of a 45° Sweptback Wing of Aspect Ratio 8 with High-Lift and Stall-Control Devices at Reynolds Numbers from 1,500,000 to 4,800,000. NACA RM L51J04, 1951.

2. Graham, Robert R.: Low-Speed Characteristics of a 45° Sweptback Wing of Aspect Ratio 8 from Pressure Distributions and Force Tests at Reynolds Numbers from 1,500,000 to 4,800,000. NACA RM L51H13, 1951.

3. Salmi, Reino J., and Jacques, William A.: Effect of Vertical Location of a Horizontal Tail on the Static Longitudinal Stability Characteristics of a 45° Sweptback-Wing - Fuselage Combination of Aspect Ratio 8 at a Reynolds Number of 4.0×10^6. NACA RM L51J08, 1951.

4. Cohen, Doris: A Method for Determining the Camber and Twist of a Surface to Support a Given Distribution of Lift, with Applications to the Load over a Sweptback Wing. NACA Rep. 826, 1945. (Supersedes NACA TN 855.)

5. Abbott, Ira H., Von Doenhoff, Albert E., and Stivers, Louis S., Jr.: Summary of Airfoil Data. NACA Rep. 824, 1945. (Supersedes NACA ACR L5C05.)

6. Sivells, James C., and Salmi, Rachel M.: Jet-Boundary Corrections for Complete and Semispan Swept Wings in Closed Circular Wind Tunnels. NACA TN 2454, 1951.

7. Salmi, Reino J.: Effects of Leading-Edge Devices and Trailing-Edge Flaps on Longitudinal Characteristics of Two 47.7° Sweptback Wings of Aspect Ratios 5.1 and 6.0 at a Reynolds Number of 6.0×10^6. NACA RM L50F20, 1950.

8. Spooner, Stanley H., and Mollenberg, Ernst F.: Low-Speed Investigation of Several Types of Split Flap on a 47.7° Sweptback-Wing - Fuselage Combination of Aspect Ratio 5.1 at a Reynolds Number of 6.0×10^6. NACA RM L51D20, 1951.

TABLE I.- WING CAMBER-LINE ORDINATES FOR A DESIGN SECTION LIFT COEFFICIENT OF 1.0.

[All values are given in percent of chord]

x/c	z/c*	x/c	z/c*
0	0	40	5.310
.5	.262	45	5.407
.75	.369	50	5.428
1.25	.566	55	5.372
2.5	.991	60	5.240
5.0	1.689	65	5.028
7.5	2.256	70	4.733
10	2.731	75	4.350
15	3.496	80	3.861
20	4.070	85	3.257
25	4.525	90	2.490
30	4.874	95	1.522
35	5.132	100	0

NACA

$$^{*}\left(\frac{z}{c}\right)_{c_{l_i}=1} = \frac{1}{1.05}\left[\left(\frac{z}{c}\right)_{a=1} + \frac{1}{6}\left(\frac{z}{c}\right)_{230}\right]$$

$\left(\frac{z}{c}\right)_{a=1}$ ordinates for a mean line of the type $a = 1$; $c_{l_i} = 1$ (reference 5).

$\left(\frac{z}{c}\right)_{230}$ ordinates for an NACA 230 series mean line; $c_{l_i} = 0.3$ (reference 5).

TABLE II.- SUMMARY OF LONGITUDINAL STABILITY CHARACTERISTICS OF THE TWISTED AND CAMBERED WING OF 45° SWEEPBACK AND ASPECT RATIO 8.0

Span of L.E. Device (b/2)	Span of T.E. Device (b/2)	Fence Location (b/2)	Configuration	$C_{L_{max}}$	$\alpha_{C_{L_{max}}}$	L/D at 0.8 $C_{L_{max}}$	C_m Characteristics	Figure
None	None	None	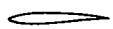	1.30	27.0°	7.5	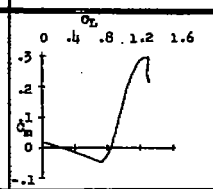	4
		.35	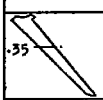 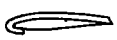	1.35	28.2°		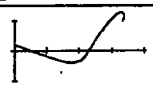	5
		.575	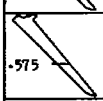 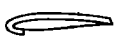	1.38	26.8°		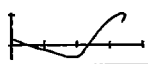	5
		.80	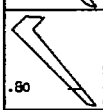 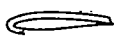	1.36	29.0°		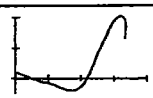	5
		.35 .575	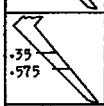 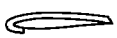	1.37	27.6°		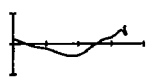	6
		.575 .80	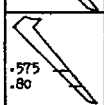 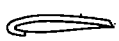	1.40	27.1°	8.2	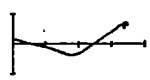	6
		.35 .575 .80	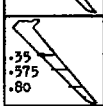 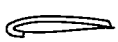	1.38	27.5°		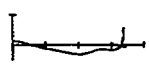	7
		.575 .80 .89	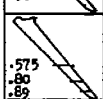 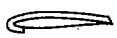	1.38	27.0°		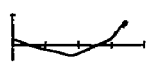	7
		.35 .575 .80 .89	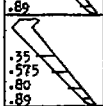 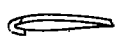	1.37	27.8°		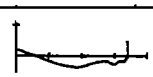	8
		.575 .80 .89	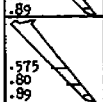 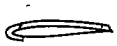	1.39	27.0[b]		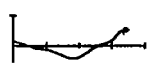	7
		.575 .70 .80	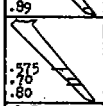 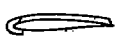	1.40	28.0°		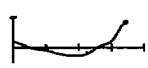	7
		.575 .70 .80 .89	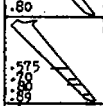 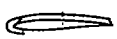	1.40	26.8°		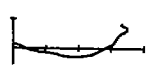	8
		.575 .80	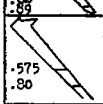 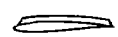	1.42	27.0°		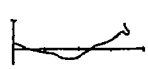	6
		.45 .70 .89	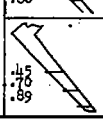 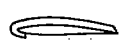	1.40	26.2°		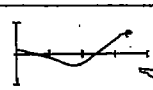	7

3P

TABLE II.- SUMMARY OF LONGITUDINAL STABILITY CHARACTERISTICS OF THE TWISTED AND CAMBERED WING OF 45° SWEEPBACK AND ASPECT RATIO 8.0 - Continued

Span of L.E. Device (b/2)	Span of T.E. Device (b/2)	Fence Location (b/2)	Configuration	$C_{L_{max}}$	$\alpha_{C_{L_{max}}}$	L/D at 0.85 $C_{L_{max}}$	C_m Characteristics	Figure
None	None	.35, .575, .80		1.39	26.5°			7
		.35, .575, .80, .89		1.39	26.5°			8
		.35, .575, .70, .80, .89		1.39	27.0°			8
	.35 Split Flaps	None	$\delta_f = 60°$	1.30	24.2°			15
		.575, .80	$\delta_f = 60°$	1.41	22.5°			16
	.50 Split Flaps	None	$\delta_f = 60°$	1.34	24.2°			15
		.575, .80	$\delta_f = 60°$	1.44	22.2°			16
		.35, .575, .80, .89	$\delta_f = 30°$	1.44	27.0°			17
	.60 Split Flaps	None	$\delta_f = 60°$	1.35	24.2°			15
		.575, .80	$\delta_f = 60°$	1.48	23.0°			16
	.50 Ext. Split Flaps	None	$\delta_f = 30°$	1.61*	31.2°			15

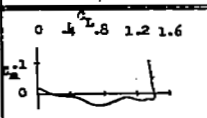

* Maximum lift coefficient probably limited by angle-of-attack range tested.

Flap deflection angles of 30° and 60° measured in plane normal to 0.80 chord line correspond to 23° and 52° measured in a plane parallel to the plane of symmetry.

TABLE II.- SUMMARY OF LONGITUDINAL STABILITY CHARACTERISTICS OF THE TWISTED AND CAMBERED WING OF 45° SWEEPBACK AND ASPECT RATIO 8.0 - Continued

Span of L.E. Device (b/2)	Span of T.E. Device (b/2)	Fence Location (b/2)	Configuration	$C_{L_{max}}$	$\alpha_{C_{L_{max}}}$	L/D at 0.85 $\alpha_{C_{L_{max}}}$	C_m Characteristics	Figure
None	.50 Ext. Split Flaps	.575 .80	$\delta_f = 30°$	1.61*	31.2°			17
		.575 .80	$\delta_f = 30°$	1.64*	31.2°			17
		.35 .575 .80	$\delta_f = 30°$	1.58	25.4°			17
		.35 .575 .80 .89	$\delta_f = 30°$	1.59	25.4°			17
.45 L.E. Flaps	None	None		1.44	27.0°	9.4		11
	.50 Split Flaps	None	$\delta_f = 60°$	1.45	21.0°			18
		.575 .80	$\delta_f = 30°$	1.49	31.2°	11.0		21
	.50 Ext. Split Flaps	None	$\delta_f = 60°$	1.61	20.2°			18
		.575 .80	$\delta_f = 30°$	1.68	24.4°	10.3		21
	None	.575 .80		1.47	26.5°	9.0		19
.50 L.E. Flaps	None	None		1.44*	31.2°			11
	.35 Split Flaps	None	$\delta_f = 60°$	1.42	21.2°			18

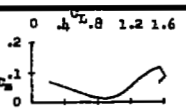

* Maximum lift coefficient probably limited by angle-of-attack range tested.

Flap deflection angles of 30° and 60° measured in plane normal to 0.80 chord line correspond to 23° and 52° measured in a plane parallel to the plane of symmetry.

TABLE II.- SUMMARY OF LONGITUDINAL STABILITY CHARACTERISTICS OF THE TWISTED AND CAMBERED WING OF 45° SWEEPBACK AND ASPECT RATIO 8.0 - Continued

Span of L.E. Device (b/2)	Span of T.E. Device (b/2)	Fence Location (b/2)	Configuration	$C_{L_{max}}$	$\alpha_{C_{L_{max}}}$	L/D at 0.85 $C_{L_{max}}$	C_m Characteristics	Figure
.50 L.E. Flaps	.50 Split Flaps	None	$\delta_f = 60°$	1.49	21.2°		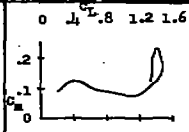	18
	.60 Split Flaps	None	$\delta_f = 60°$	1.49	20.0°		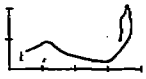	18
	.35 Split Flaps	.80	$\delta_f = 60°$	1.44	20.4°		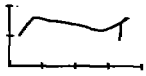	22
		.575 .80	$\delta_f = 60°$	1.46	21.2°	10.5	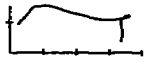	22
	.50 Split Flaps	.575 .80	$\delta_f = 60°$	1.51	21.0°		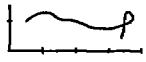	19
	.60 Split Flaps	.575 .80	$\delta_f = 60°$	1.55	21.2°		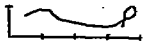	19
	.35 Split Flaps	.575 .80	$\delta_f = 30°$	1.47	24.2°	11.5	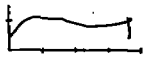	19
	.50 Split Flaps	.575 .80	$\delta_f = 30°$	1.49	22.4°		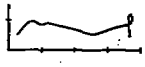	19
	.60 Split Flaps	.575 .80	$\delta_f = 30°$	1.54	25.0°		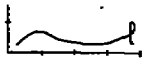	19
	.35 Ext. Split Flaps	.575 .80	$\delta_f = 60°$	1.57	20.4°		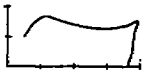	20
	.50 Ext. Split Flaps	.575 .80	$\delta_f = 60°$	1.66	20.4°		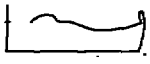	20
	.60 Ext. Split Flaps	.575 .80	$\delta_f = 60°$	1.72	30.0°		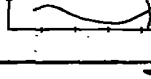	20

Flap deflection angles of 30° and 60° measured in plane normal to 0.80 chord line correspond to 23° and 52° measured in a plane parallel to the plane of symmetry.

TABLE II.- SUMMARY OF LONGITUDINAL STABILITY CHARACTERISTICS OF THE TWISTED AND CAMBERED WING OF 45° SWEEPBACK AND ASPECT RATIO 8.0 - Continued

Span of L.E. Device (b/2)	Span of T.E. Device (b/2)	Fence Location (b/2)	Configuration	$C_{L_{max}}$	$\alpha_{C_{L_{max}}}$	L/D at 0.85 $C_{L_{max}}$	C_m Characteristics	Figure
.50 L.E. Flaps	.35 Ext. Split Flaps	.575 .80	$\delta_f = 30°$	1.61	28.0°	10.8	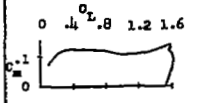	20
	.50 Ext. Split Flaps	.575 .80	$\delta_f = 30°$	1.74	28.0°		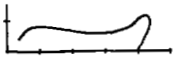	20
	.60 Ext. Split Flaps	.575 .80	$\delta_f = 30°$	1.78*	30.2°			20
	None	.575 .80		1.50	31.2°		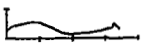	14
		.35 .575 .80		1.47	30.4°			14
		.35 .575 .80 .89		1.48	30.0°		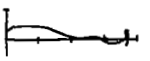	14
.575 L.E. Flaps	None	None		1.40	30.0°		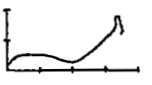	11
		.575 .80		1.51*	31.2°		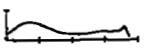	13
.32 L.E. Flaps	None	None	Inboard end of L.E. flap at .40b/2	1.39	30.0°	11.0		11
		.575 .80	Inboard end of L.E. flap at .40b/2	1.43	29.0°		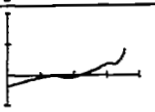	13
.195 L.E. Flaps	None	.575 .80	Inboard end of L.E. flap at .525b/2	1.43	26.5°		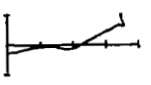	13

* Maximum lift coefficient probably limited by angle-of-attack range tested.

Flap deflection angles of 30° and 60° measured in plane normal to 0.80 chord line correspond to 23° and 52° measured in a plane parallel to the plane of symmetry.

TABLE II.- SUMMARY OF LONGITUDINAL STABILITY CHARACTERISTICS OF THE TWISTED AND CAMBERED WING OF 45° SWEEPBACK AND ASPECT RATIO 8.0 - Concluded

Span of L.E. Device (b/2)	Span of T.E. Device (b/2)	Fence Location (b/2)	Configuration	$C_{L_{max}}$	$\alpha_{C_{L_{max}}}$	L/D at 0.85 $C_{L_{max}}$	C_m Characteristics	Figure
None	None	.575 .80	Fence height = $0.15t_{max}$	1.39	26.2°		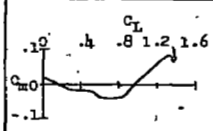	9
		.575 .80	Fence height = $0.15t_{max}$ $0.30t_{max}$	1.41	26.5°		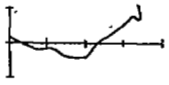	9
		None	$i_w = 0°$	1.31	27.2°	7.5		27
			$i_w = 4°$	1.32	27.2°		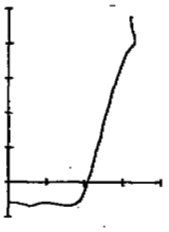	27
		.575 .80	$i_w = 0°$	1.43	28.2°	8.5	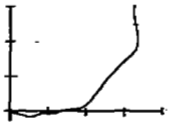	27
		.575 .80	$i_w = 4°$	1.45	27.4°			27
.45 L.E. Flaps	.50 Ext Split Flaps	.575 .80	$i_w = 4°$ $\delta_f = 30°$	1.68*	31.2°		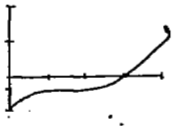	27

* Maximum lift coefficient probably limited by angle-of-attack range tested.

NACA

Flap deflection angles of 30° and 60° measured in plane normal to 0.80 chord line correspond to 23° and 52° measured in a plane parallel to the plane of symmetry.

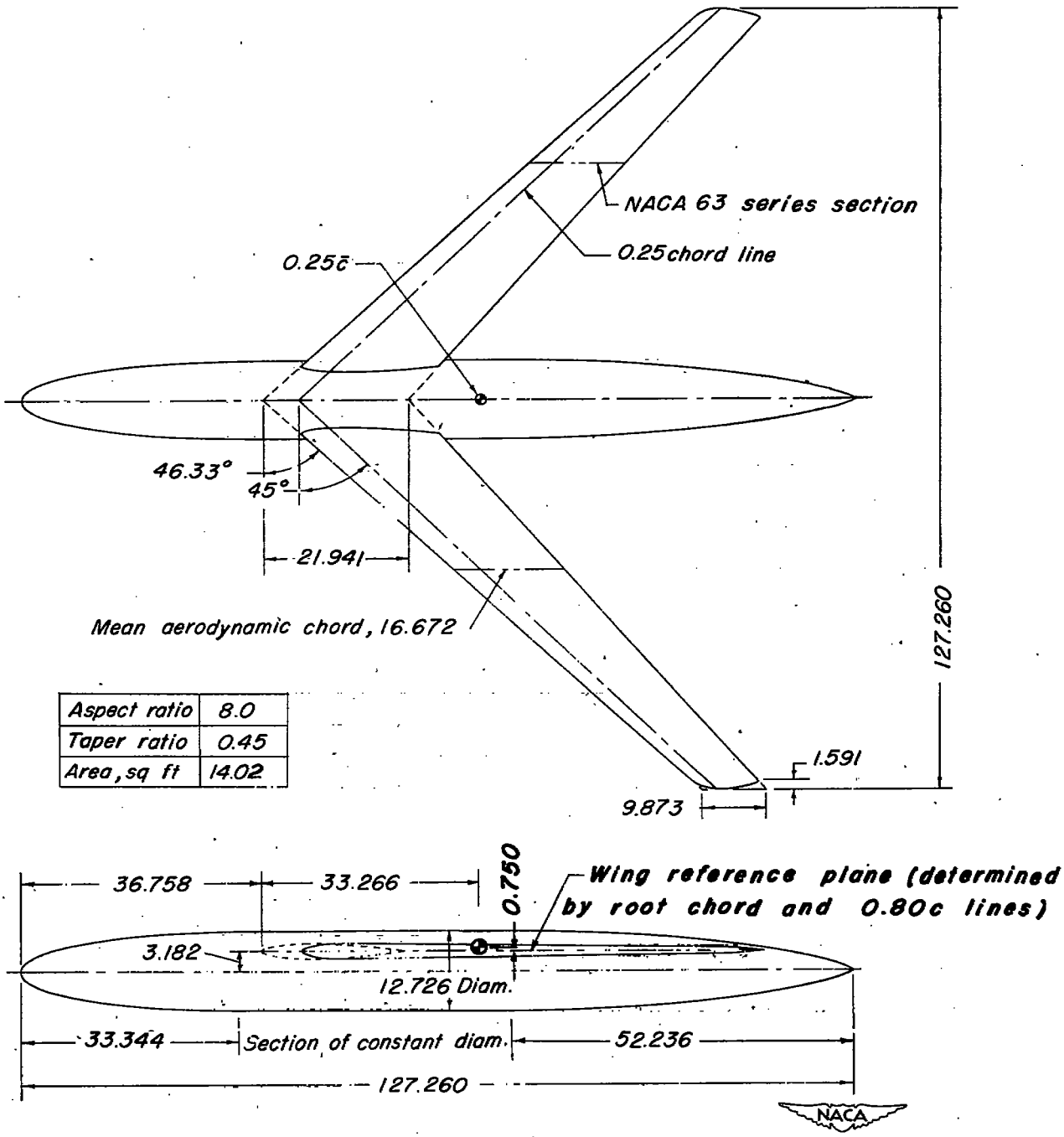

(a) Wing and fuselage.

Figure 1.- Geometric details of the twisted and cambered wing of 45° sweepback and aspect ratio 8.0 and the various devices tested. All dimensions in inches unless otherwise noted.

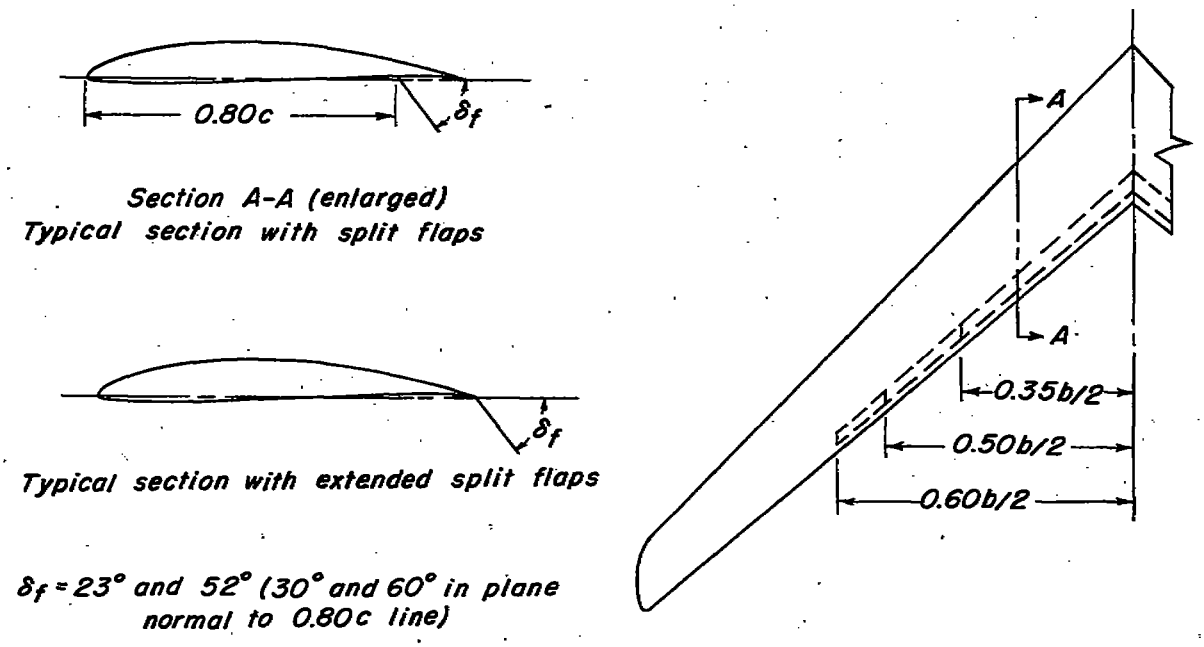

(b) Trailing-edge flaps.

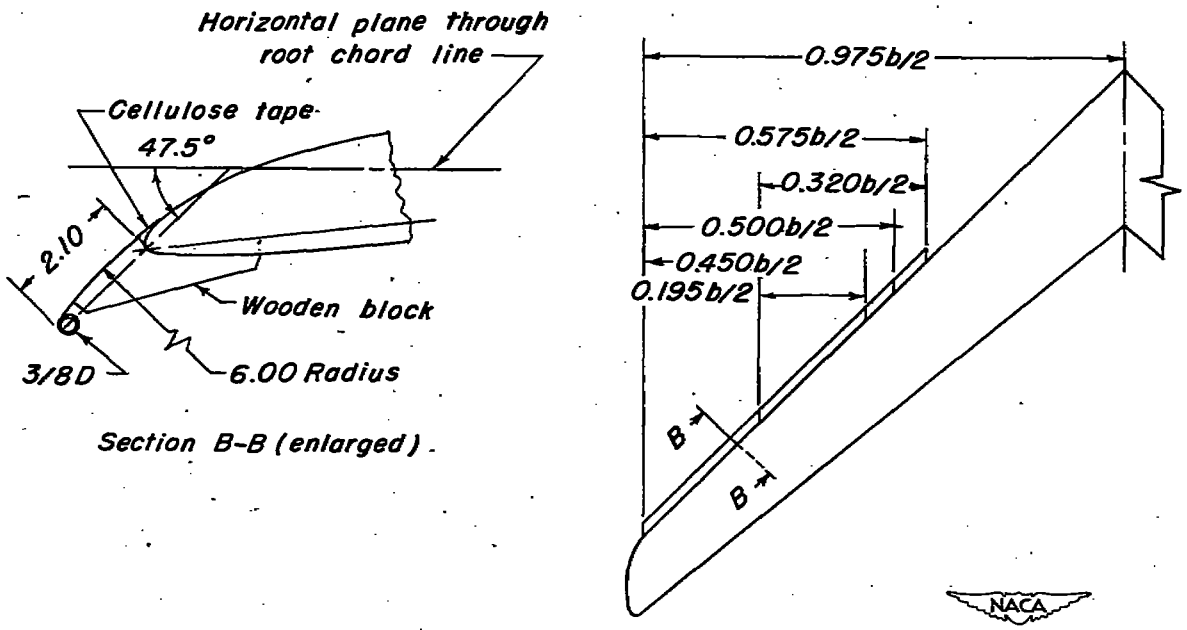

(c) Leading-edge flaps.

Figure 1.- Continued.

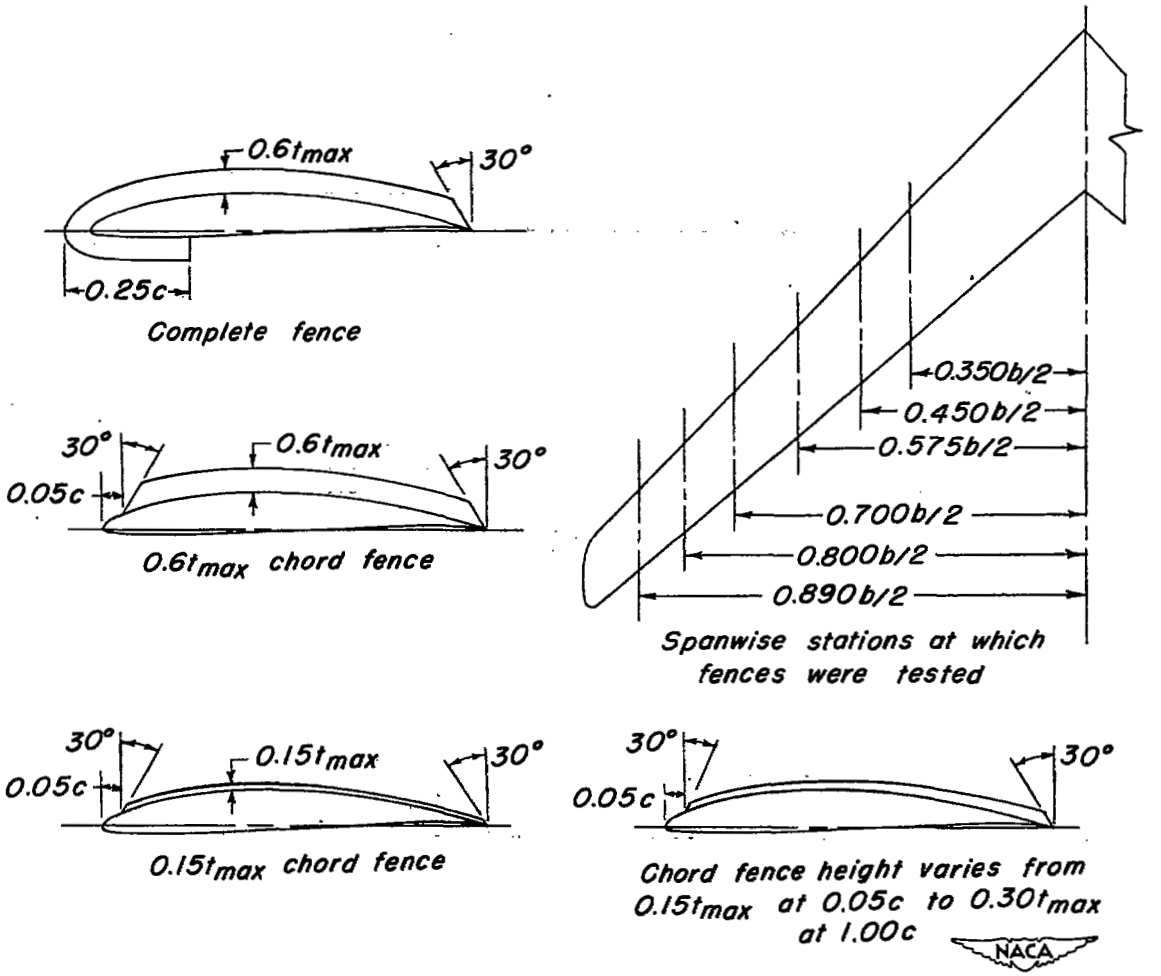

(d) Fences.

Figure 1.- Concluded.

4P

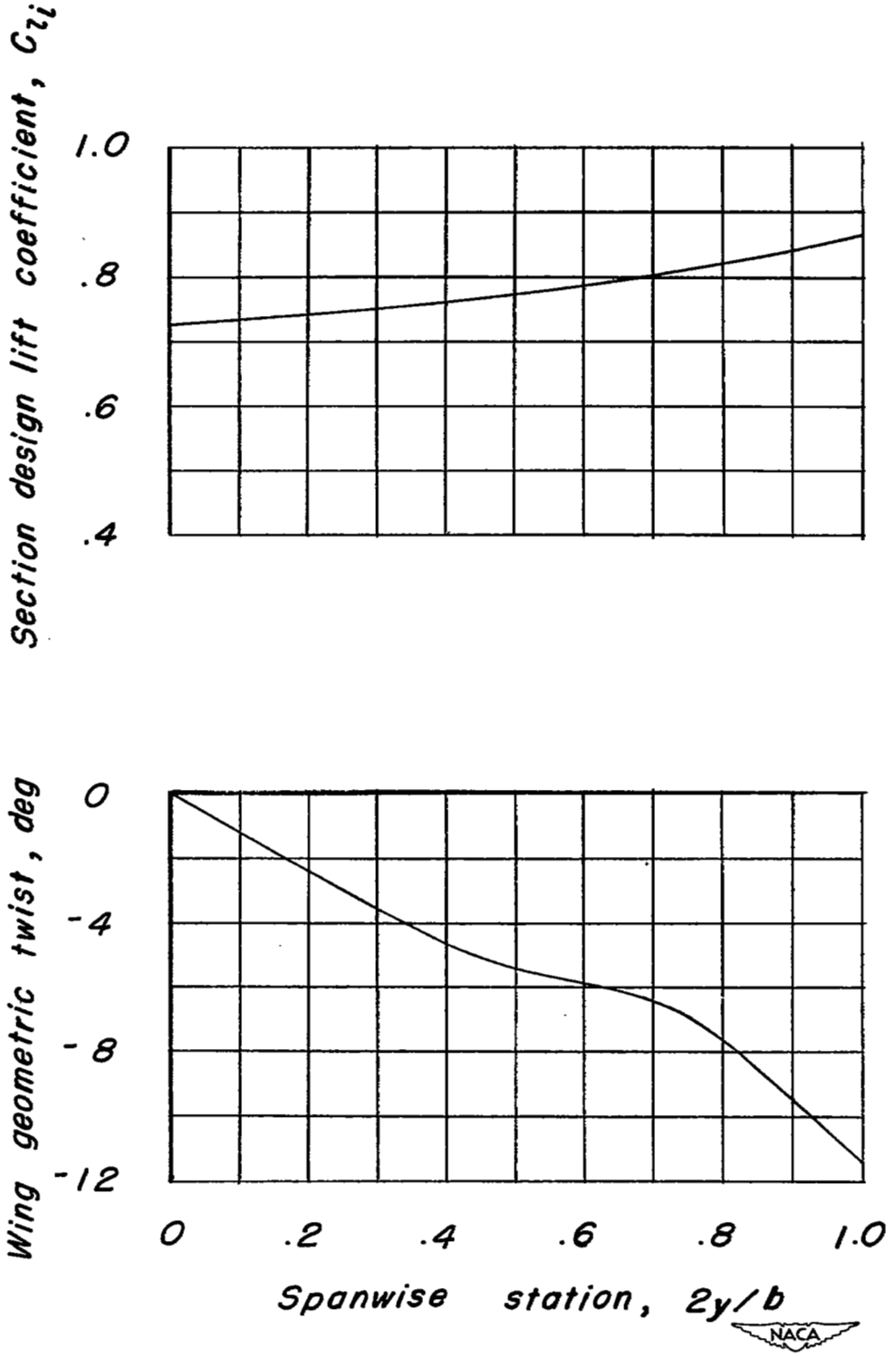

Figure 2.- Spanwise variation of wing geometric twist and design section lift coefficient.

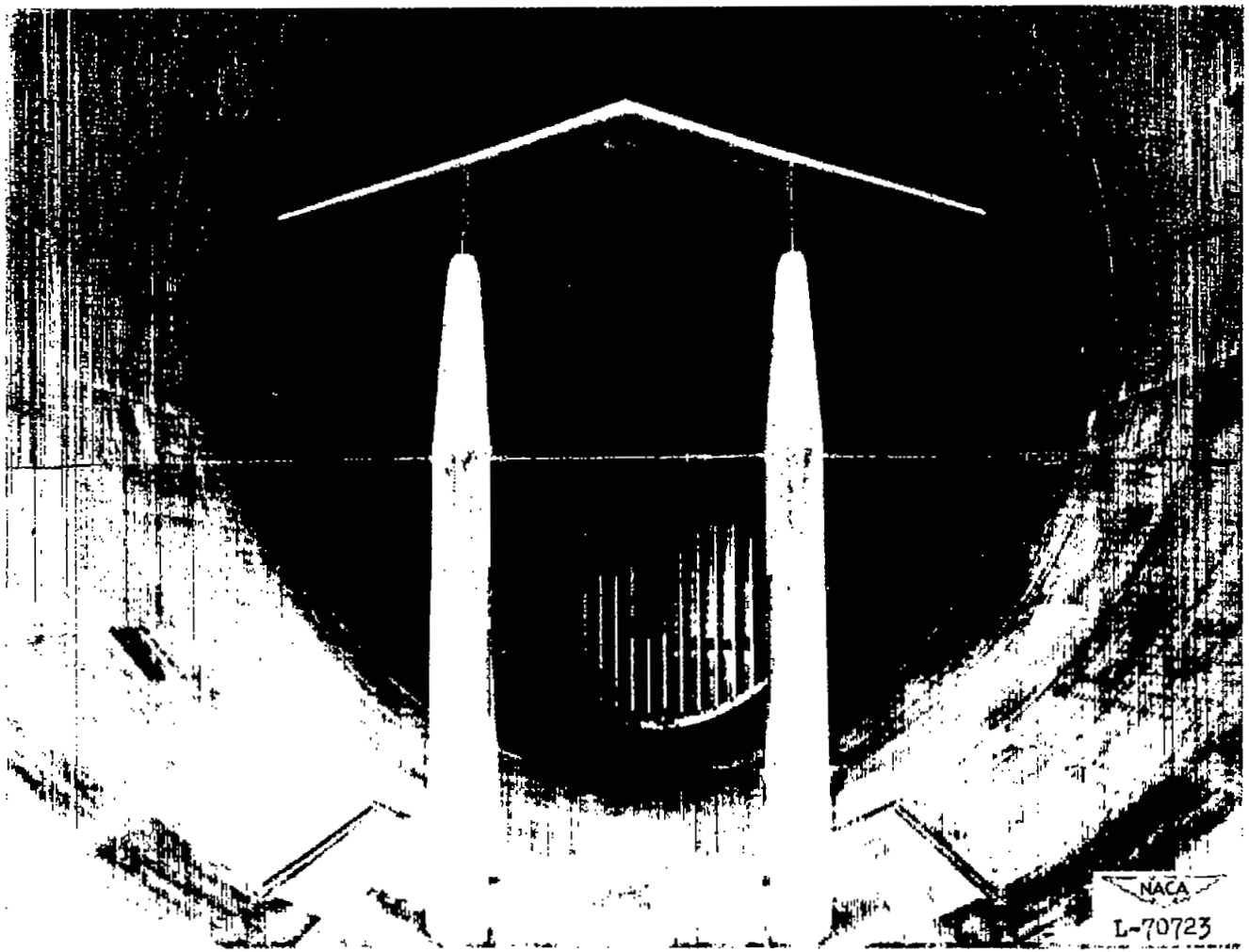

Figure 3.- The twisted and cambered wing of 45° sweepback and aspect ratio 8.0 mounted in the Langley 19-foot pressure tunnel.

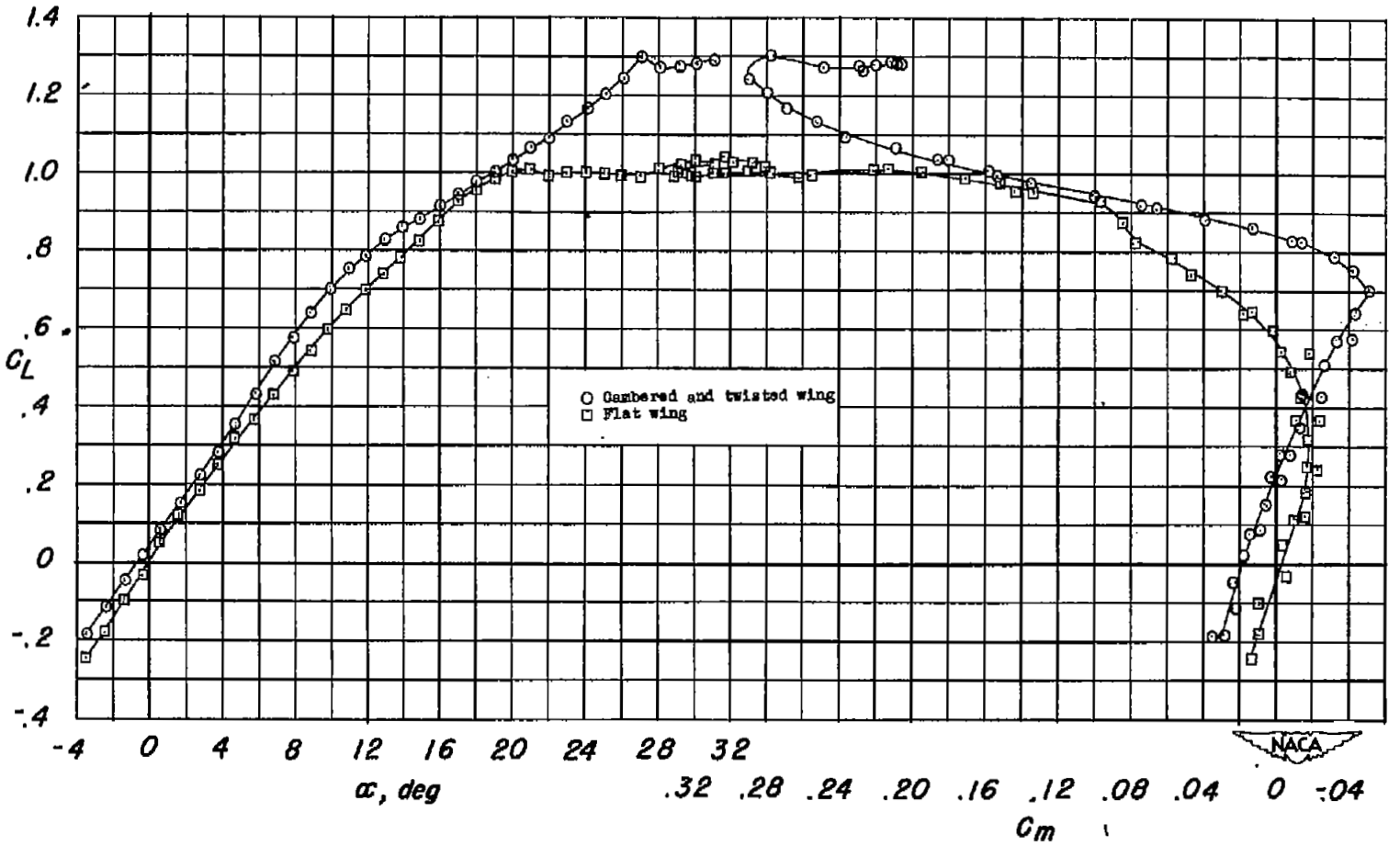

Figure 4.- Lift and pitching-moment characteristics of the cambered and twisted wing and the flat wing at a Reynolds number of 4.0×10^6.

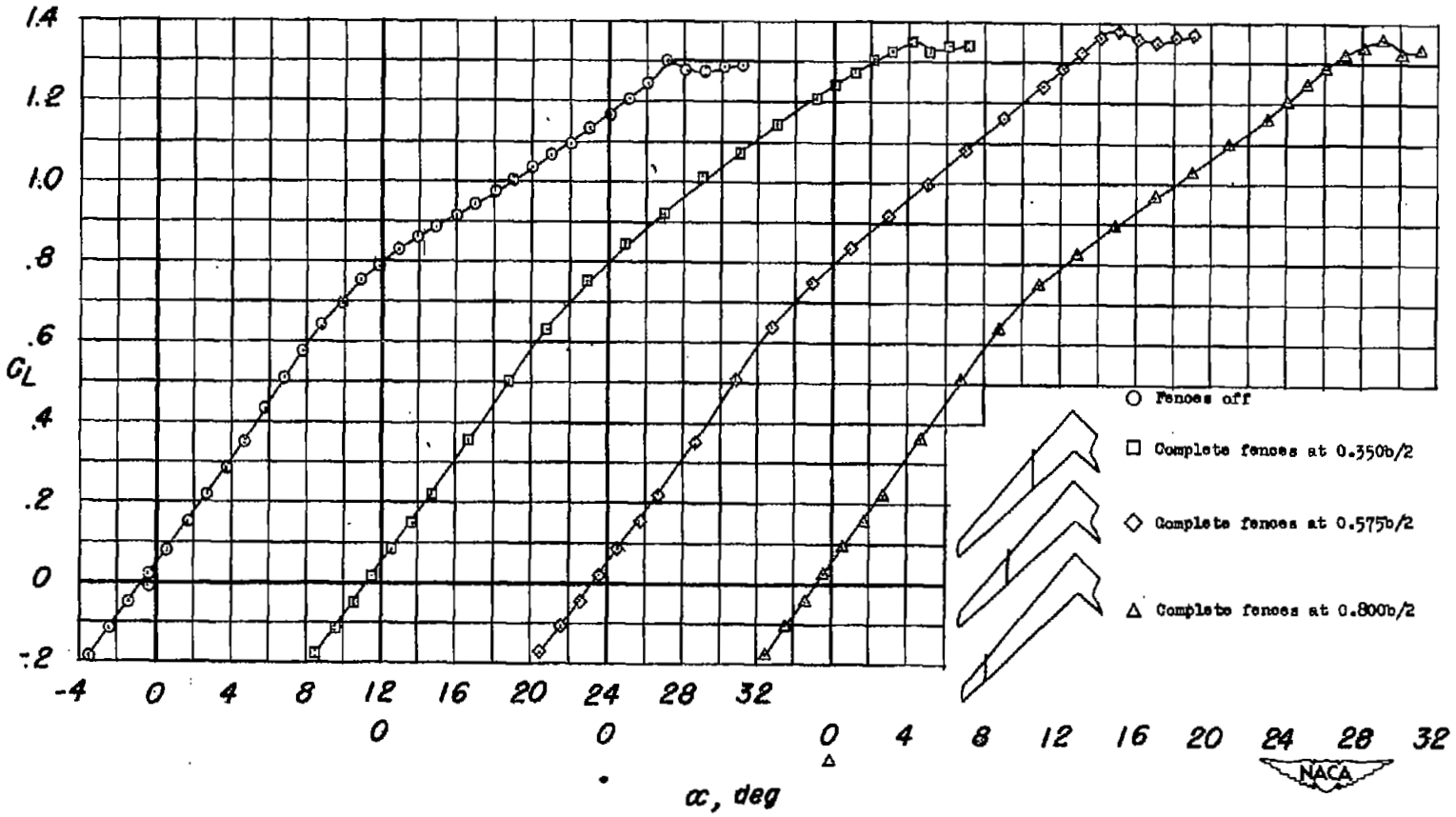

(a) C_L against α.

Figure 5.- Lift and pitching-moment characteristics of the wing with a single fence on each semispan at various spanwise locations.

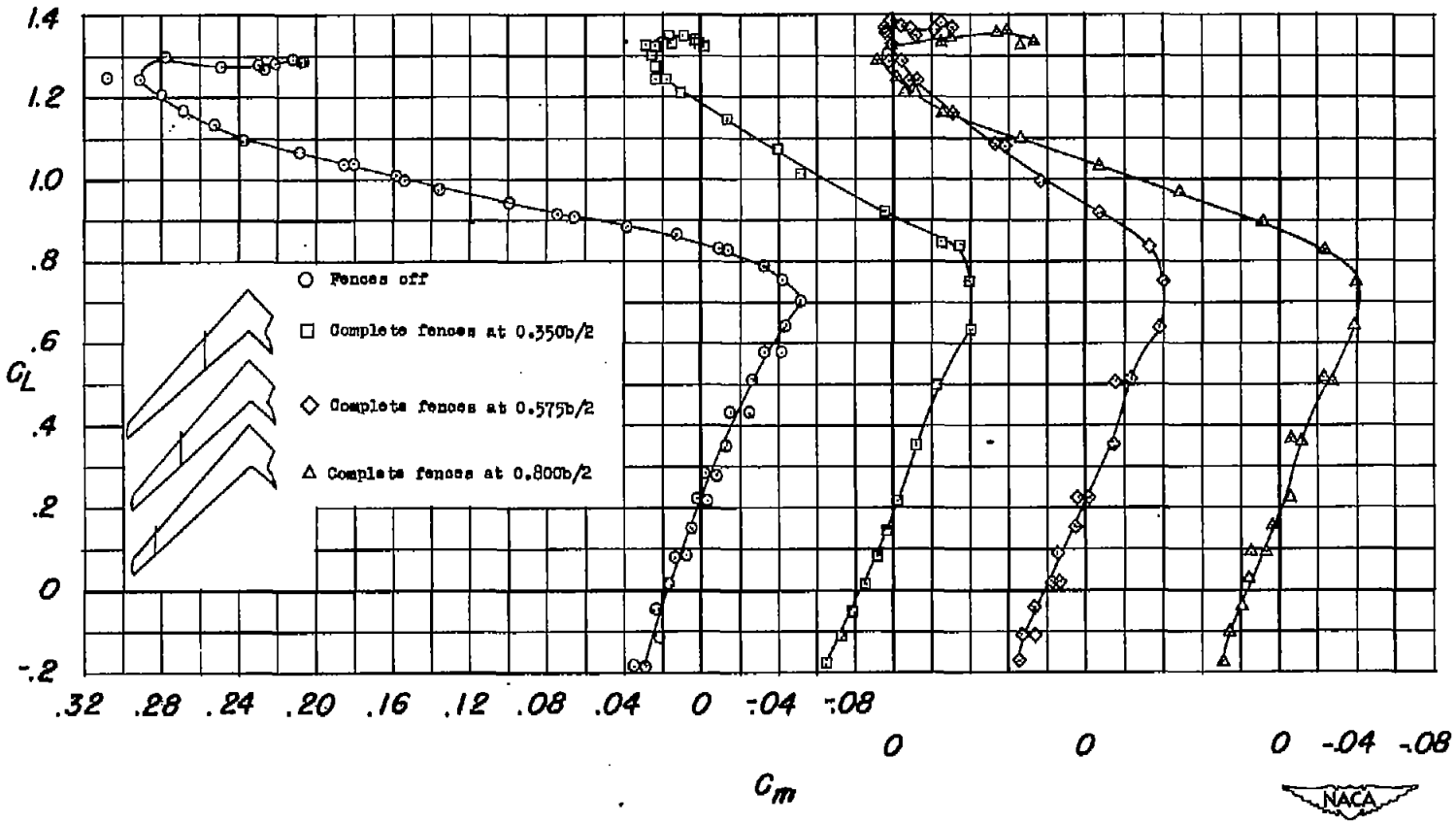

(b) C_L against C_m.

Figure 5.- Concluded.

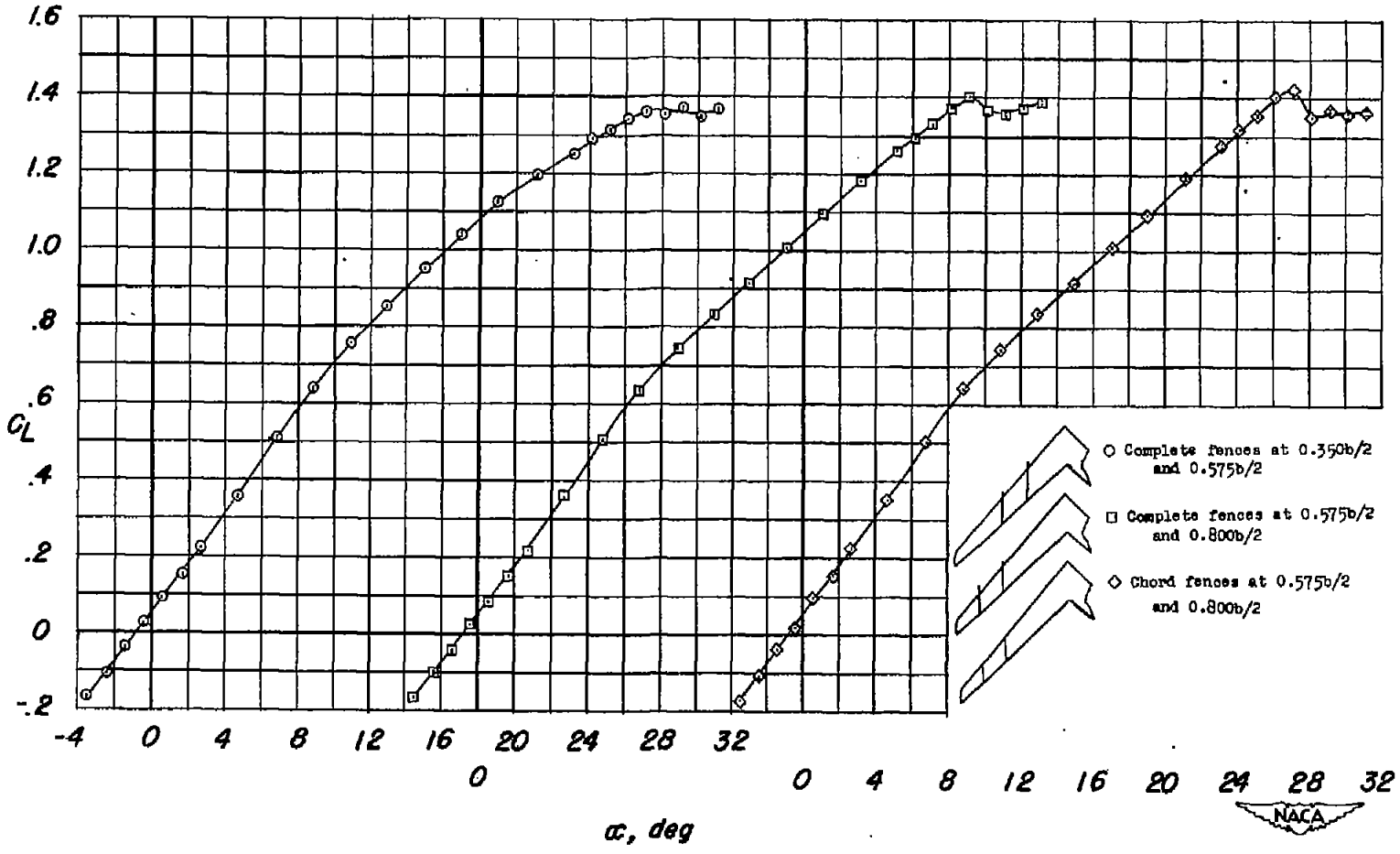

(a) C_L against α.

Figure 6.- Lift and pitching-moment characteristics of the wing with two fences on each semispan at various spanwise locations.

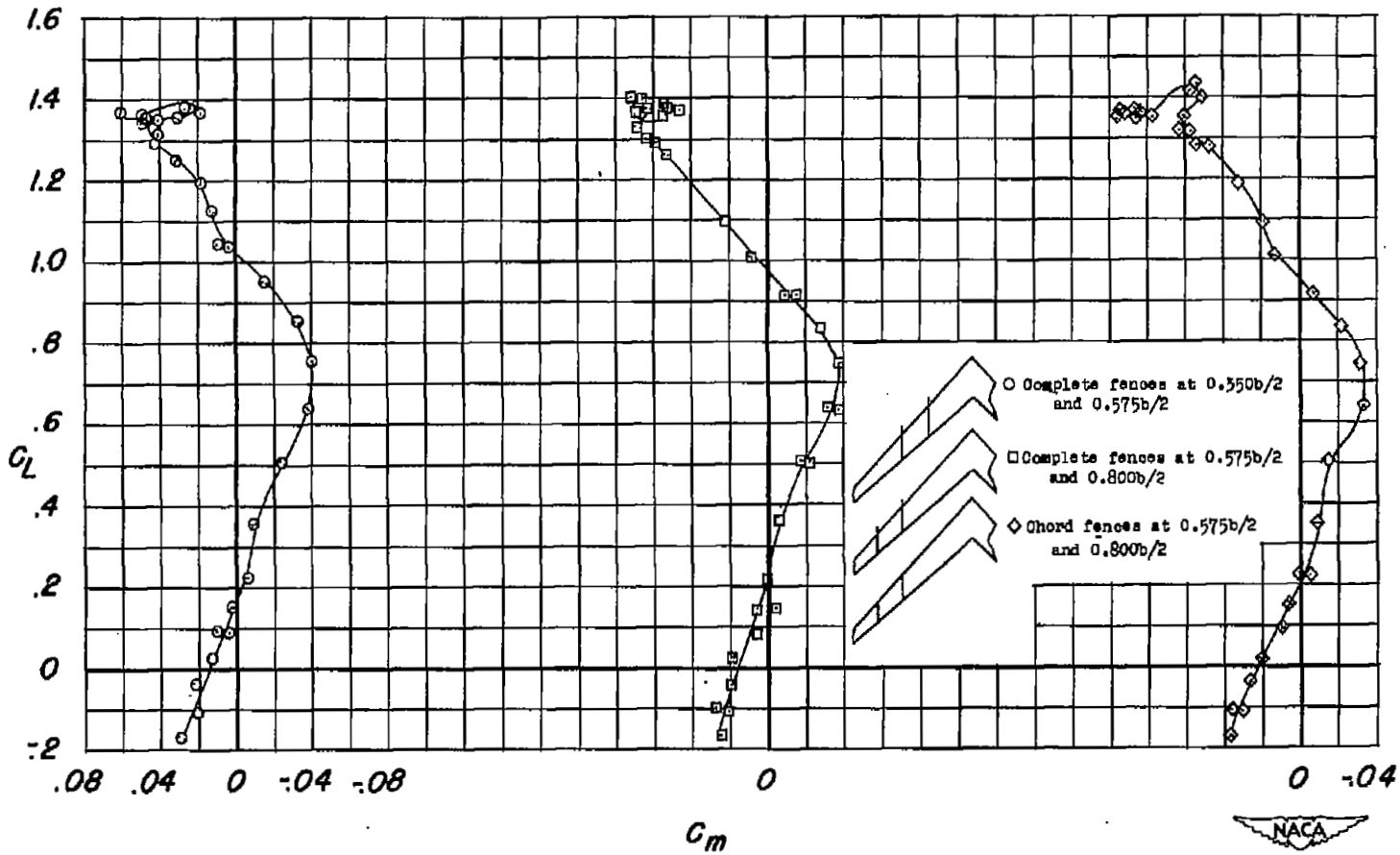

(b) C_L against C_m.

Figure 6.- Concluded.

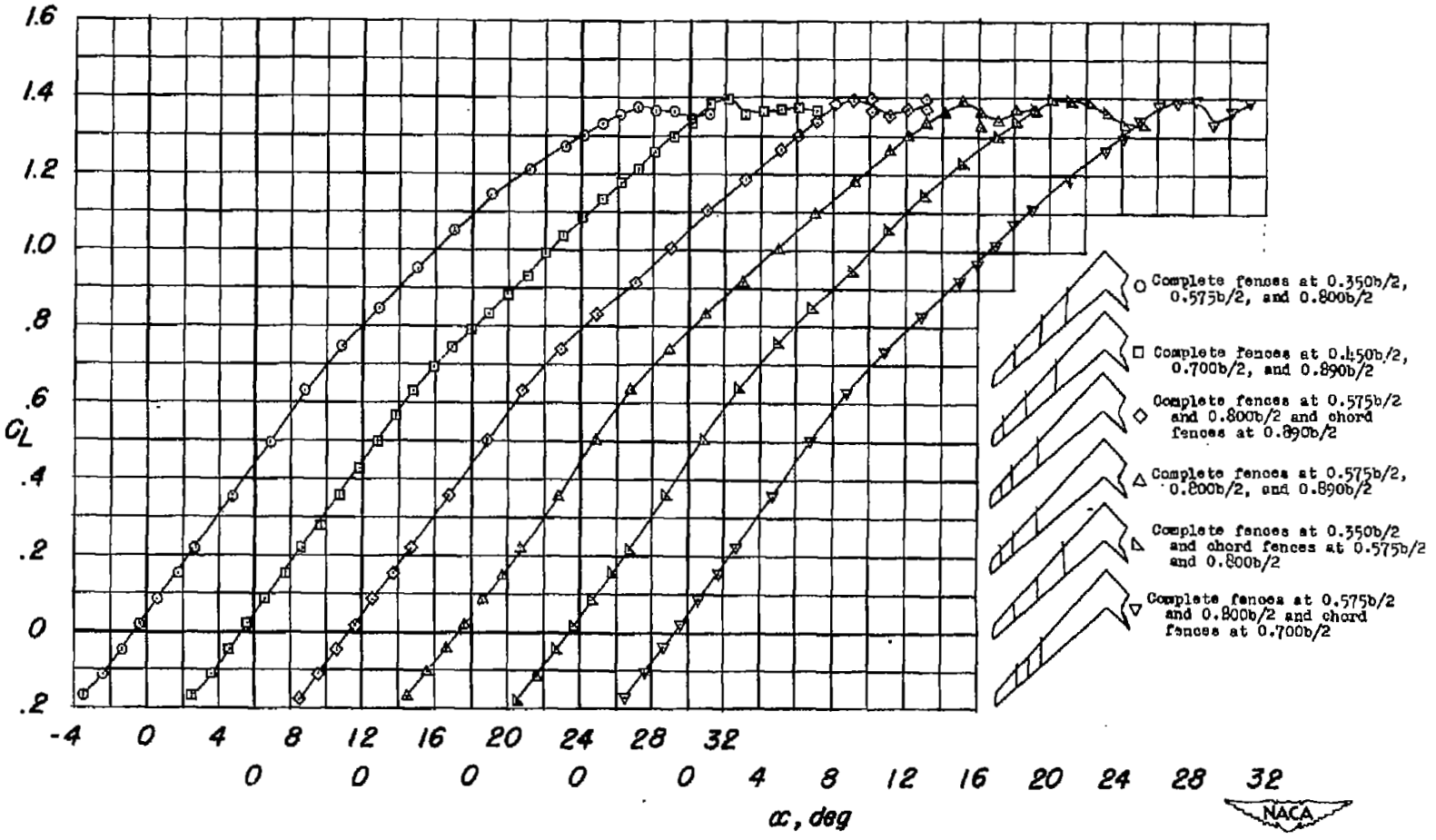

(a) C_L against α.

Figure 7.- Lift and pitching-moment characteristics of the wing with three fences on each semispan at various spanwise positions.

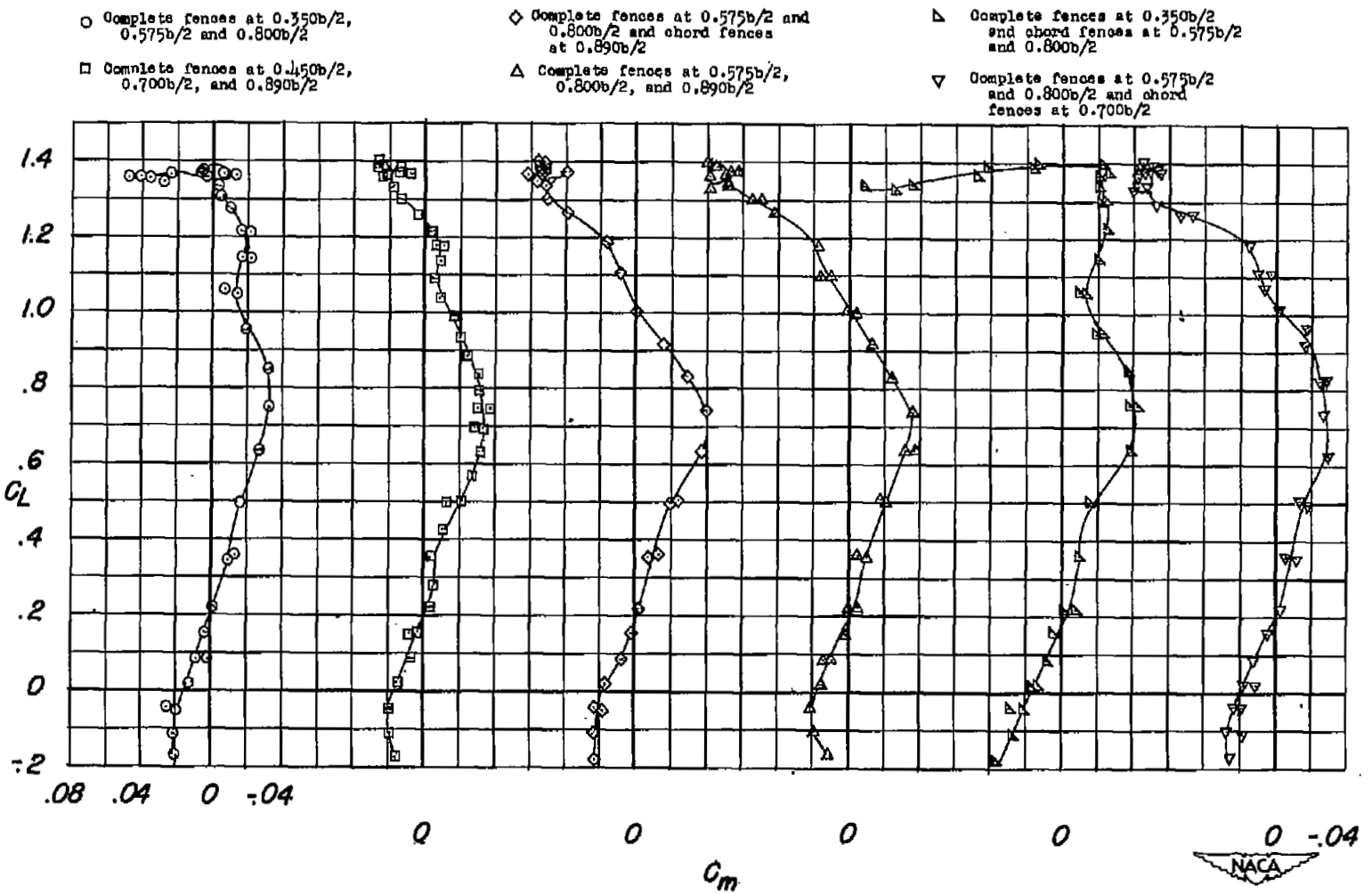

(b) C_L against C_m.

Figure 7.- Concluded.

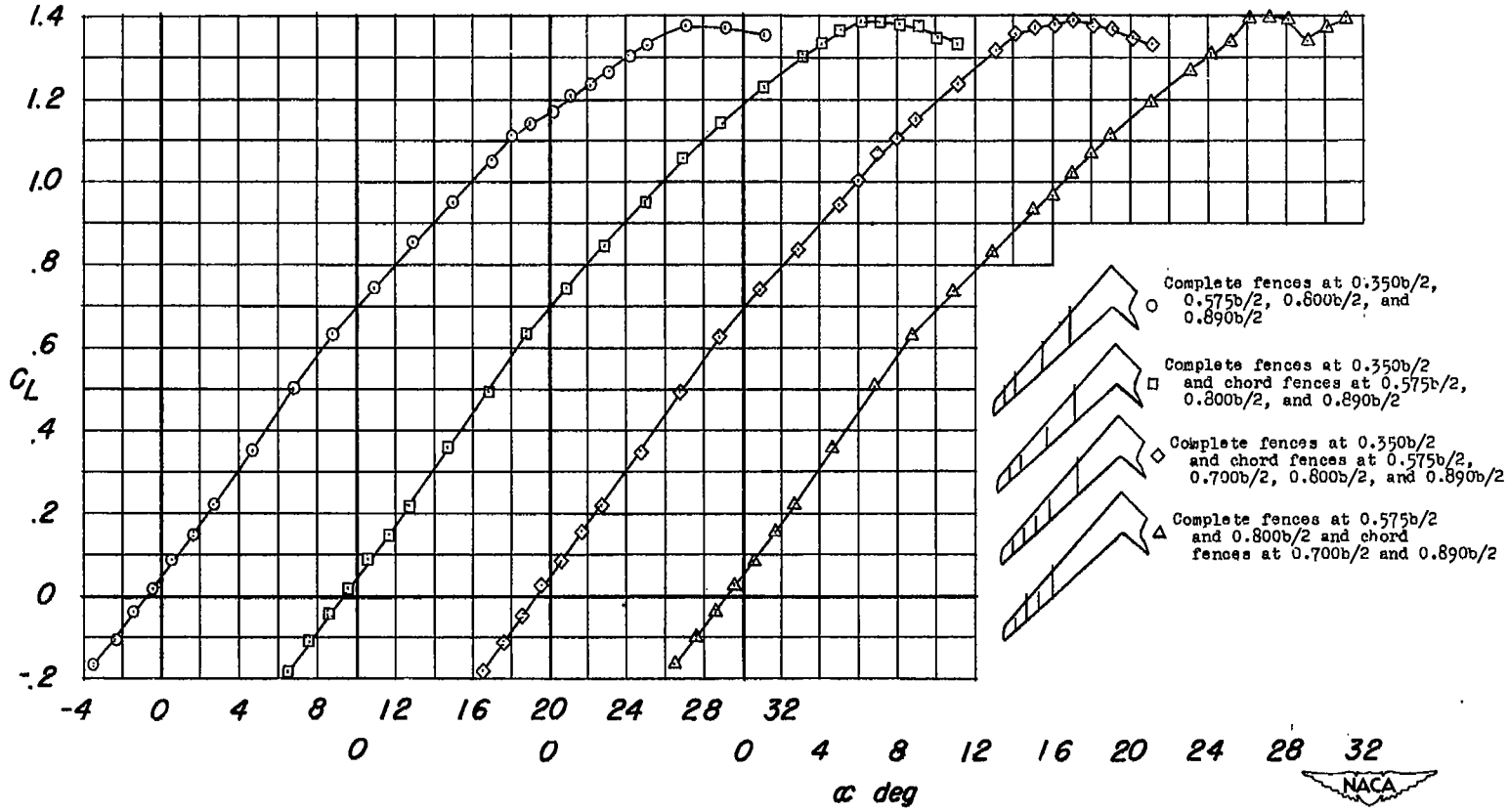

(a) C_L against α.

Figure 8.- Lift and pitching-moment characteristics of the wing with four or five fences on each semispan at various spanwise positions.

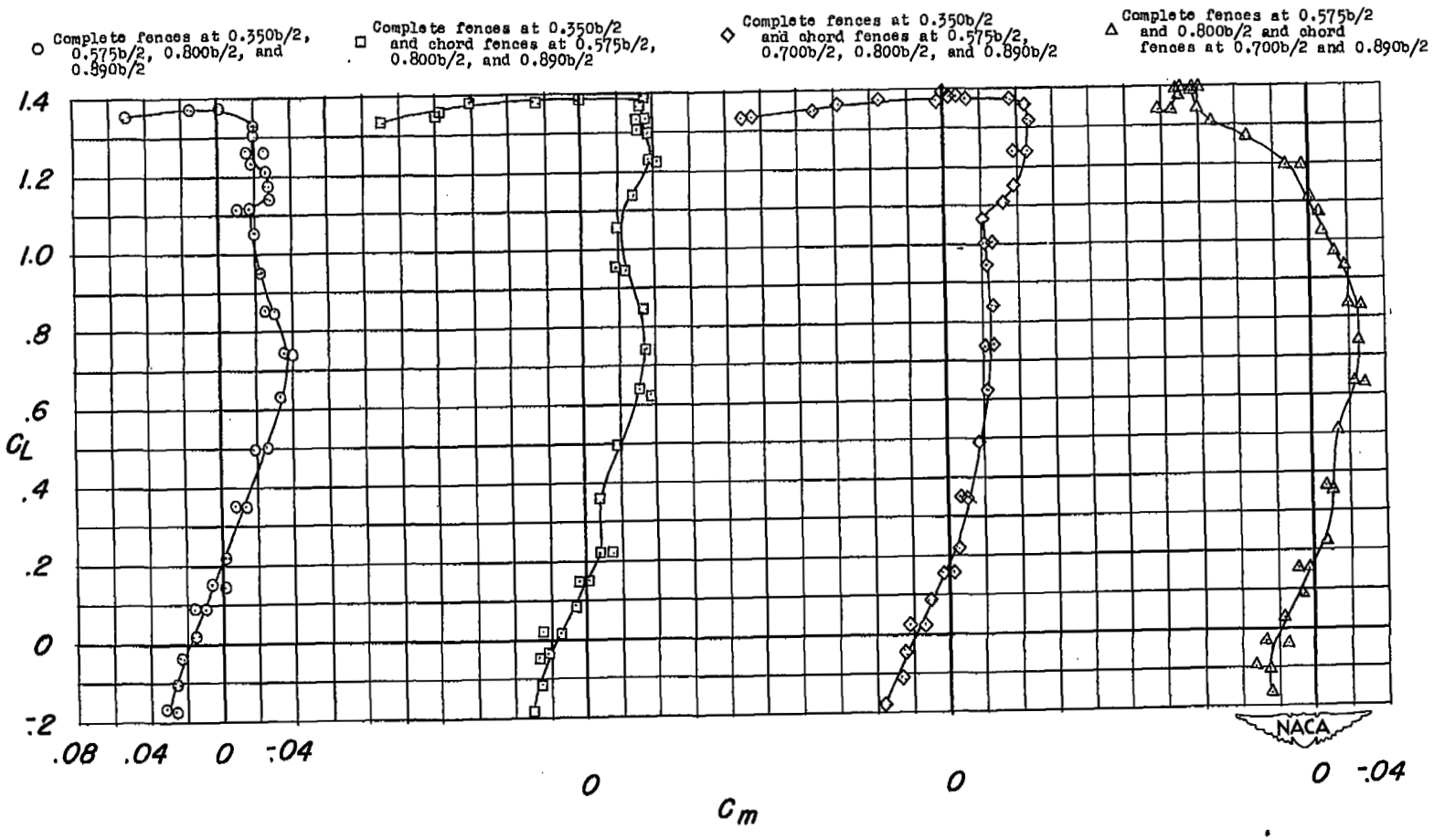

(b) C_L against C_m.

Figure 8.- Concluded.

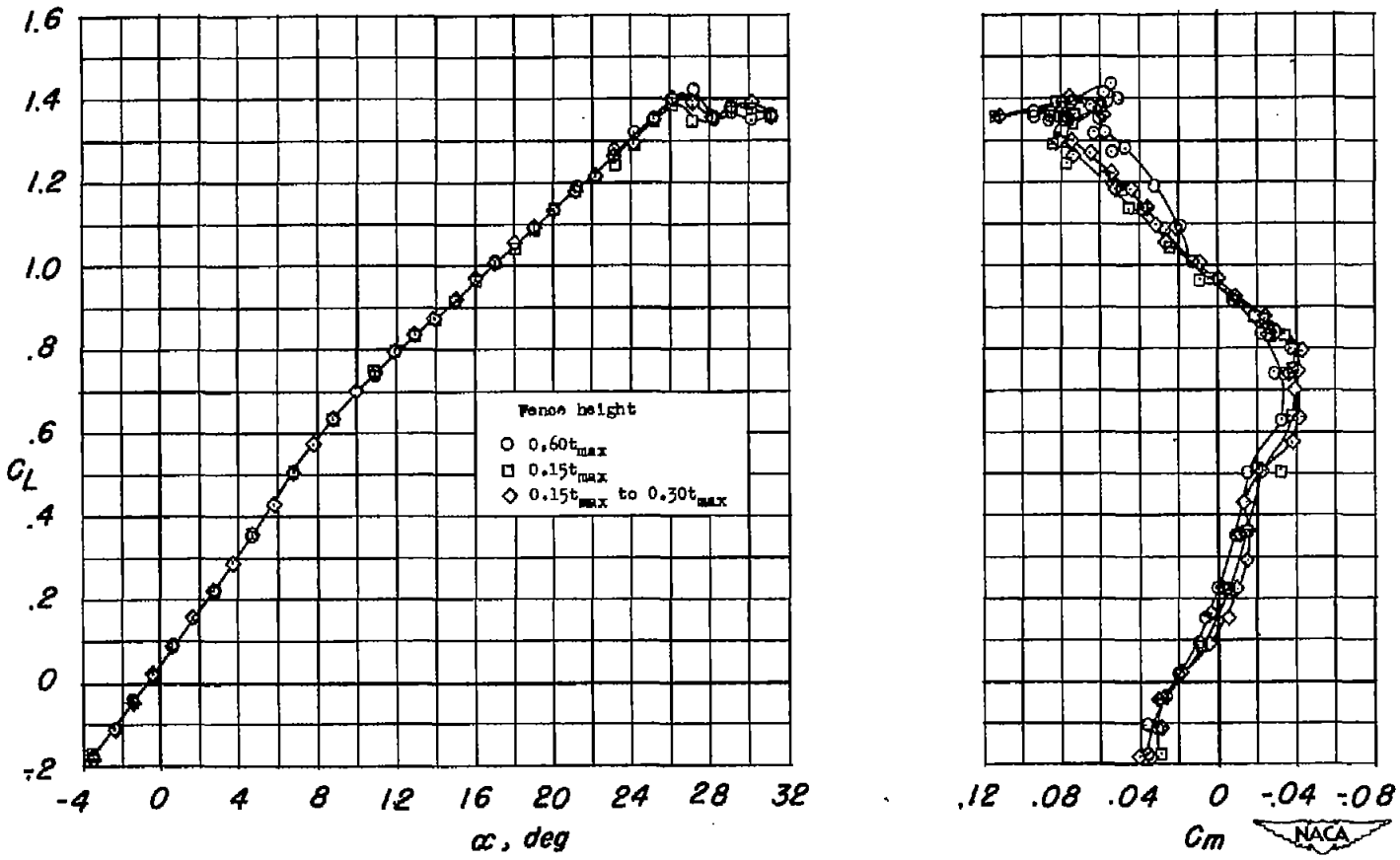

Figure 9.- Effect of fence height on the lift and pitching-moment characteristics of the wing with chord fences at 0.575b/2 and 0.800b/2.

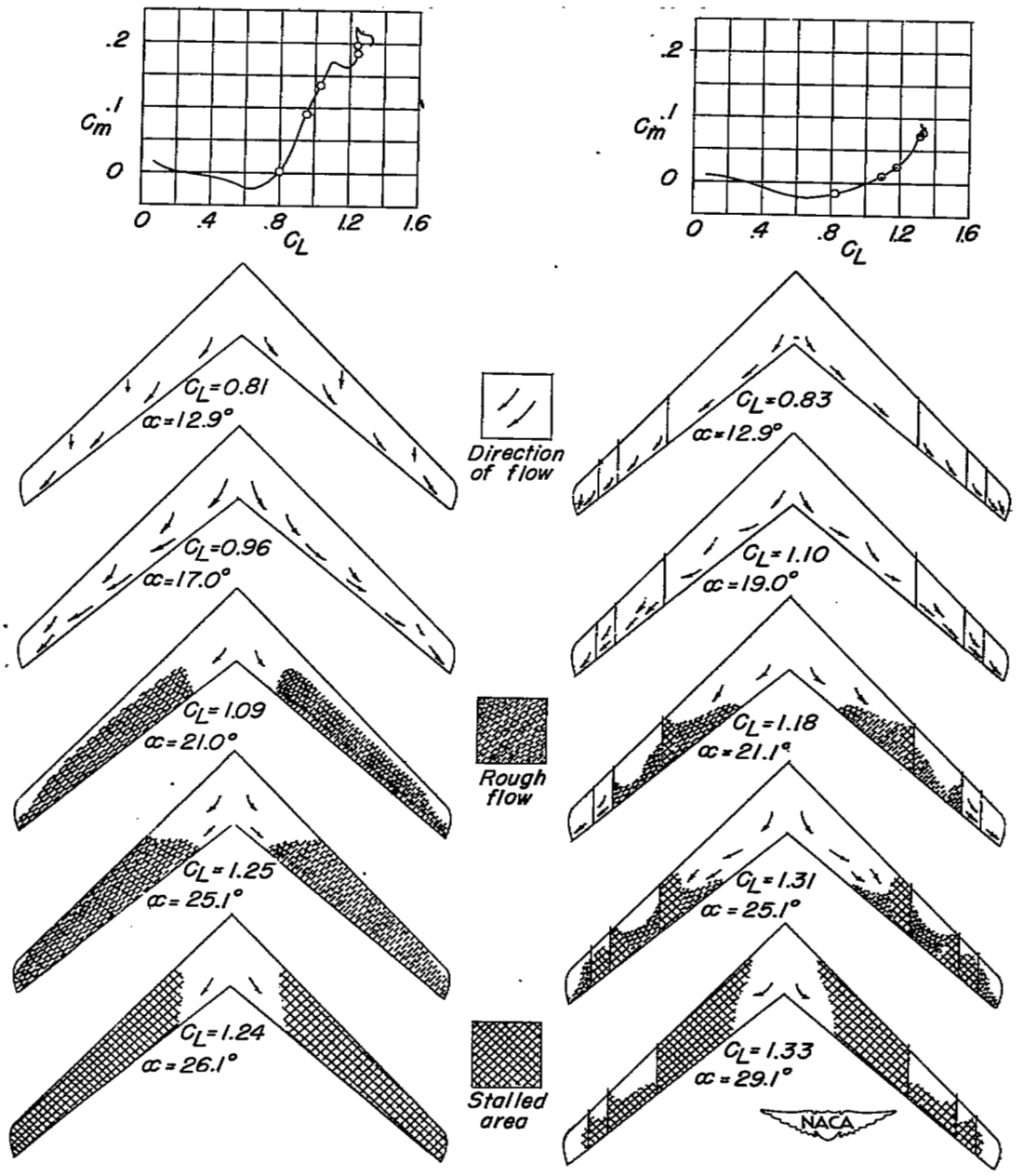

(a) Plain wing.

(b) 0.575, 0.80, and 0.89b/2 complete fences.

Figure 10.- Airflow characteristics near the wing surface as obtained by observations of wool tufts. Plain wing and wing with complete fences at 0.575b/2, 0.800b/2, and 0.890b/2.

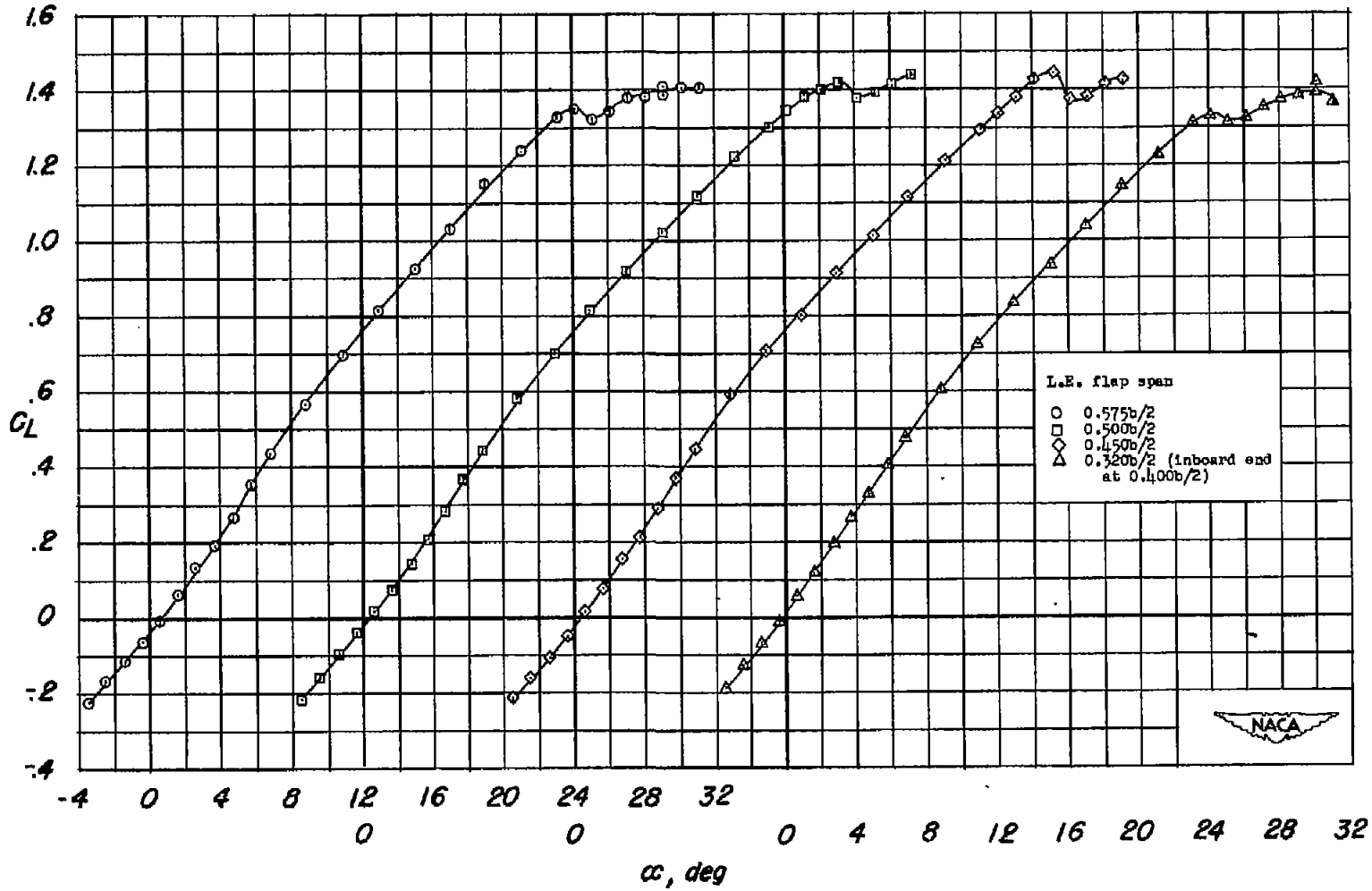

(a) C_L and α.

Figure 11.- Lift and pitching-moment characteristics of the wing with various spans of leading-edge flaps.

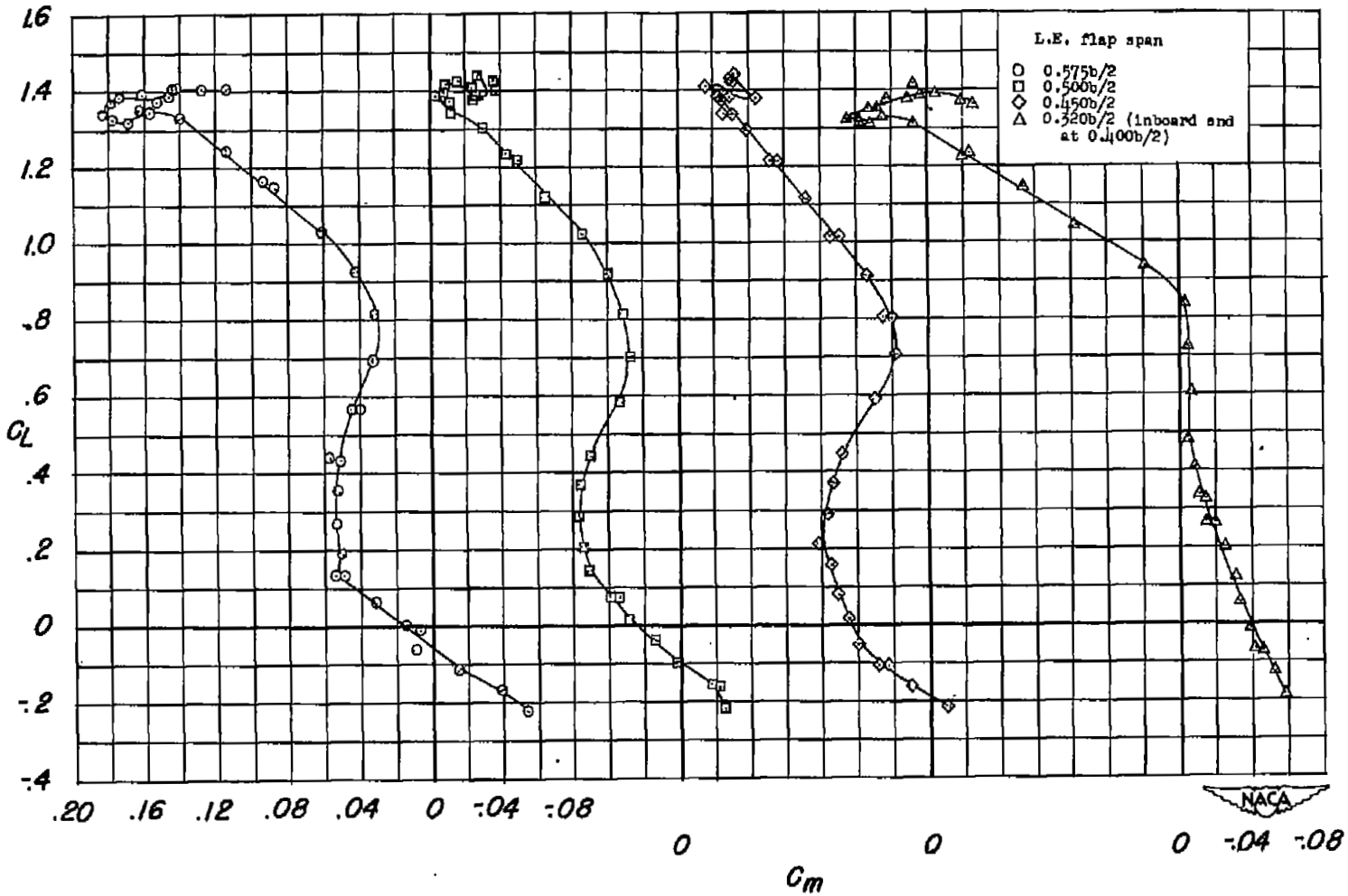

(b) C_L against C_m.

Figure 11.- Concluded.

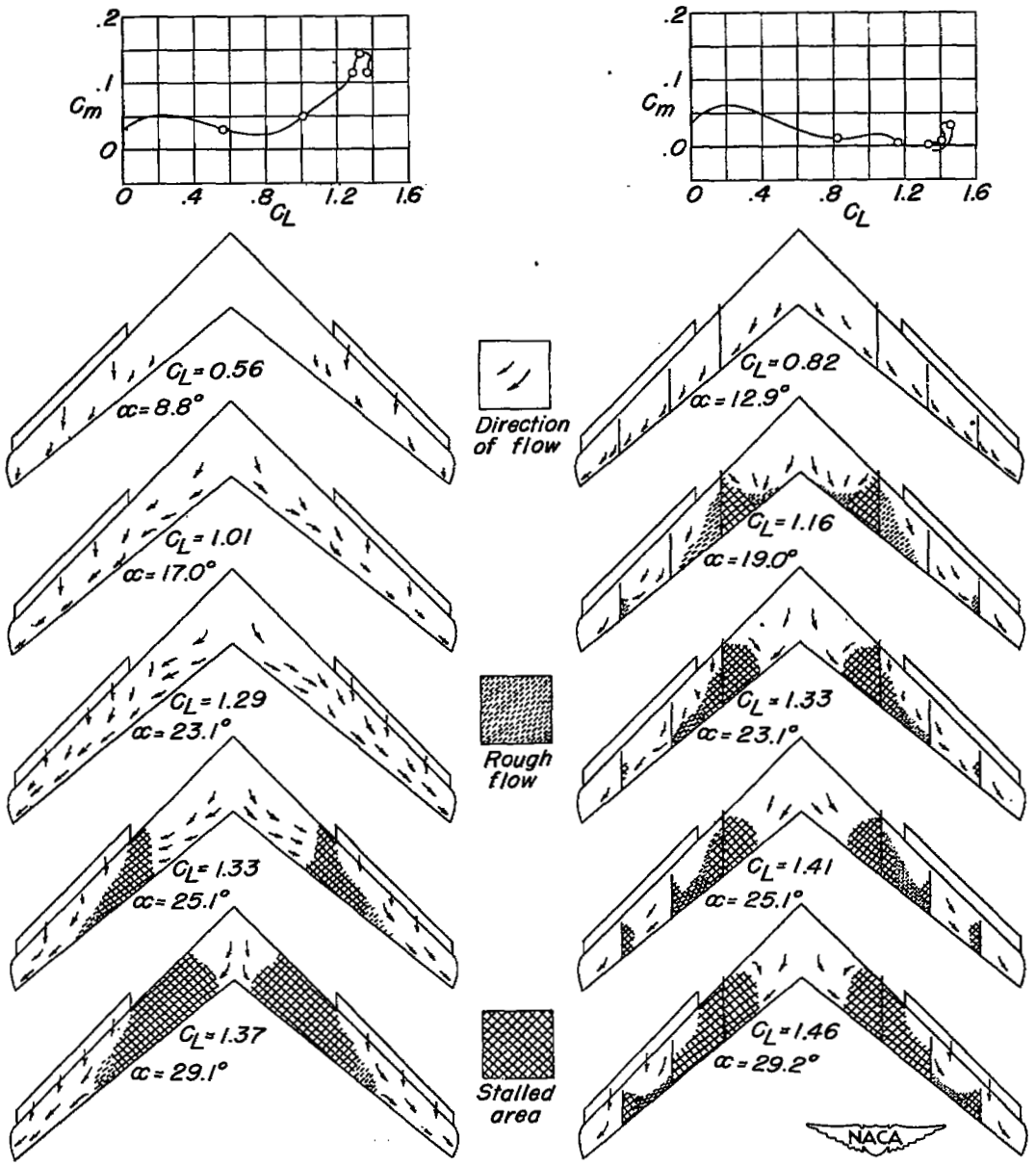

(a) 0.500b/2 leading-edge flap.

(b) 0.500b/2 leading-edge flaps, 0.350b/2 complete fences and 0.575b/2 and 0.800b/2 chord fences.

Figure 12.- Airflow characteristics near the wing surface as obtained by observations of wool tufts. Wing with 0.500b/2 leading-edge flaps with and without fences.

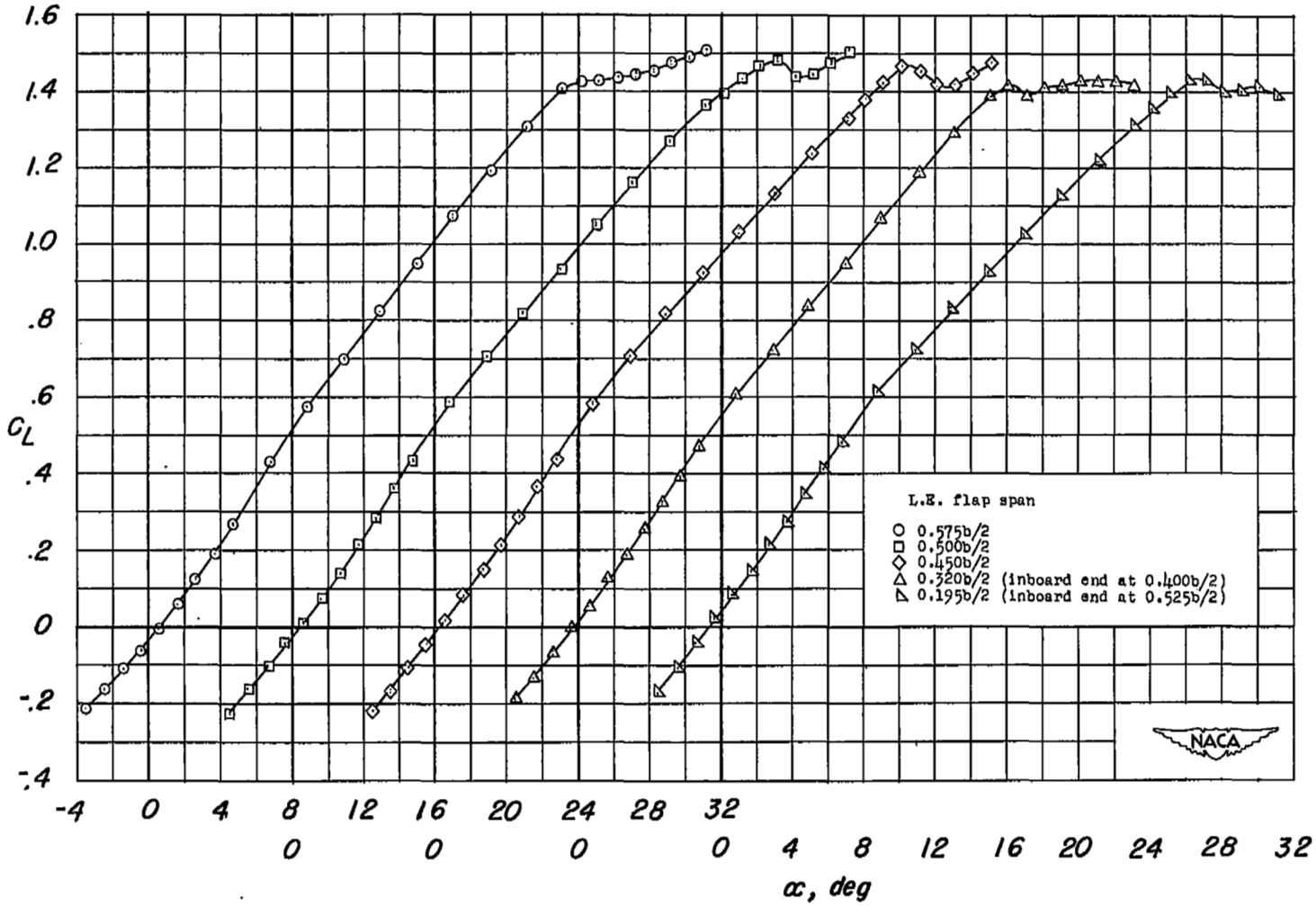

(a) C_L against α.

Figure 13.- Lift and pitching-moment characteristics of the wing with chord fences at 0.575b/2 and 0.800b/2, and various spans of leading-edge flaps.

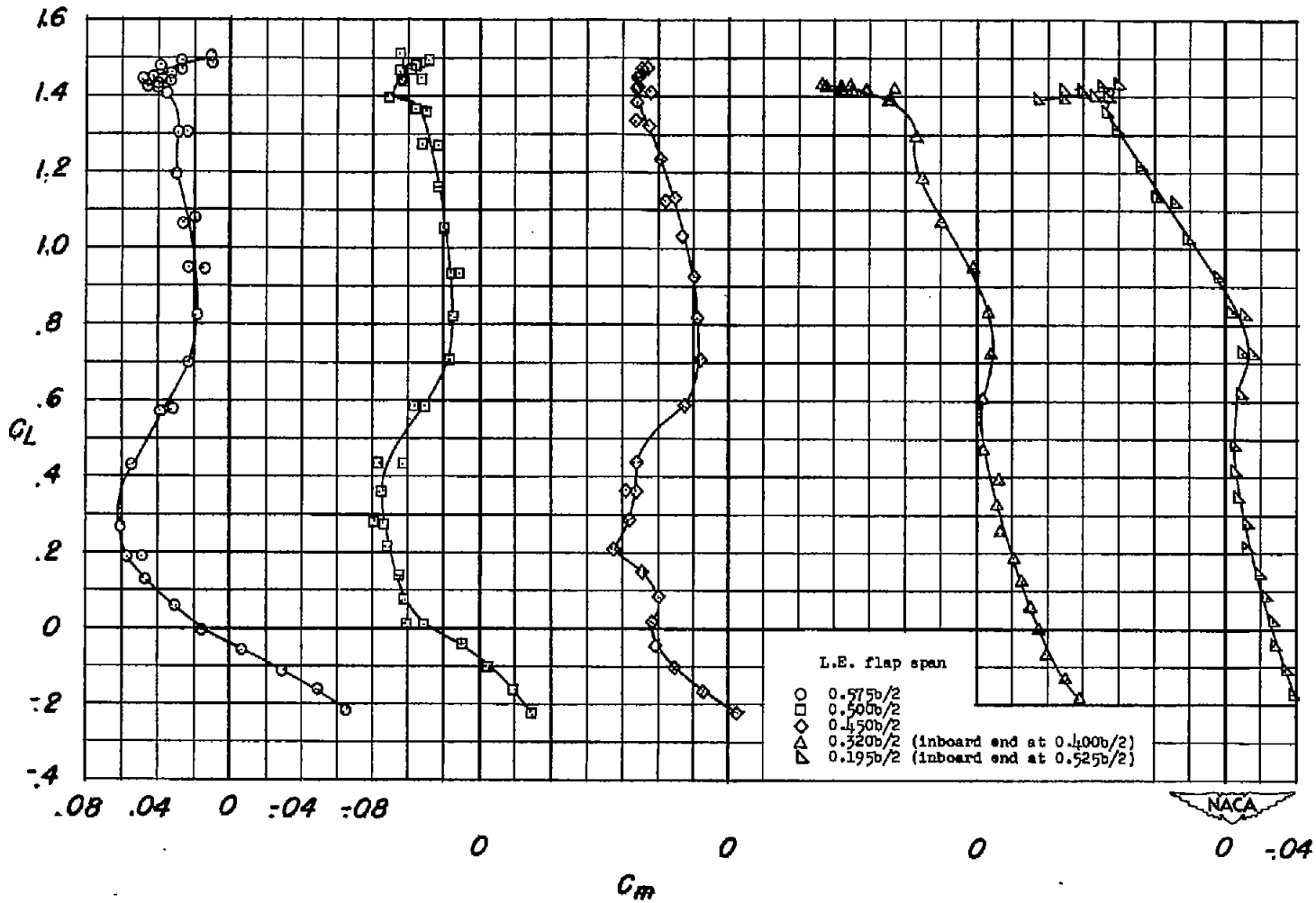

(b) C_L against C_m.

Figure 13.- Concluded.

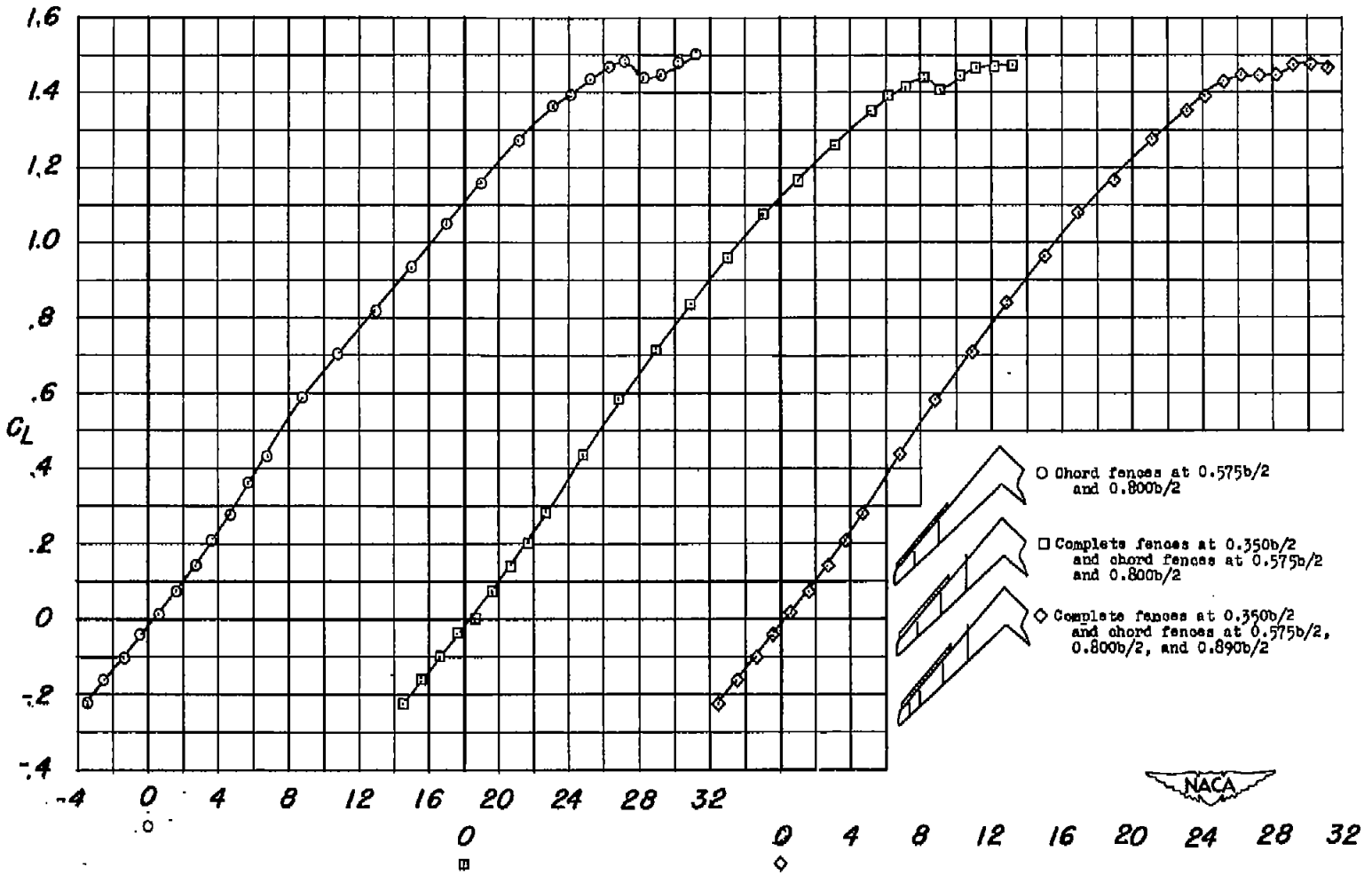

(a) C_L against α.

Figure 14.- Lift and pitching-moment characteristics of the wing with 0.500b/2 leading-edge flaps and various fence arrangements.

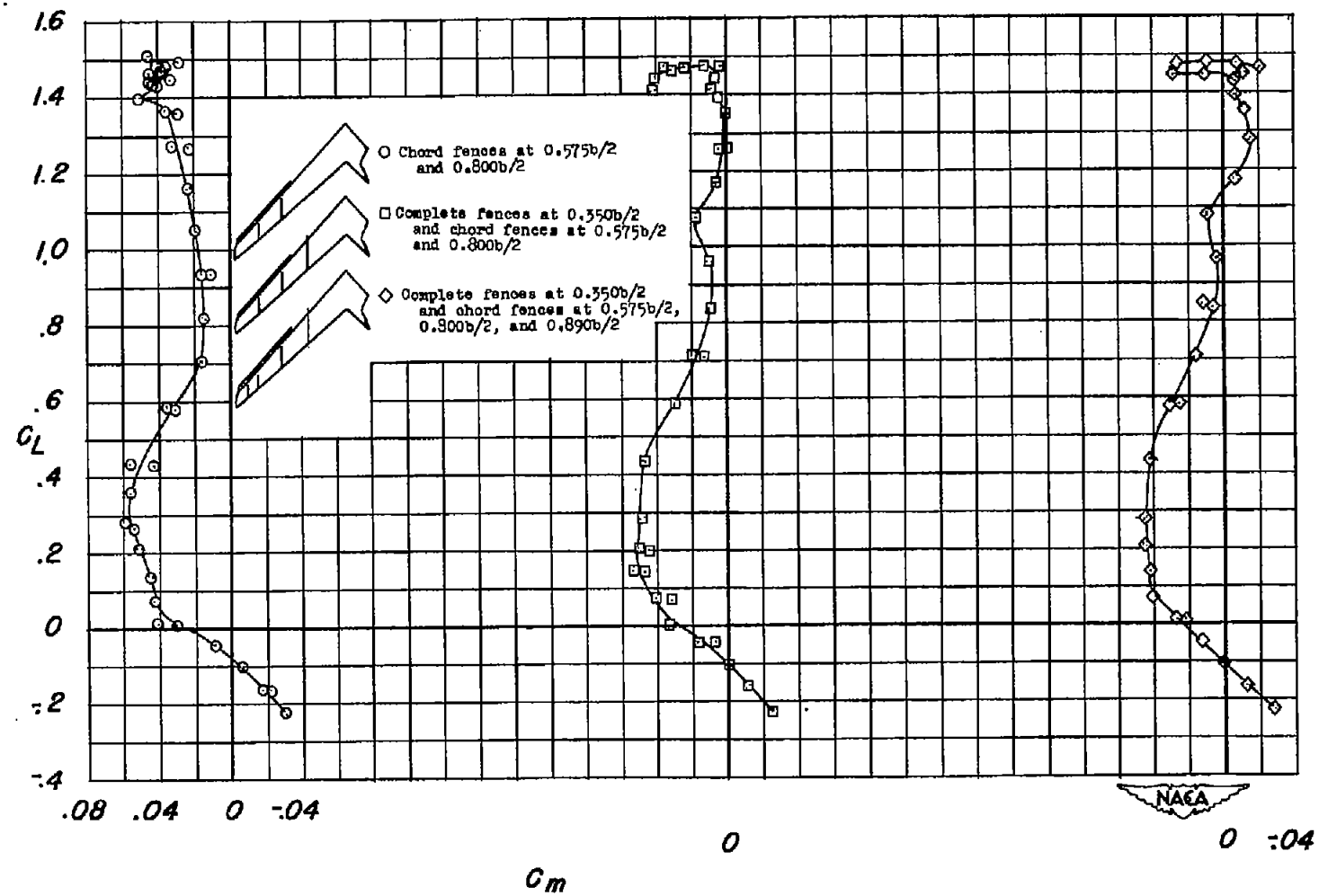

(b) C_L against C_m.

Figure 14.- Concluded.

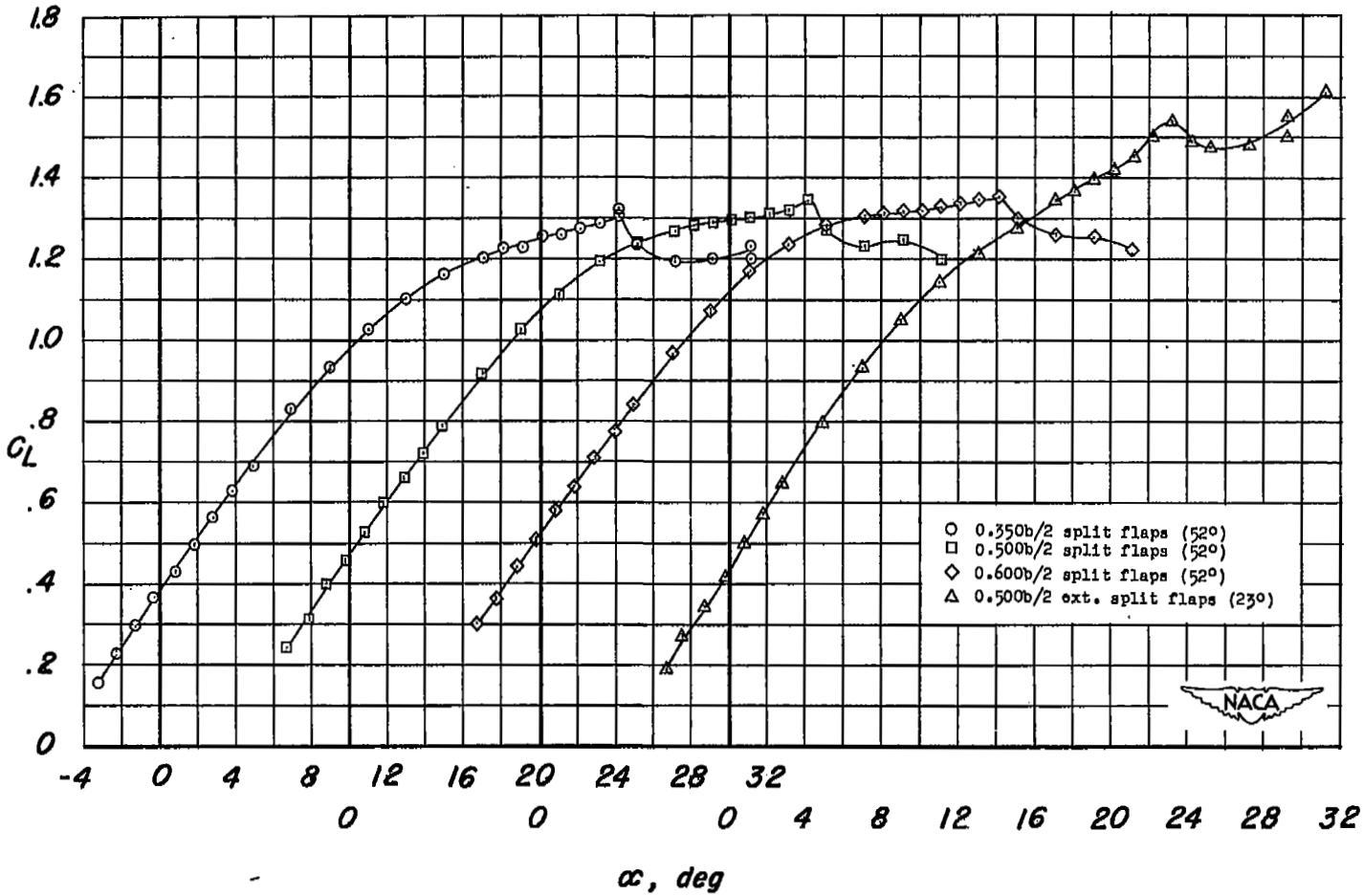

(a) C_L against α.

Figure 15.- Lift and pitching-moment characteristics of the wing with various spans of split flaps deflected 52° and with 0.500b/2 extended-split flaps deflected 23°.

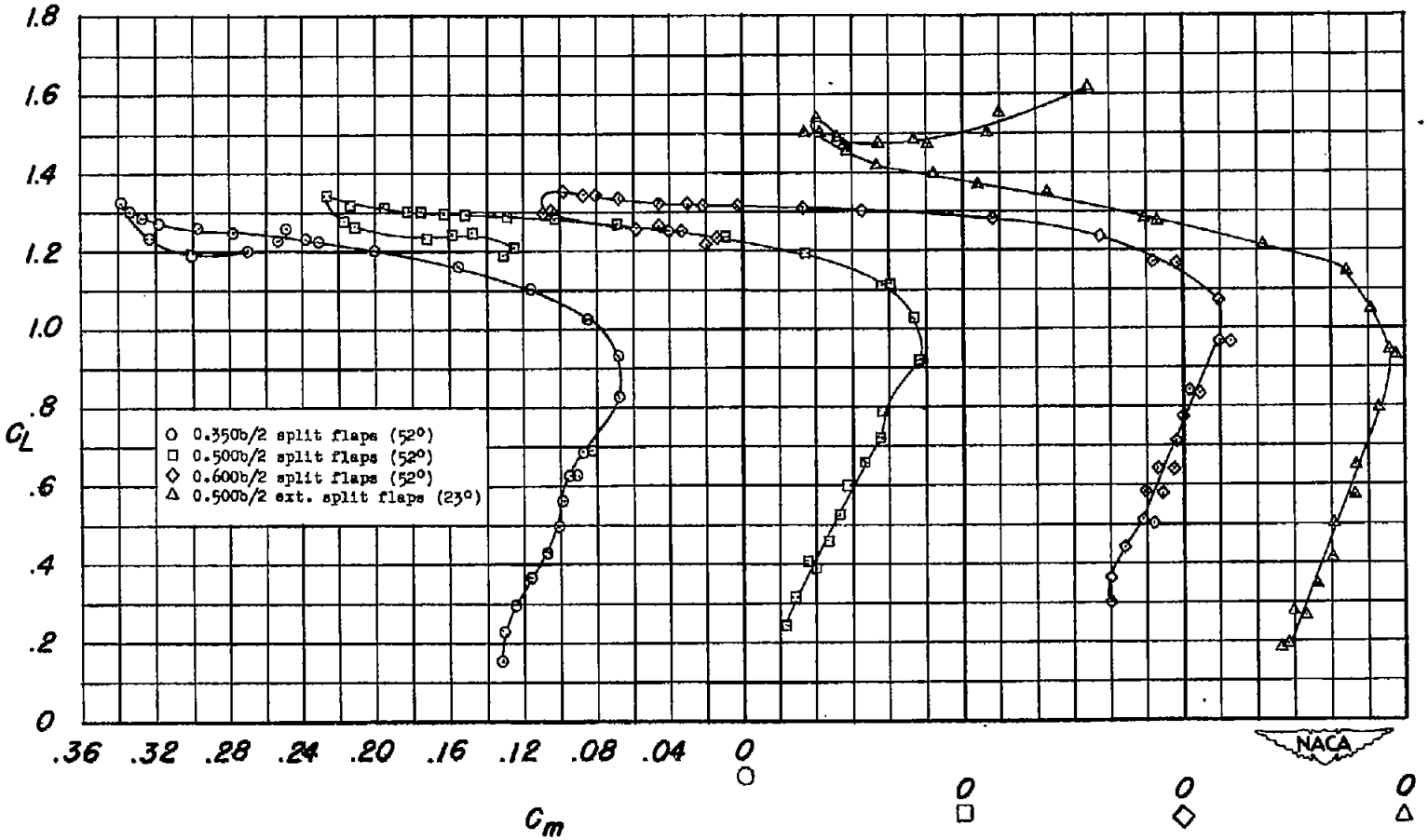

(b) C_L against C_m.

Figure 15.- Concluded.

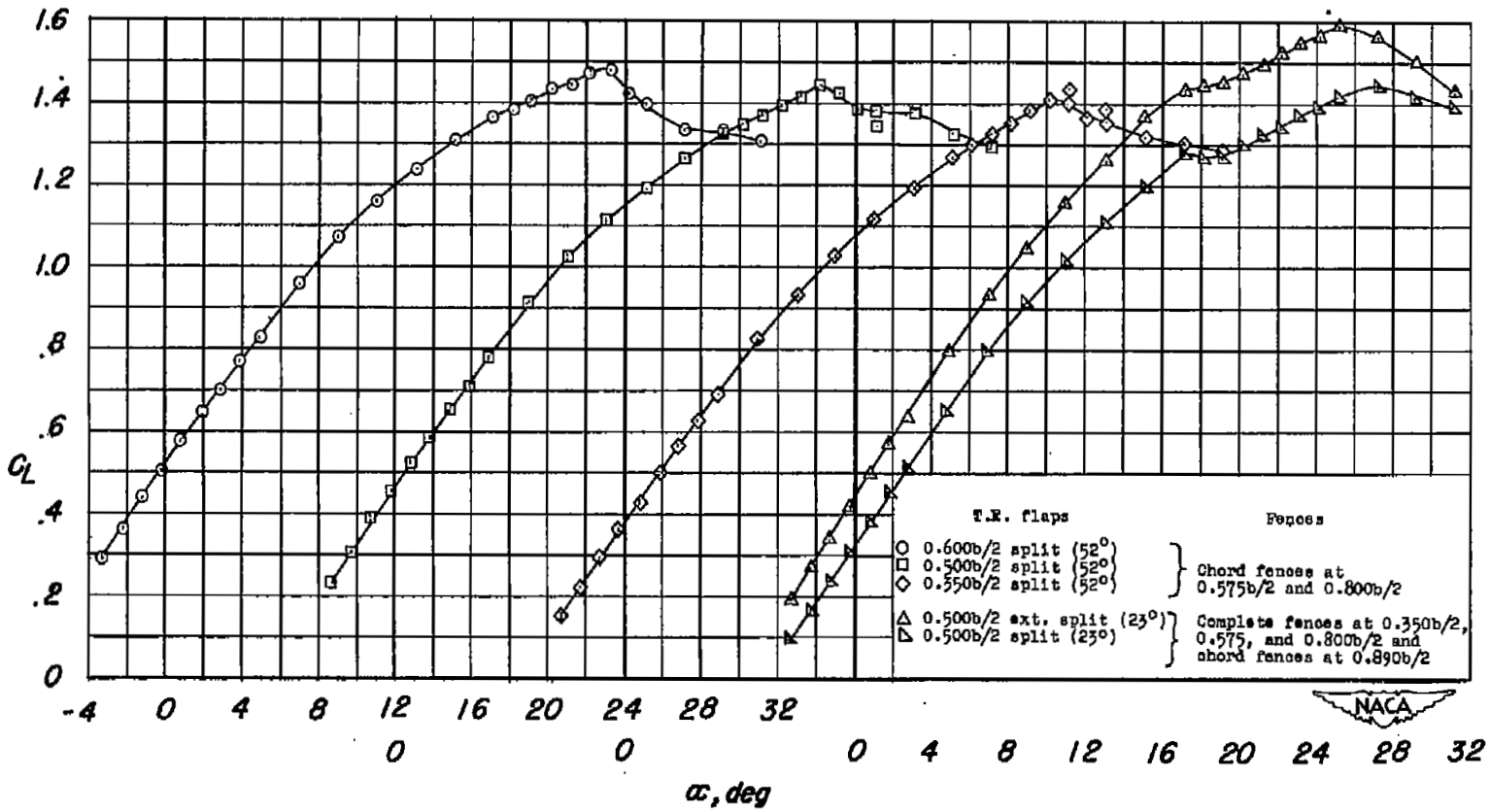

(a) C_L against α.

Figure 16.- Lift and pitching-moment characteristics of the wing with various spans of split flaps deflected 52° and chord fences at 0.575b/2 and 0.800b/2, and comparison of 0.500b/2 split and 0.500b/2 extended-split flaps deflected 23° on the wing with four fences on each semispan.

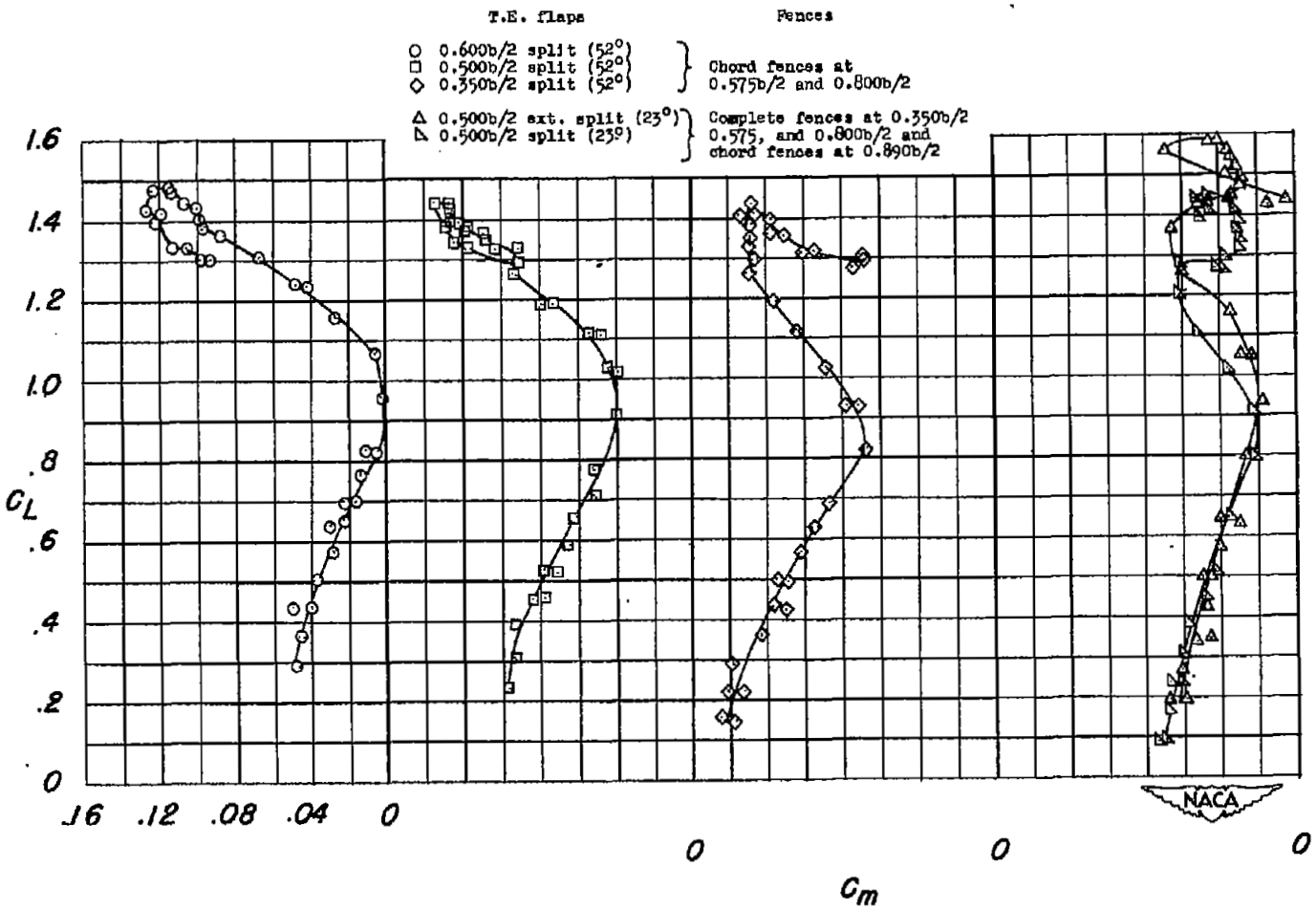

(b) C_L against C_m.

Figure 16.- Concluded.

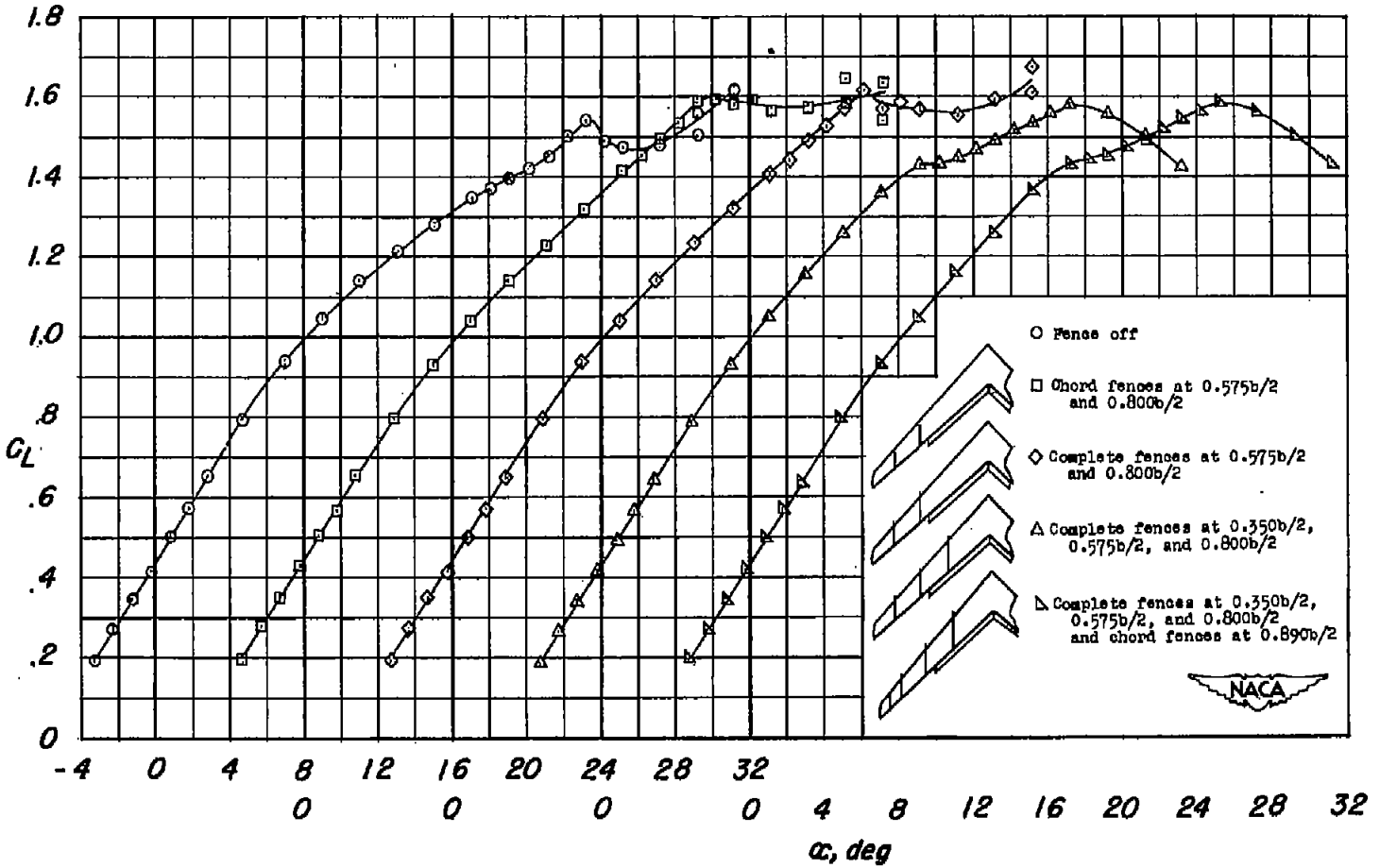

(a) C_L against α.

Figure 17.- Effect of fences on the lift and pitching moment characteristics of the wing with 0.500b/2 extended split flaps deflected 23°.

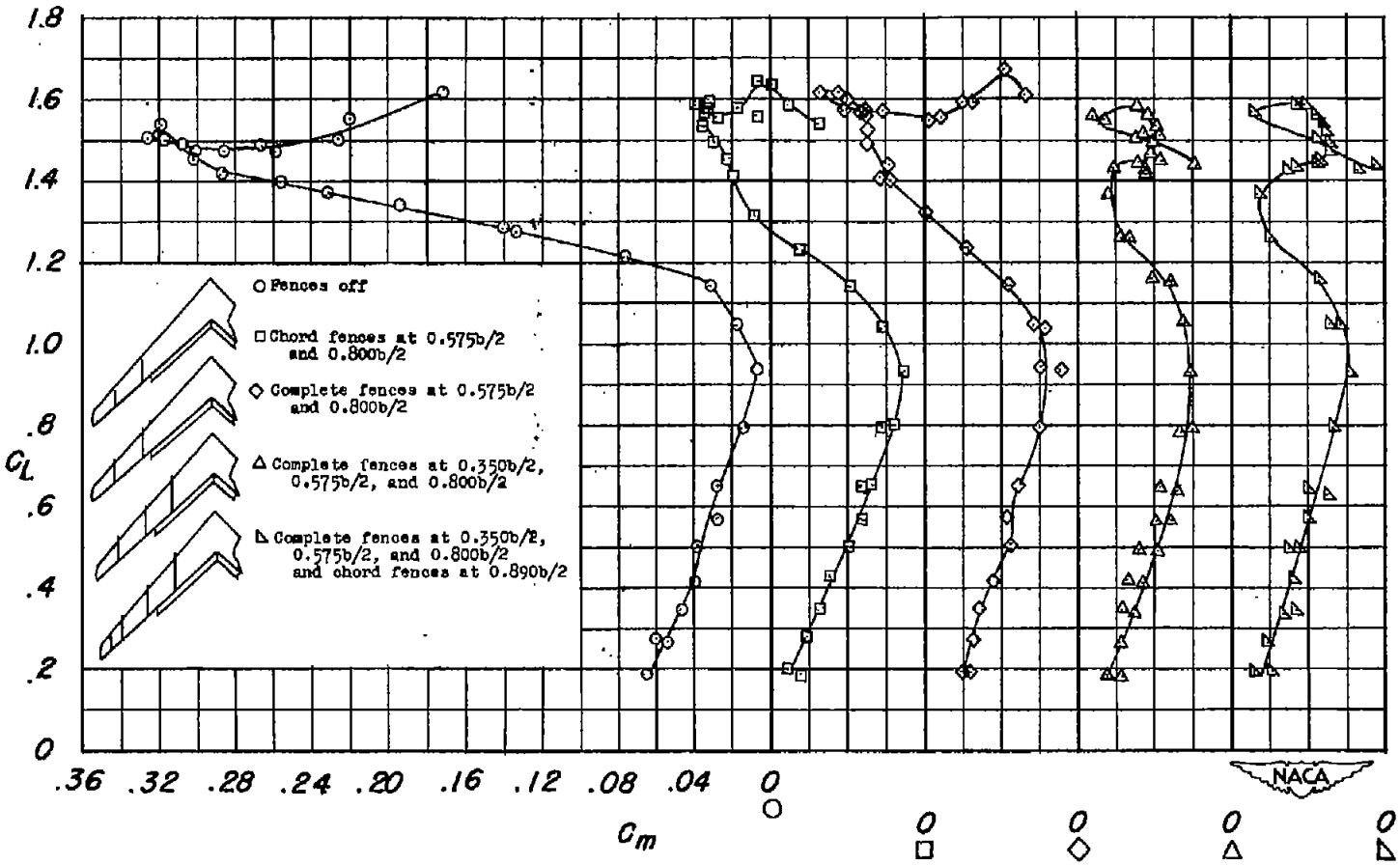

(b) C_L against C_m.

Figure 17.- Concluded.

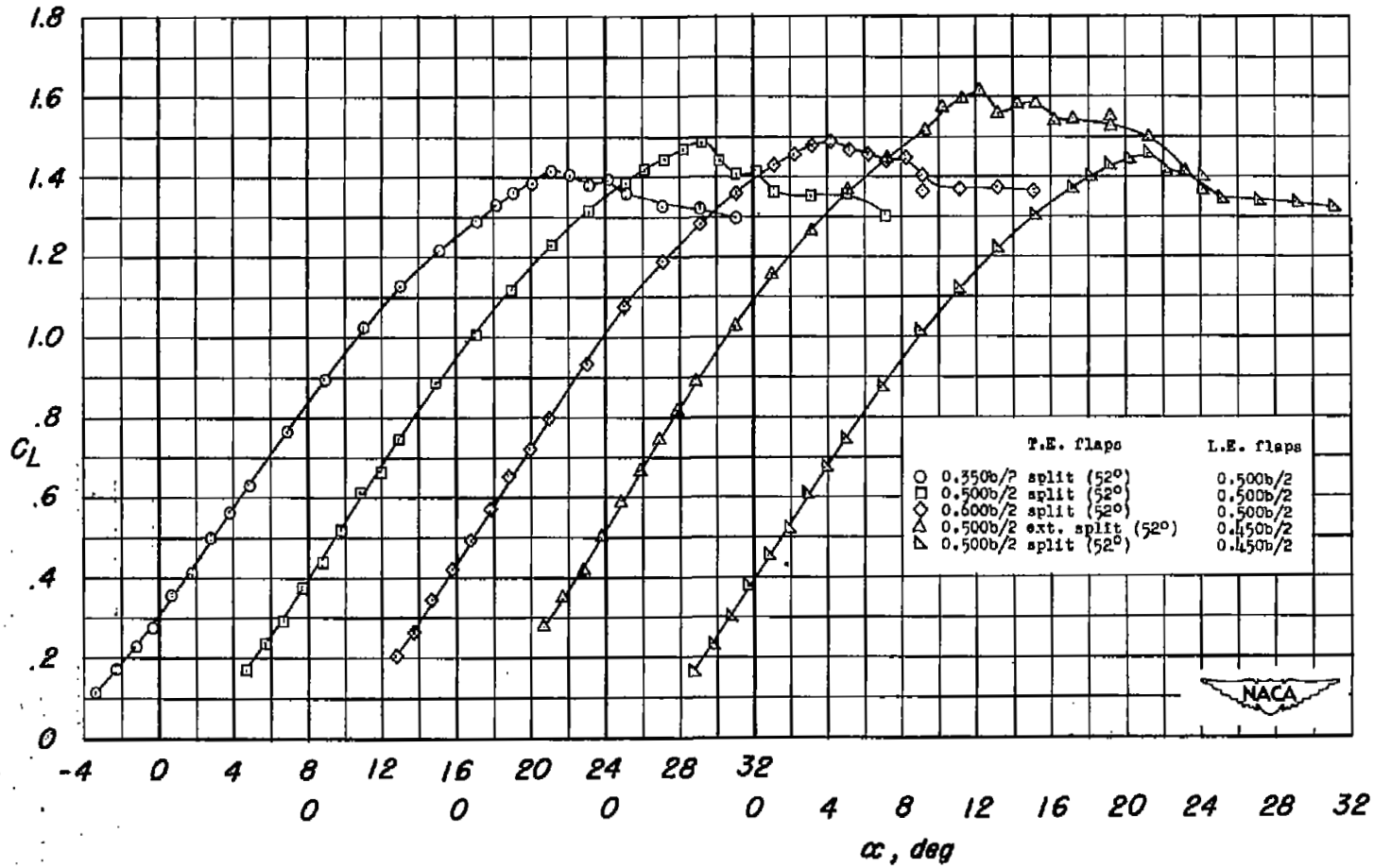

(a) C_L against α.

Figure 18.- Lift and pitching-moment characteristics of the wing with various combinations of leading- and trailing-edge flaps.

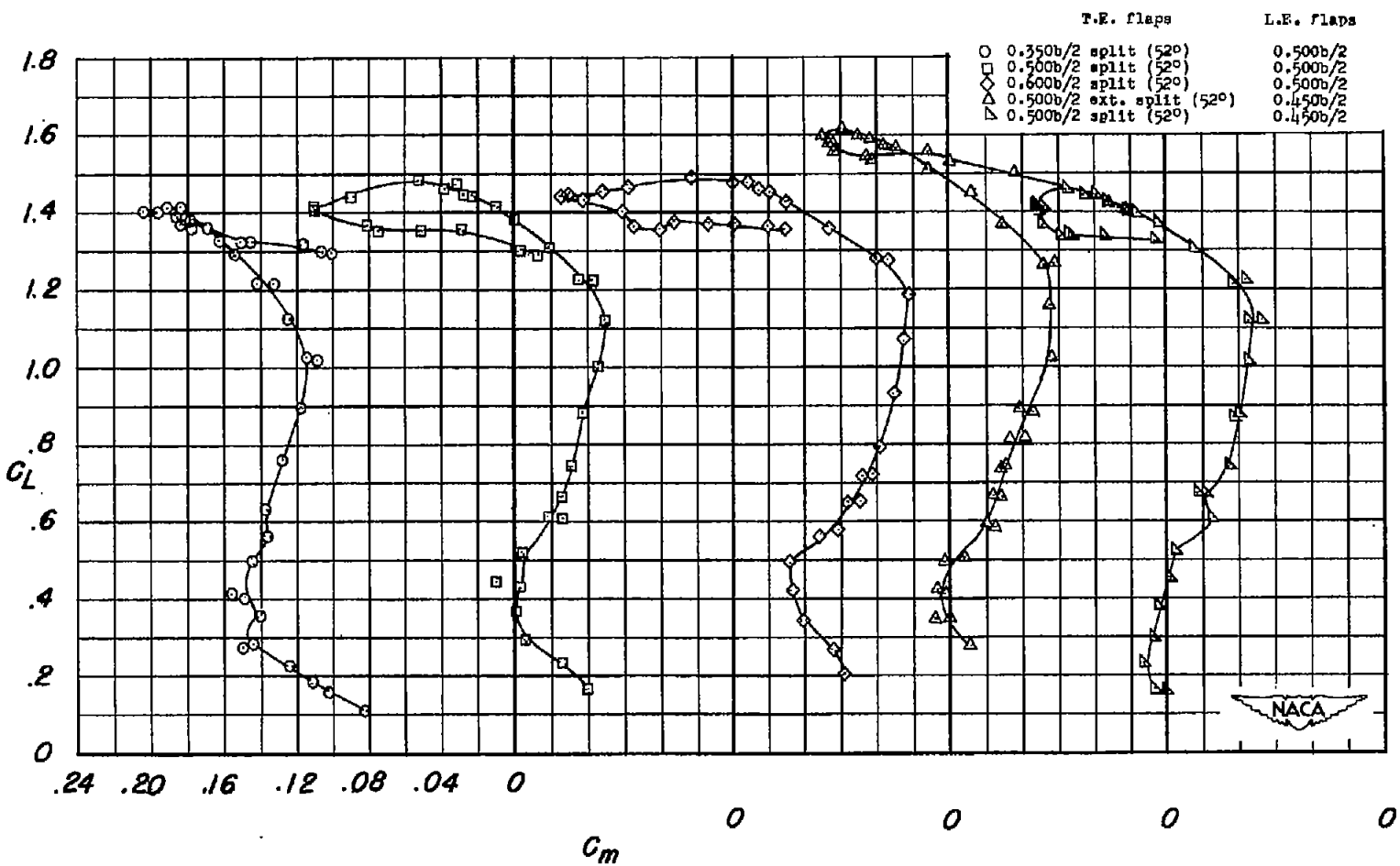

(b) C_L against C_m.

Figure 18.- Concluded.

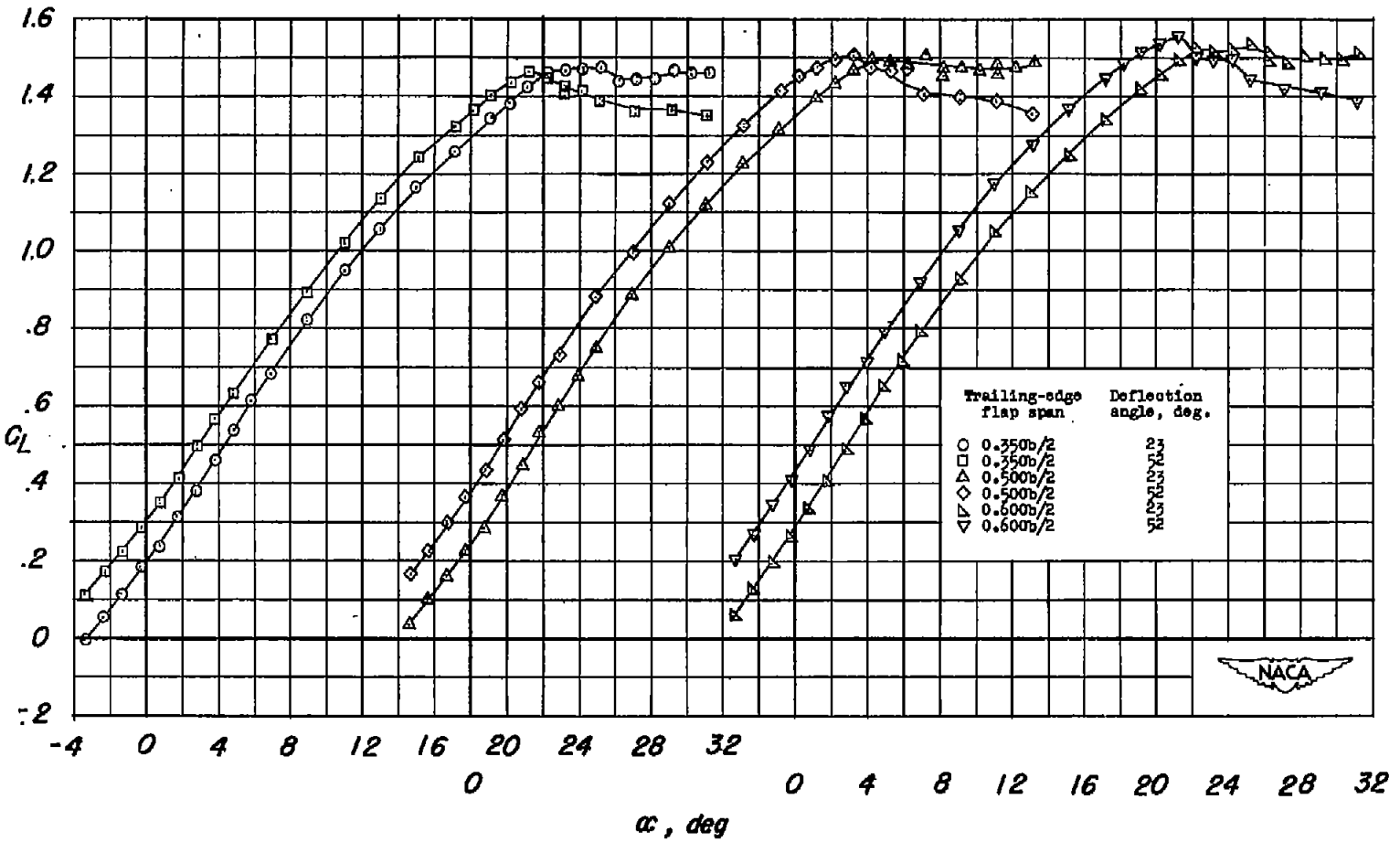

(a) C_L against α.

Figure 19.- Effect of split flap span and deflection angle on the lift and pitching-moment characteristics of the wing with 0.500b/2 leading-edge flaps and chord fences at 0.575b/2 and 0.800b/2.

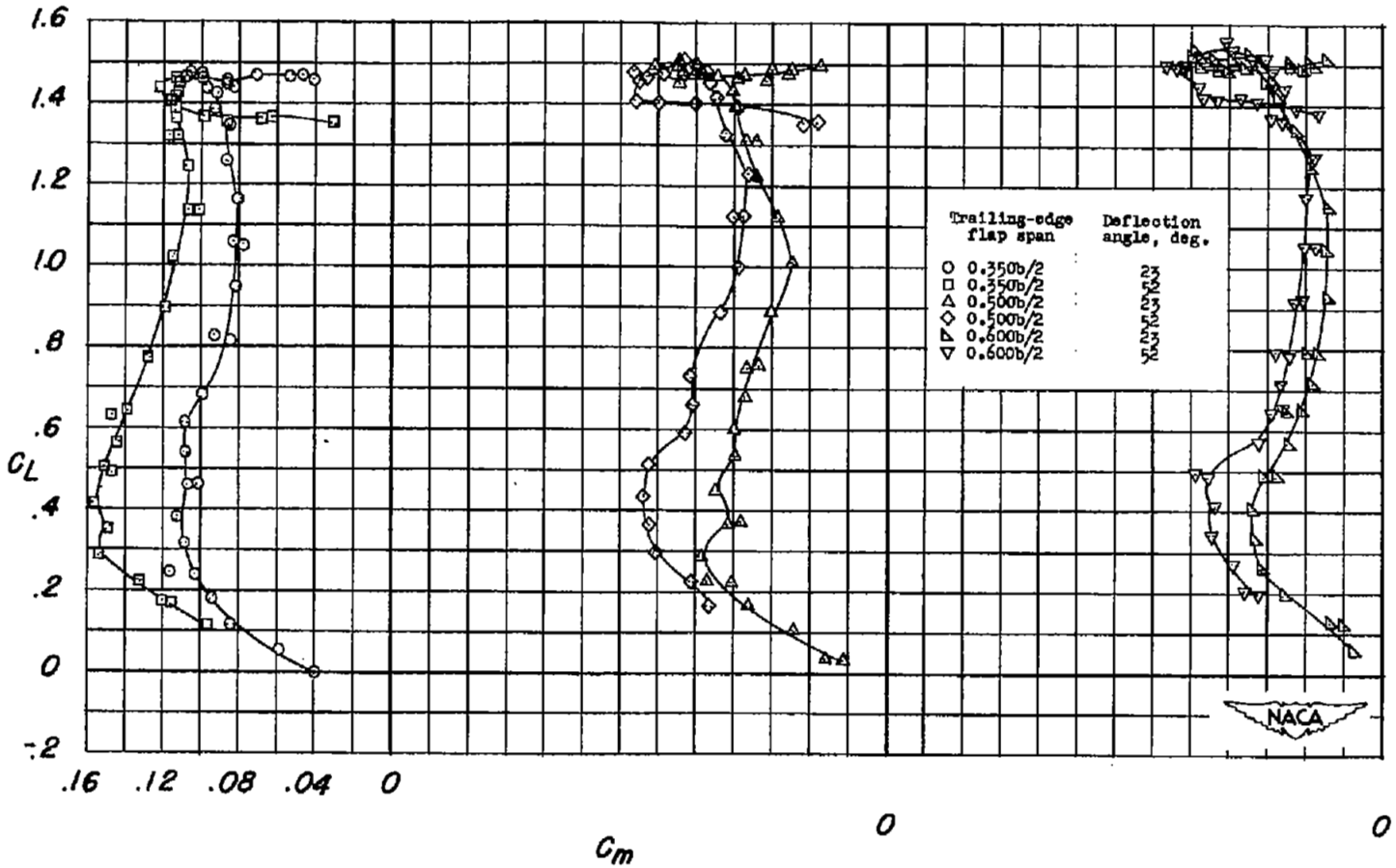

(b) C_L against C_m.

Figure 19.- Concluded.

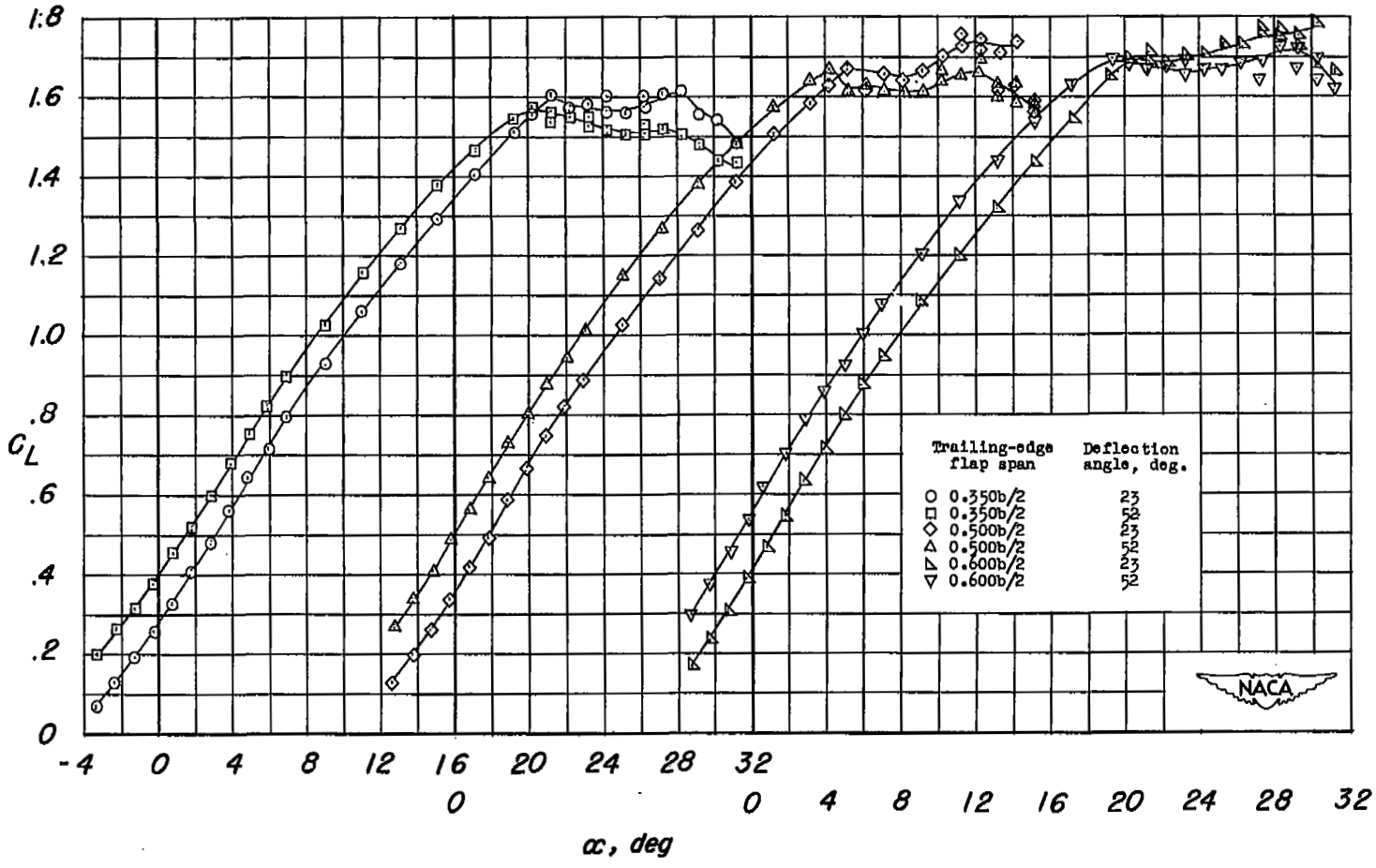

(a) C_L against α.

Figure 20.- Effect of extended-split flap span and deflection angle on the lift and pitching-moment characteristics of the wing with 0.500b/2 leading-edge flaps and chord fences at 0.575b/2 and 0.800b/2.

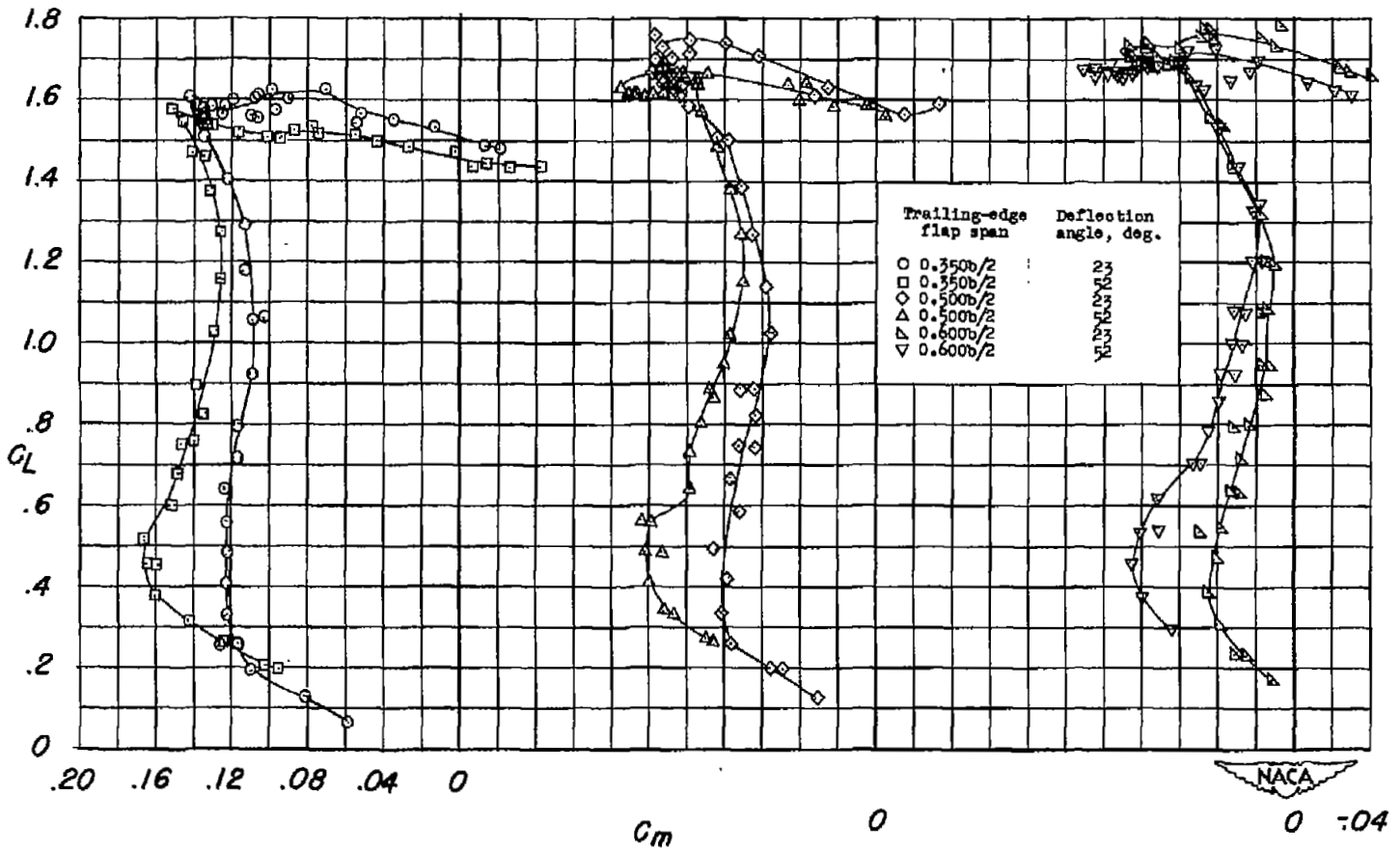

(b) C_L against C_m.

Figure 20.- Concluded.

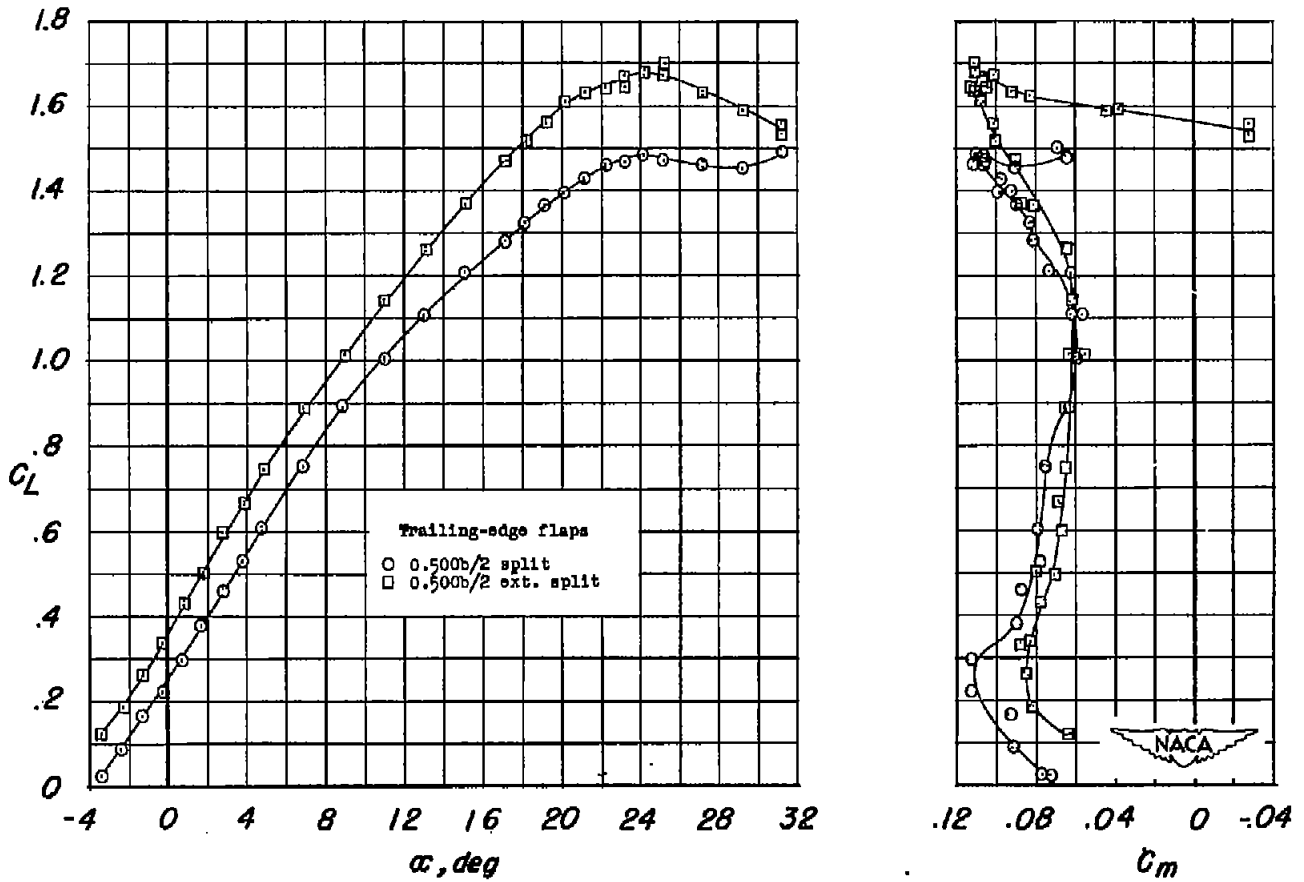

Figure 21.- Comparison of 0.500b/2 split and 0.500b/2 extended-split flaps deflected 23° on the wing with 0.450b/2 leading-edge flaps and chord fences at 0.575b/2 and 0.800b/2.

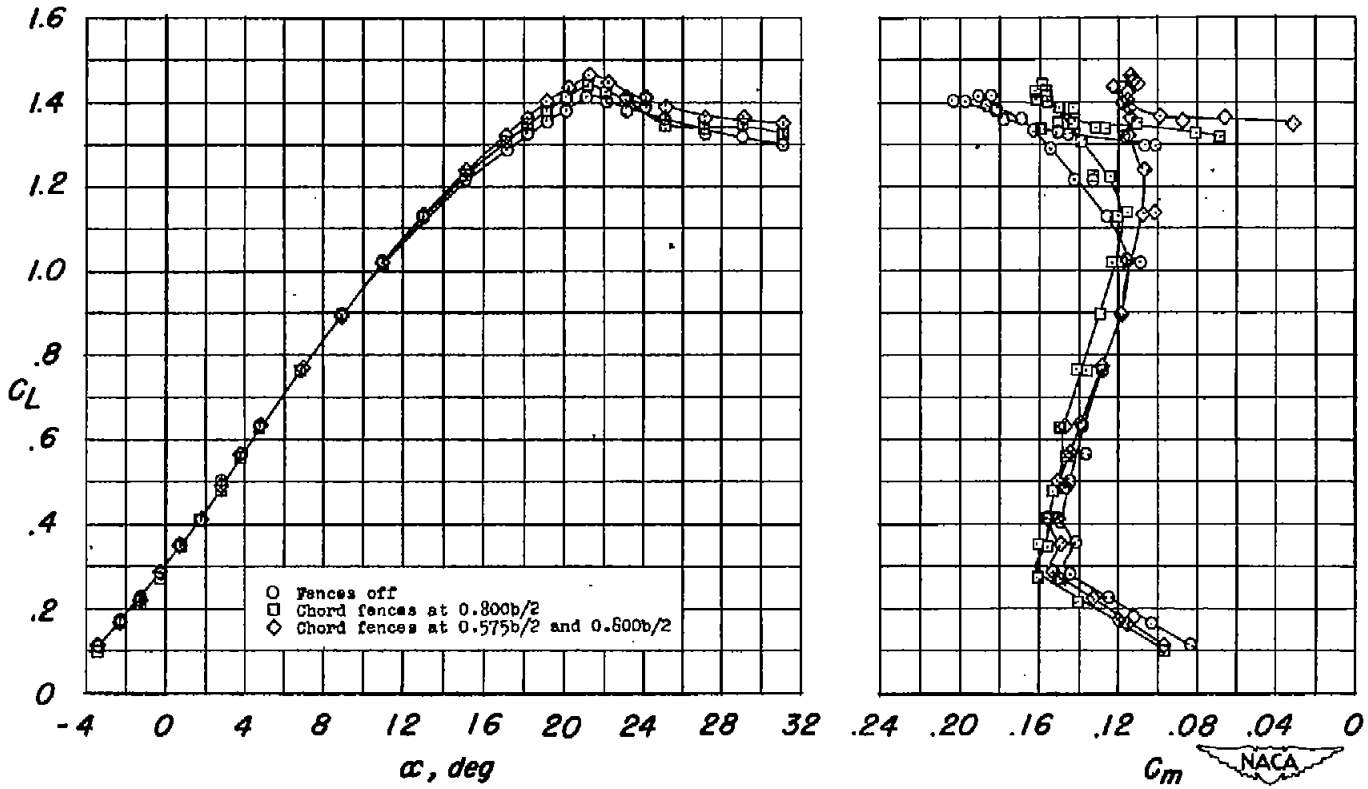

Figure 22.- Effect of chord fences on the lift and pitching-moment characteristics of the wing with 0.350b/2 split flaps deflected 52° and 0.500b/2 leading-edge flaps.

[redacted]

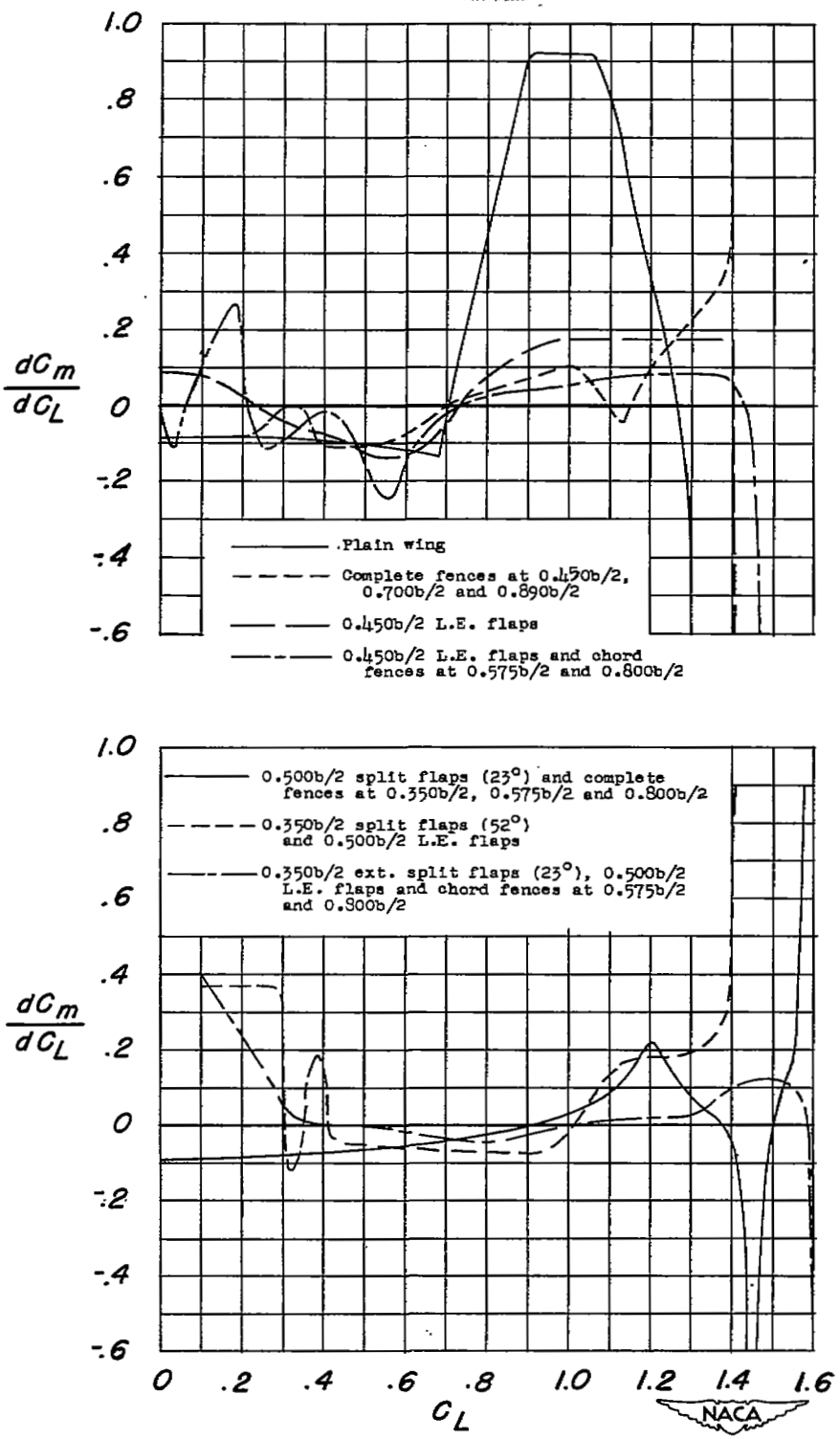

Figure 23.- Comparison of the most favorable stability characteristics obtained with various combinations of high-lift and stall-control devices.

[redacted]

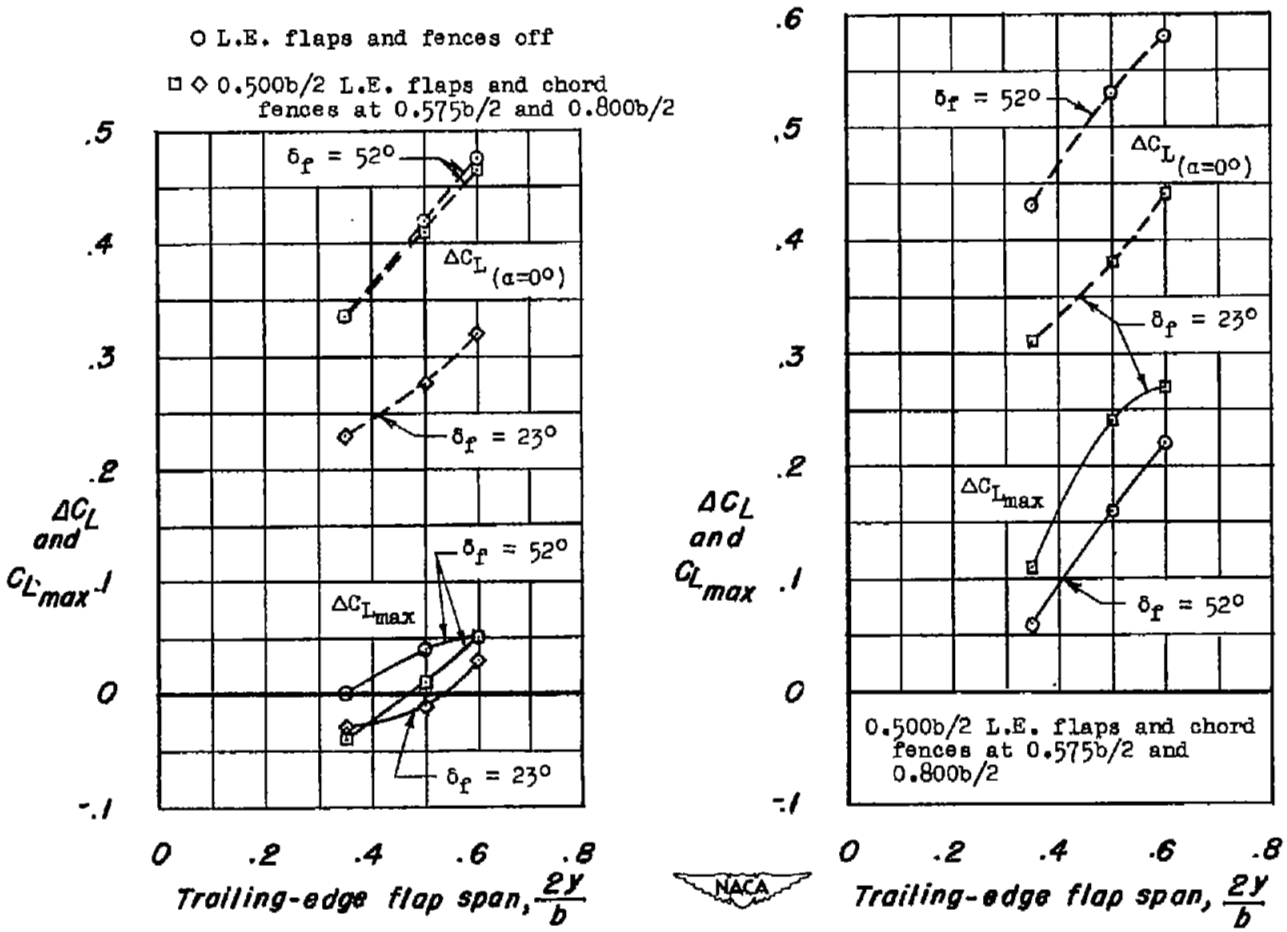

(a) Split flaps.

(b) Extended split flaps.

Figure 24.- Variation with trailing-edge flap span of the increment in lift due to the trailing-edge flaps at zero angle of attack and at maximum lift.

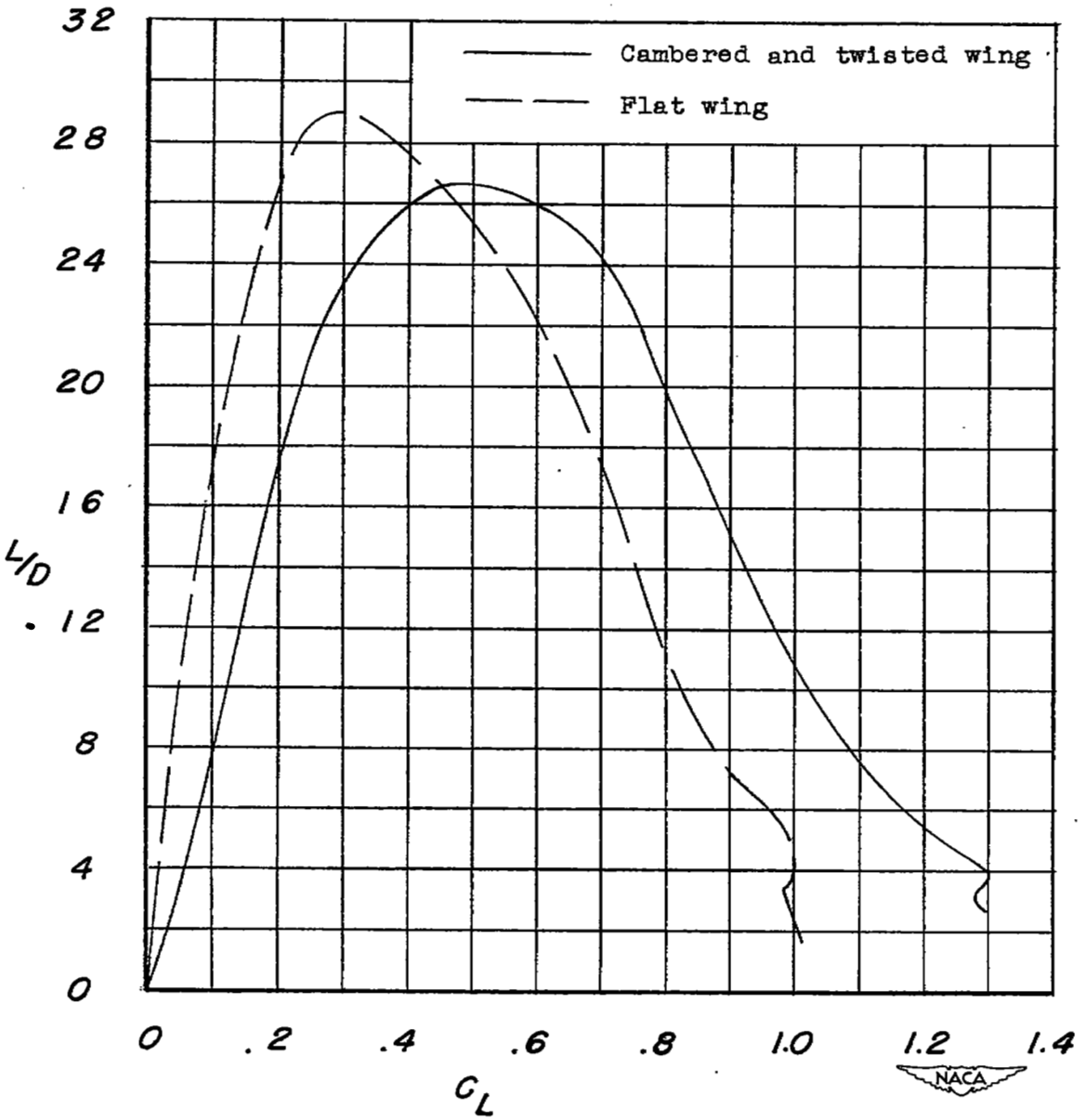

Figure 25.- Lift-drag ratios of the cambered and twisted wing and the flat wing at a Reynolds number of 4.0×10^6.

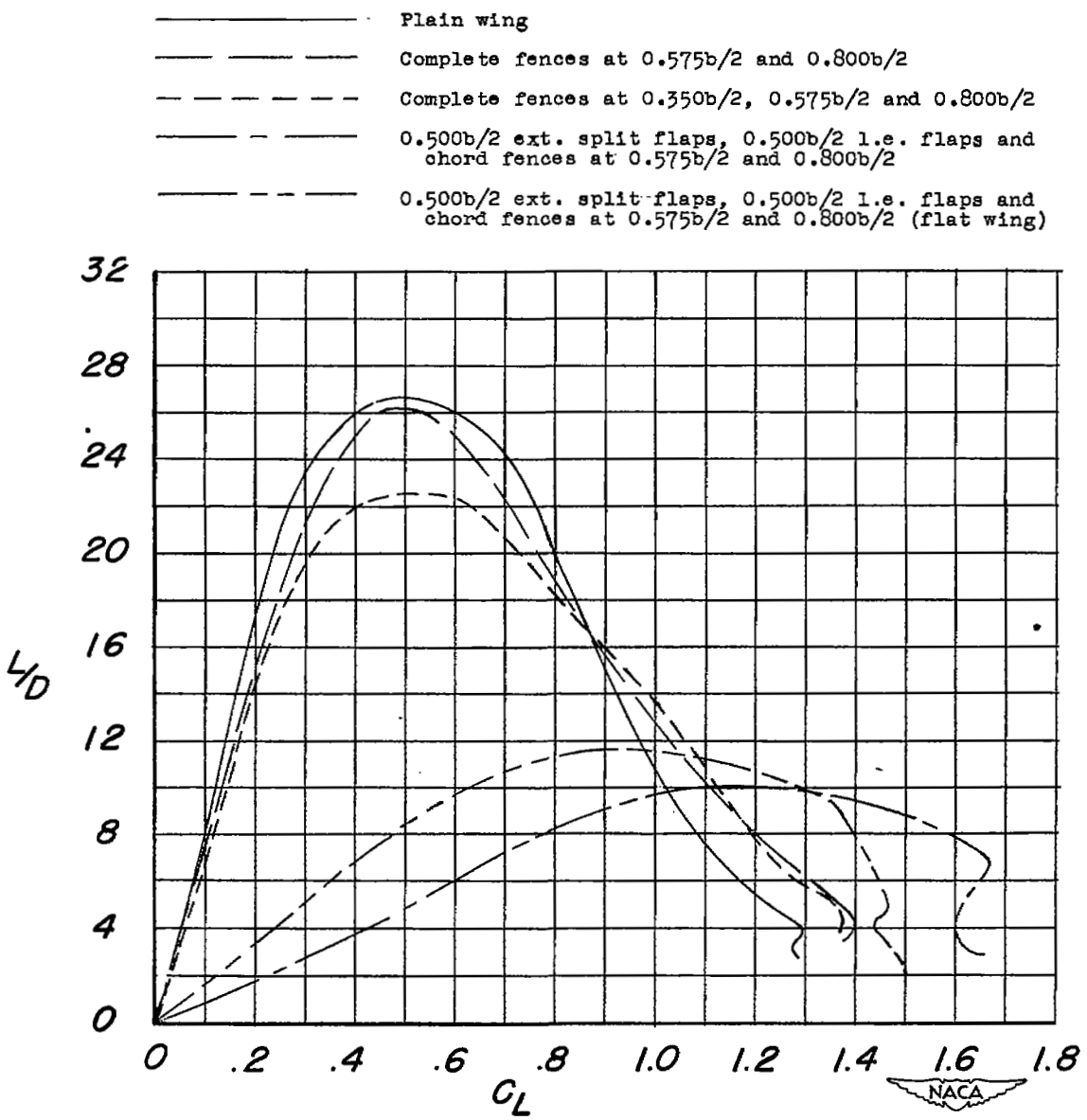

Figure 26.- Lift-drag ratios of the twisted and flat wings with high-lift and stall-control devices. $R = 4.0 \times 10^6$.

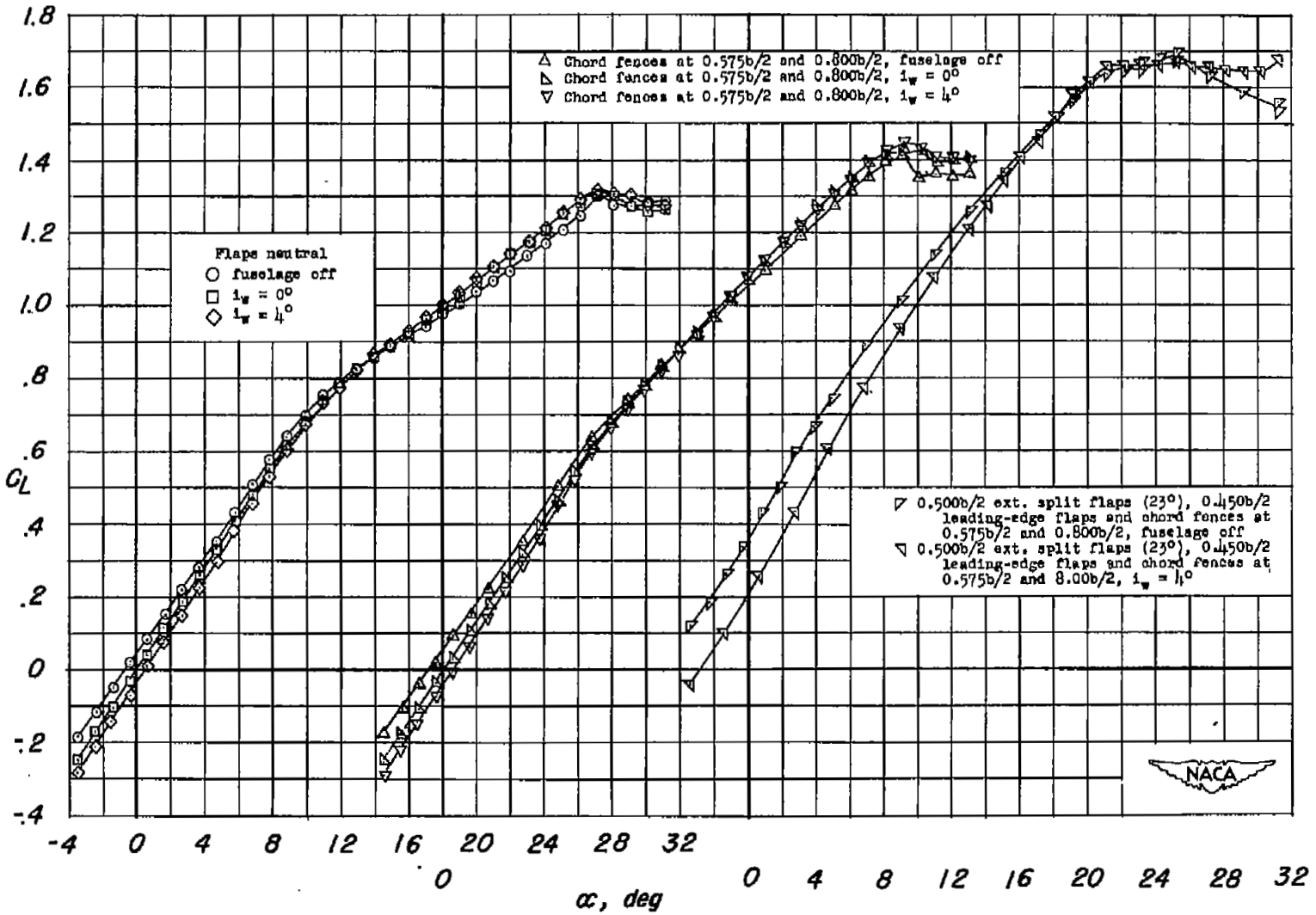

(a) C_L against α.

Figure 27.- Lift and pitching-moment characteristics of the plain wing and the wing with various flap and fence configurations with and without a fuselage.

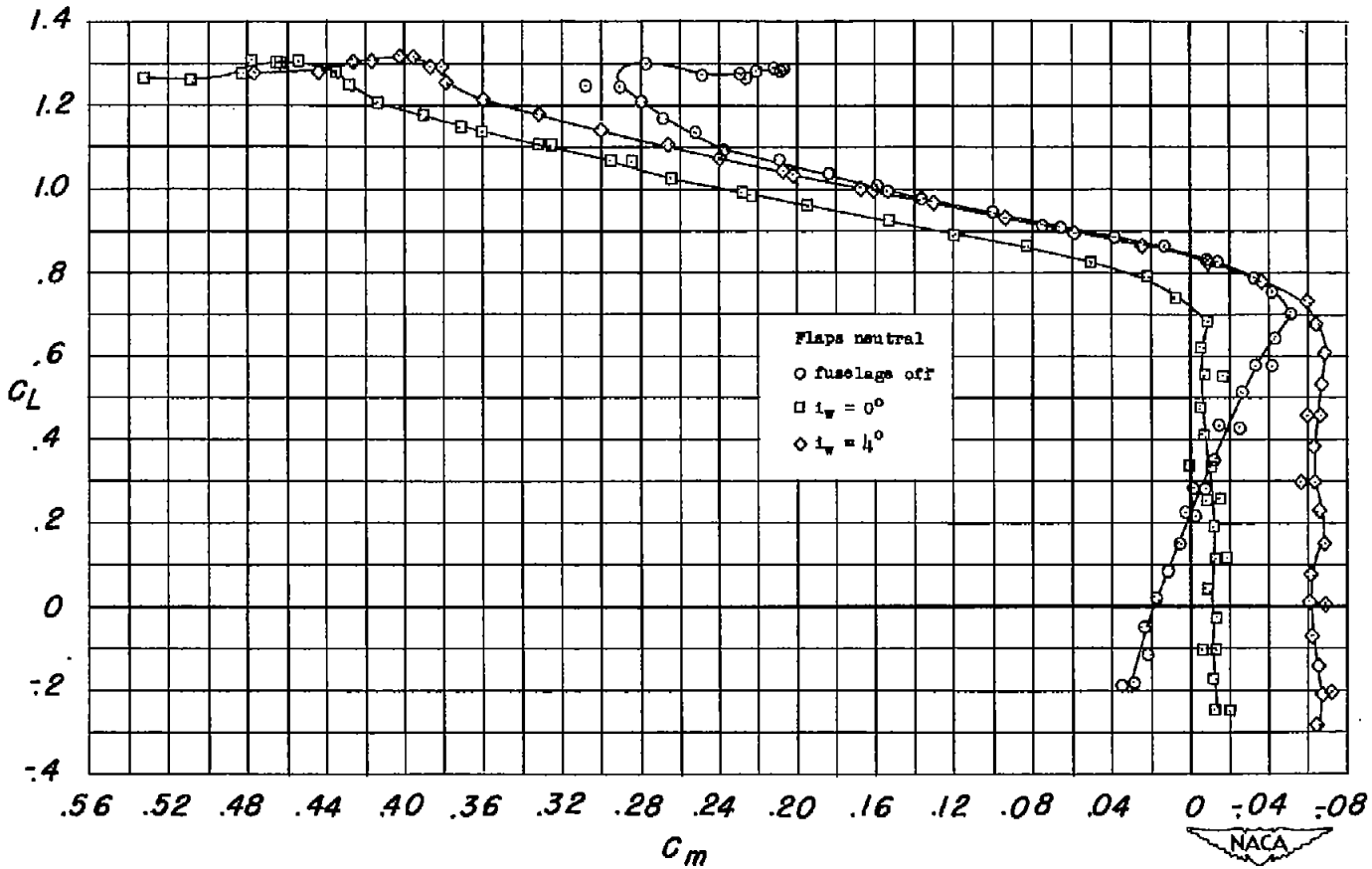

(b) C_L against C_m.

Figure 27.- Continued.

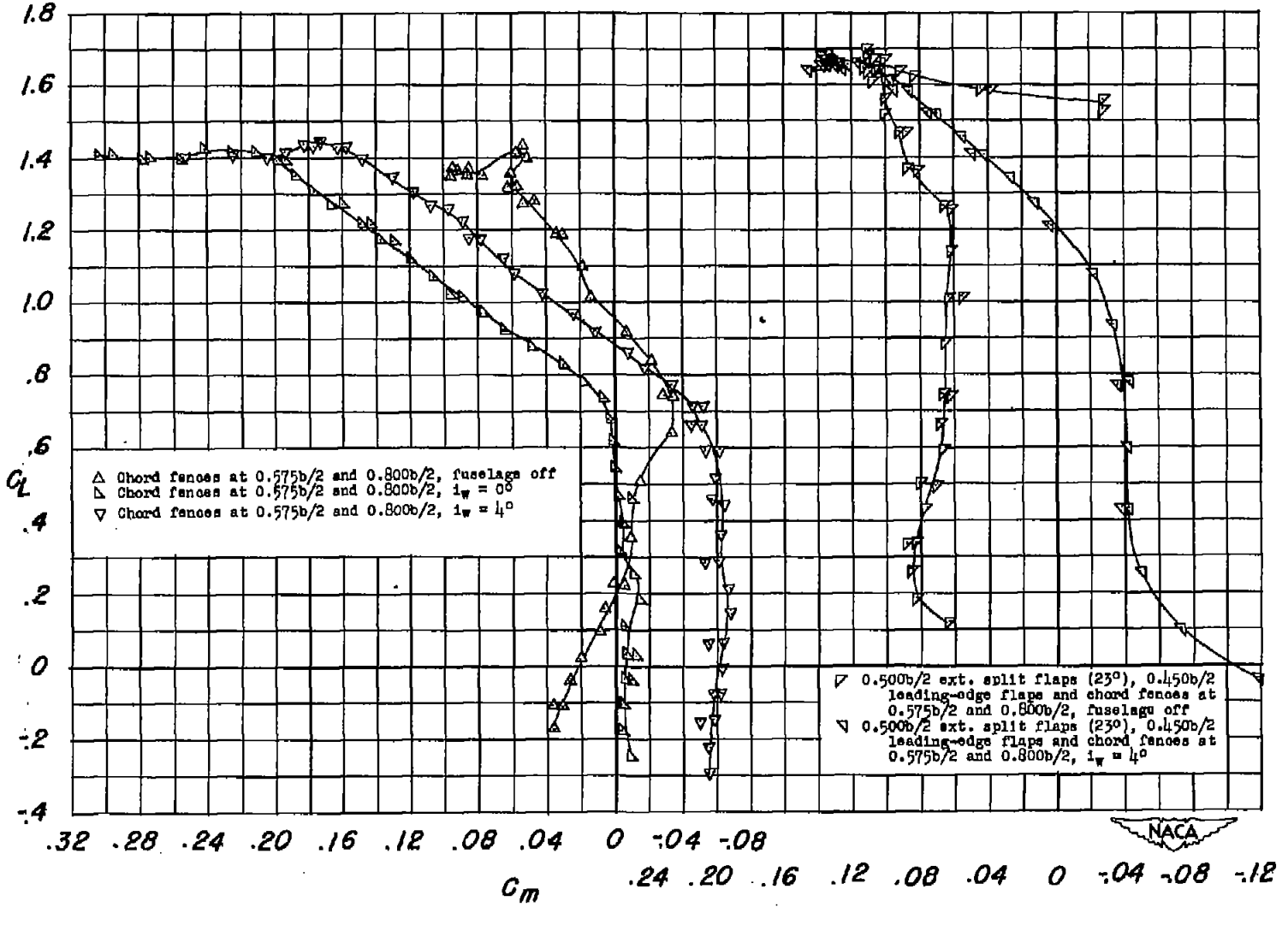

(b) Concluded.

Figure 27.- Concluded.

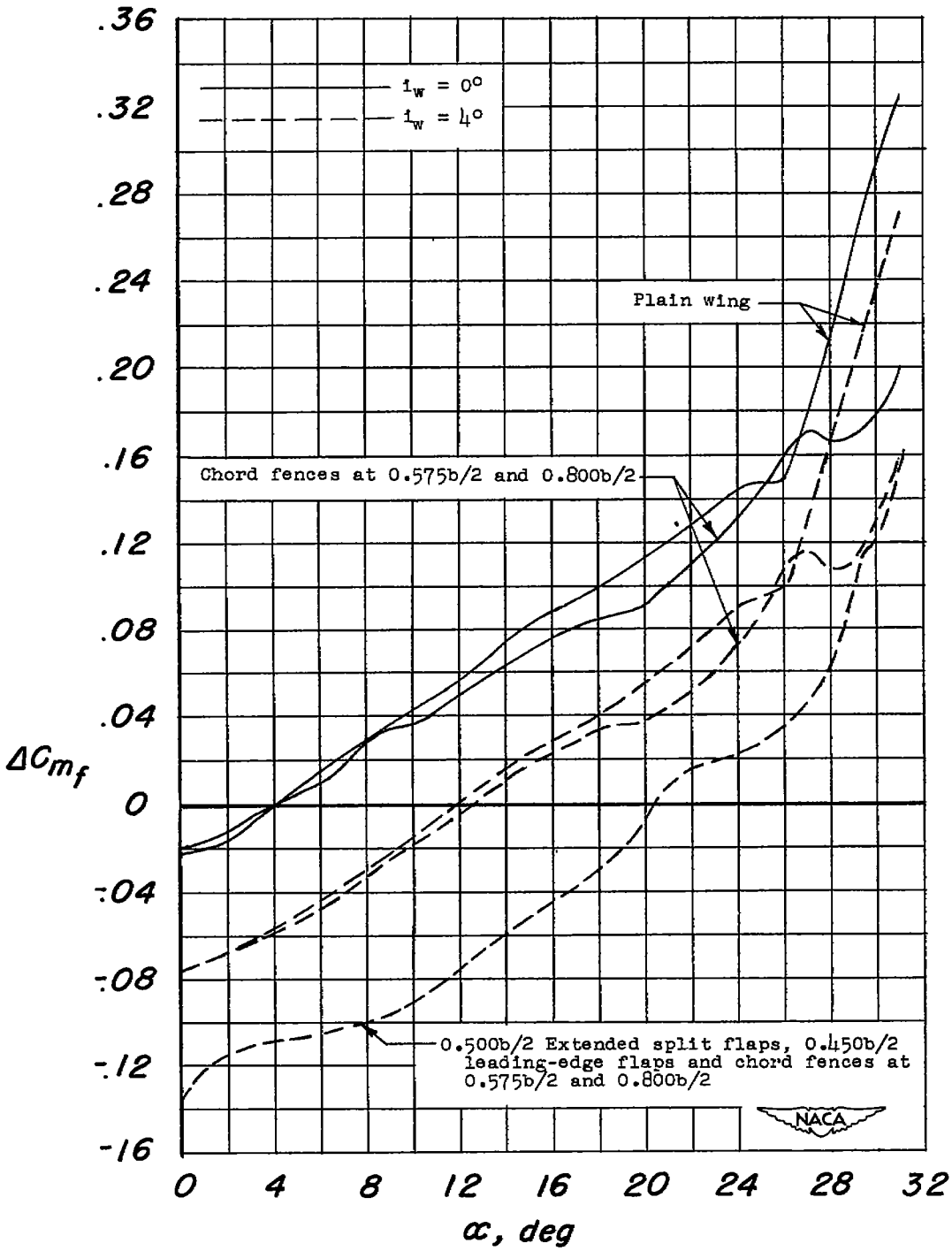

Figure 28.- Increment in pitching moment due to the addition of the fuselage.

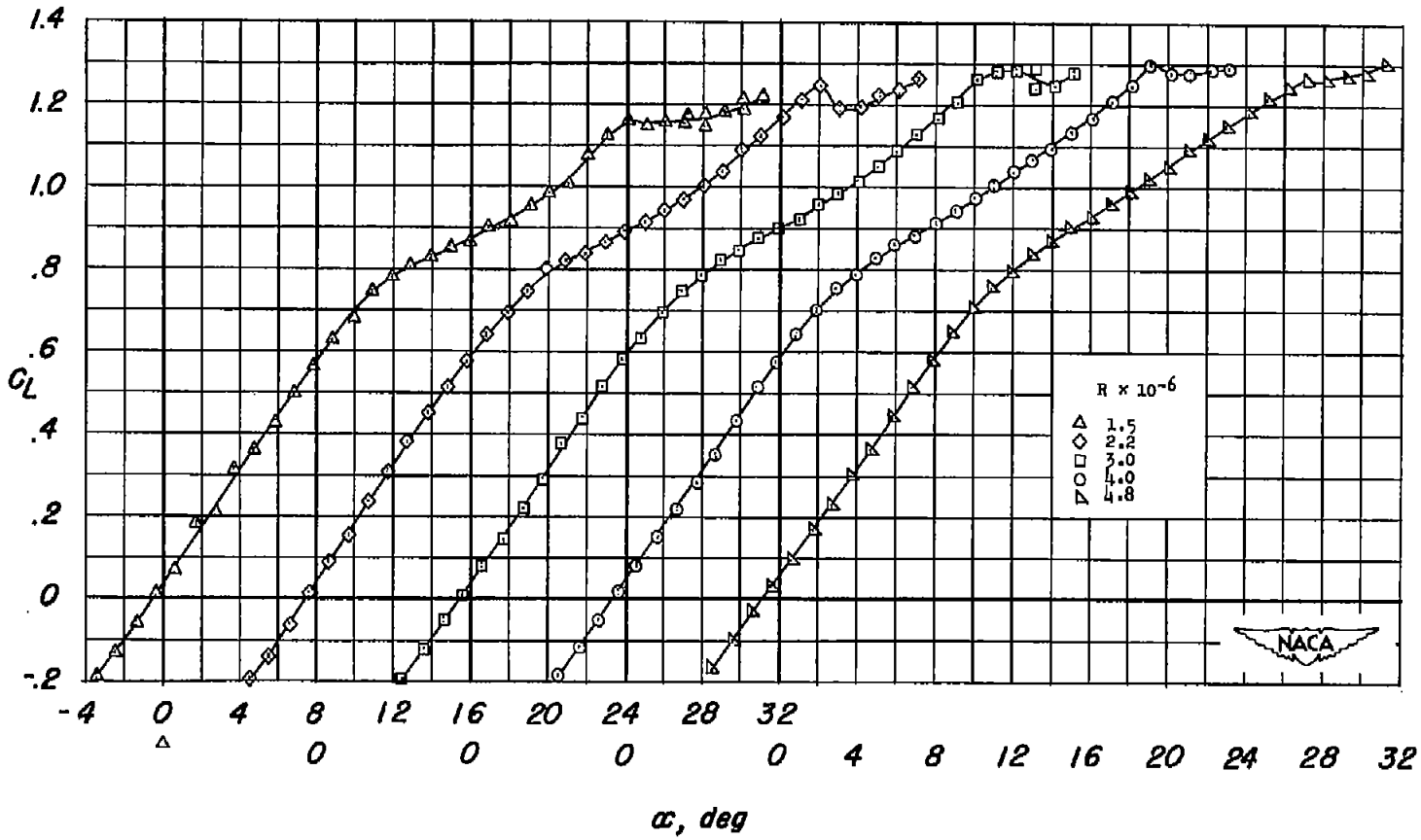

(a) C_L against α.

Figure 29.- Effect of Reynolds number on lift, drag, and pitching-moment characteristics of the plain wing.

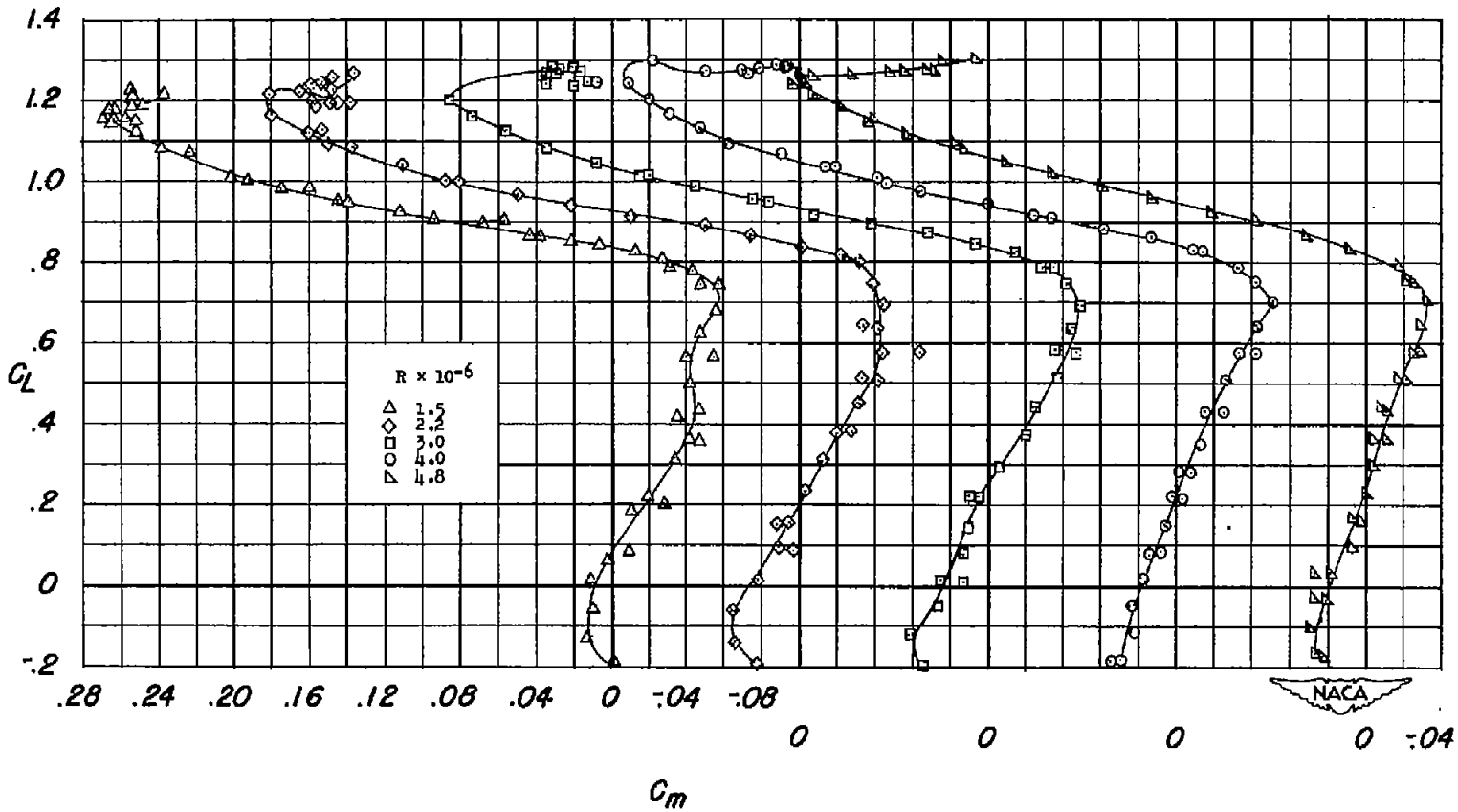

(b) C_L against C_m.

Figure 29.- Continued.

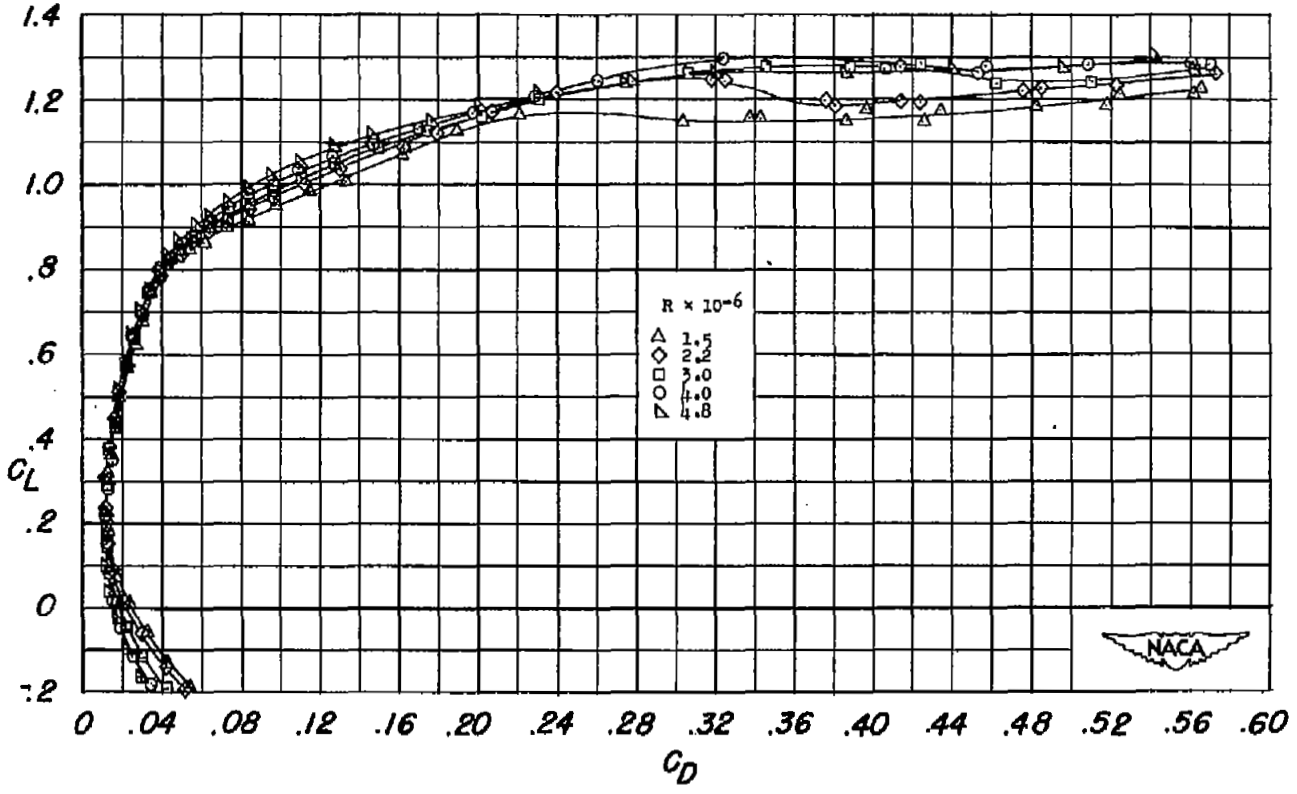

(c) C_L against C_D.

Figure 29.- Concluded.

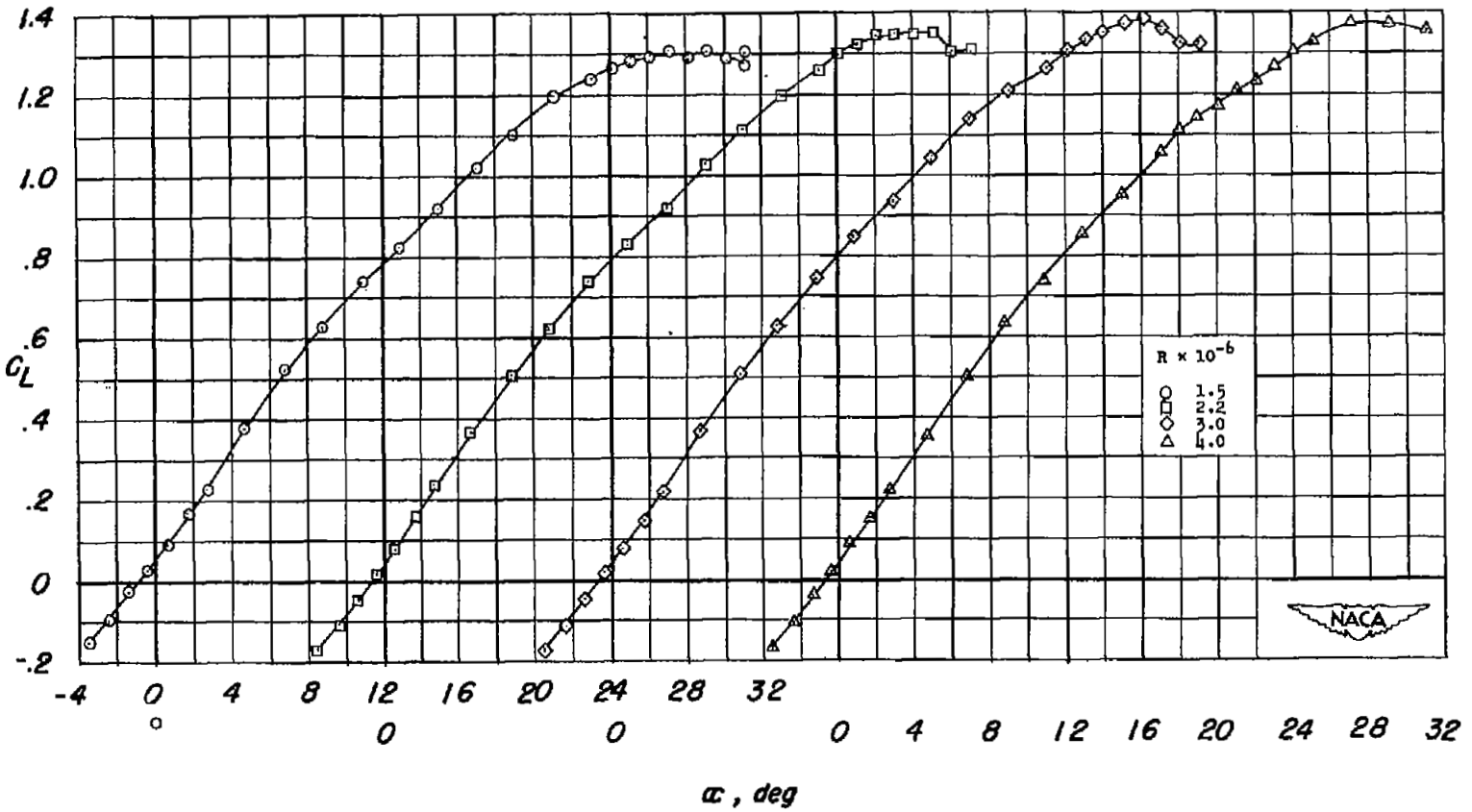

(a) C_L against α.

Figure 30.- Effect of Reynolds number on the lift and pitching-moment characteristics of the wing with complete fences at 0.35b/2, 0.575b/2, 0.800b/2, and 0.890b/2.

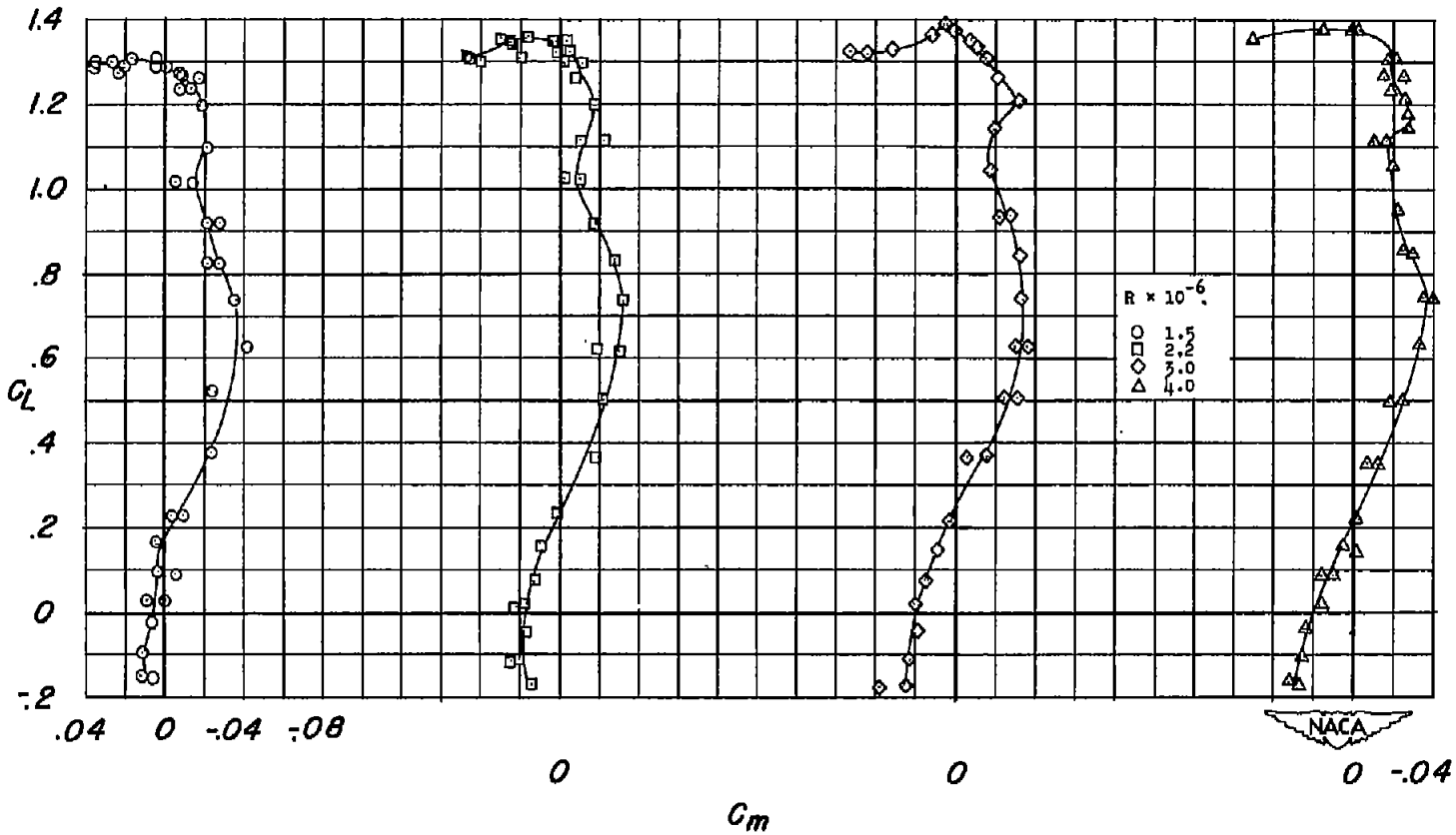

(b) C_L against C_m.

Figure 30.- Concluded.

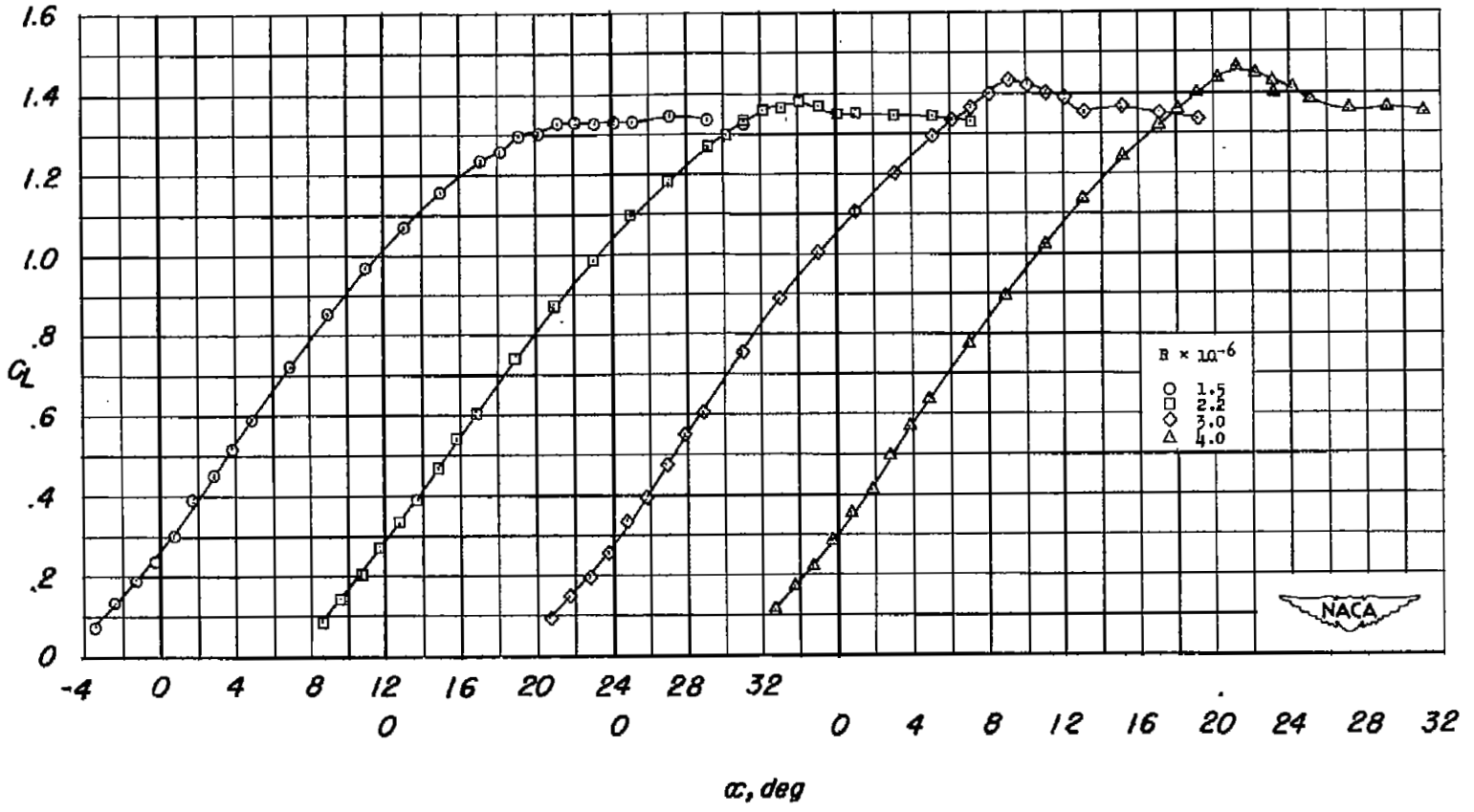

(a) C_L against α.

Figure 31.- Effect of Reynolds number on the lift and pitching-moment characteristics of the wing with 0.350b/2 split flaps, 0.500b/2 leading-edge flaps and chord fences at 0.575b/2 and 0.800b/2.

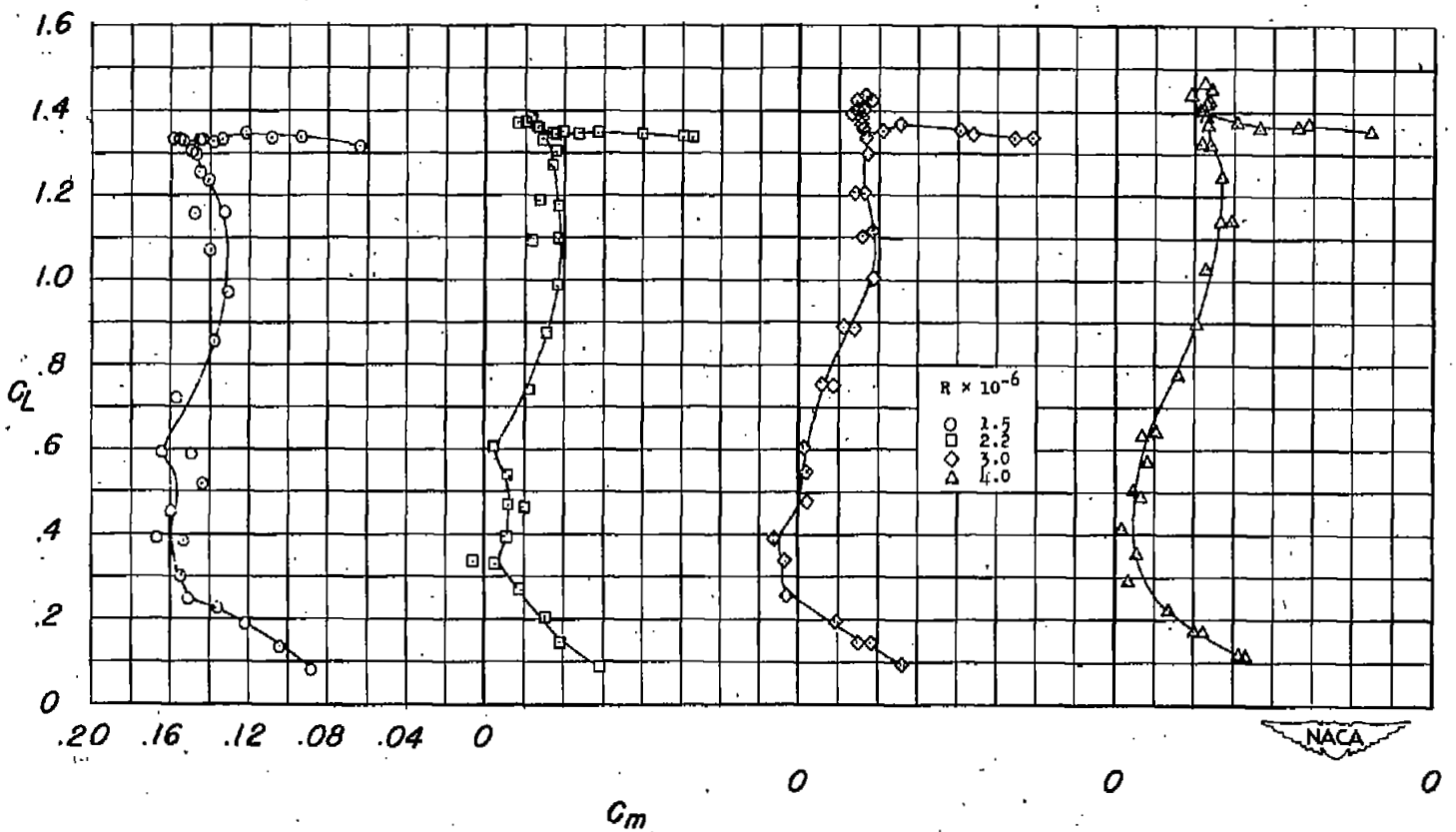

(b) C_L against C_m.

Figure 31.- Concluded.

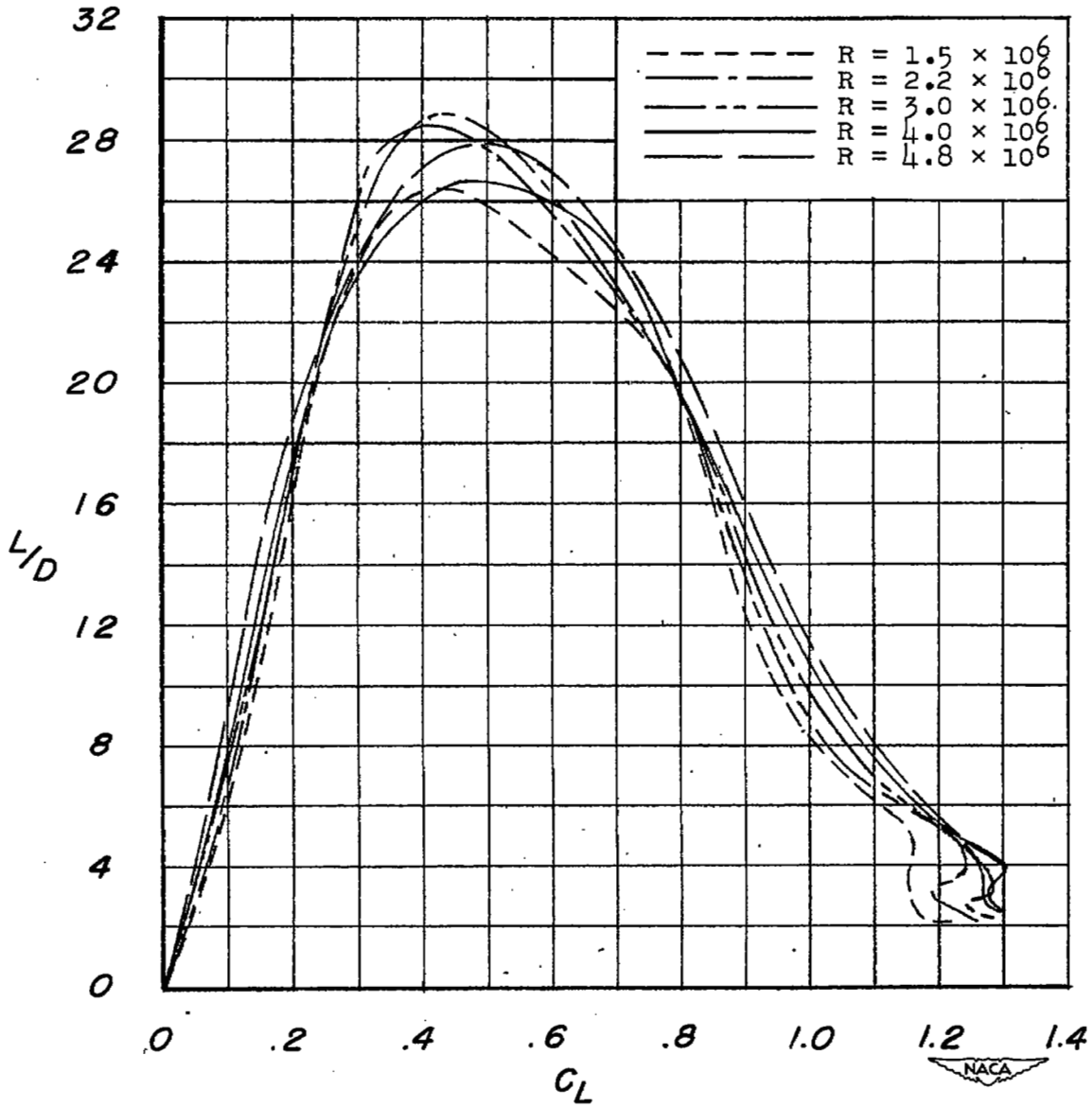

Figure 32.- Effect of Reynolds number on the lift-drag ratio of the plain wing.

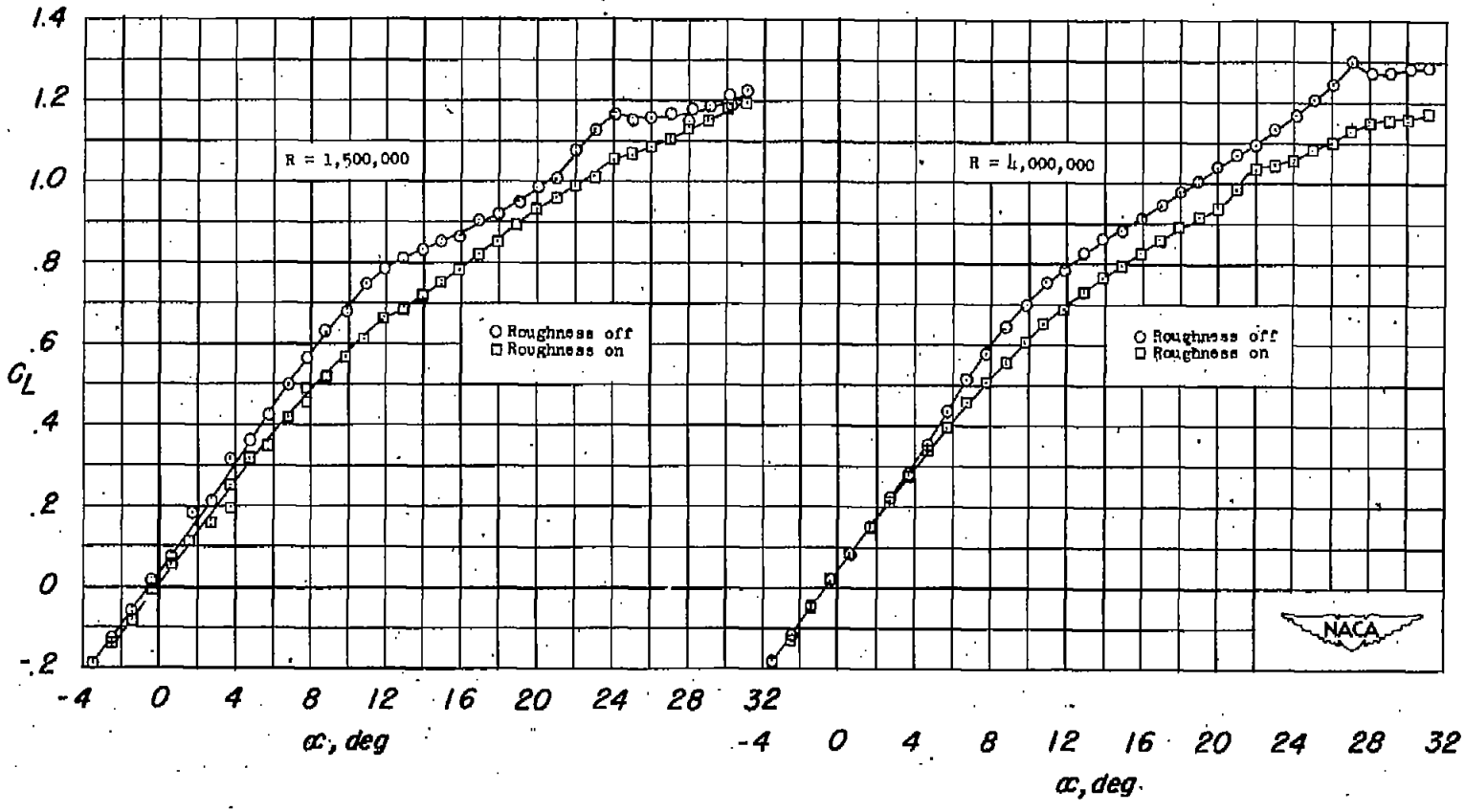

(a) C_L against α.

Figure 33.- Effect of roughness on the lift and pitching-moment characteristics of the plain wing at two Reynolds numbers.

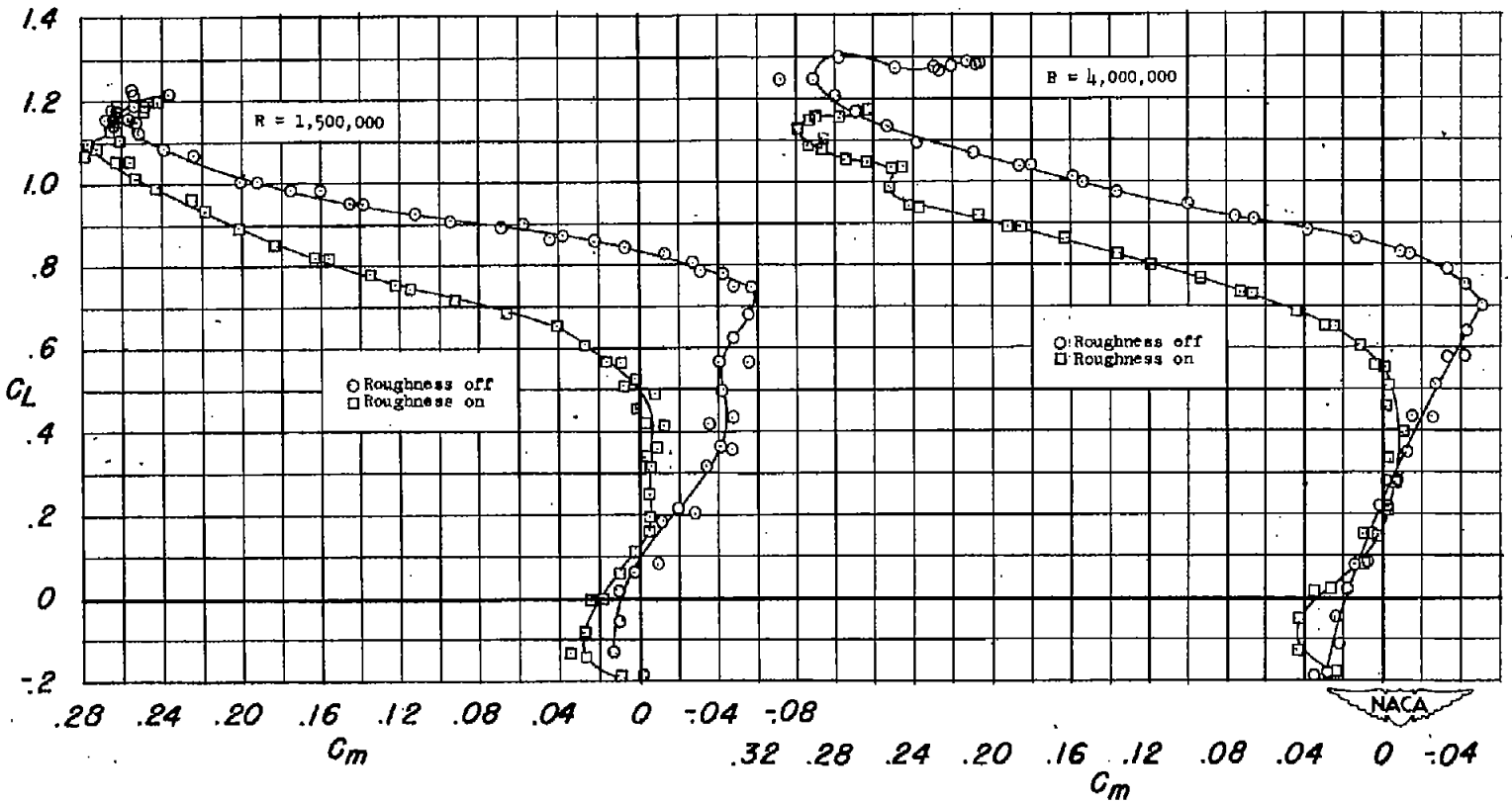

(b) C_L against C_m.

Figure 33.- Concluded.

SECURITY INFORMATION

[redacted]

NASA Technical Library
3 1176 01437 0770

[redacted]